Neuro-synergy Model Imitating Biological Control Principle and Its Application for Neuro-rehabilitation

Shotaro OKAJIMA

Abstract

Recently, robots have been developed for aiming to replace heavy duty work by human being, and demonstration experiments have been conducted. On the other hand, we are interested in the robot to be a partner for human beings. When considering technologies to make the robot be the partner, is is considered that current robots are missing abilities of motion generation and motion support. Human beings can generate their action from a symbolized action purpose like "Walk", and human beings can support the other people without disturbing the motion of the other people. Since a biological information processing structure is a basis of human activities, the biological information processing structure will be a key factor for the robot to acquire the ability of the motion generation and the motion support.

In this study, the biological information processing structure is modeled as a hierarchical control structure called Neuro-synergy model. Neuro-synergy model has two features: top-down process and bottom-up process. In the top-down process, the motion is generated by the symbolized action purpose being gradually divided into high-dimensional detail control signals as layers goes down. In the bottom-up process, control signals in each layer forms feedback control loops, and the feedback control loops adjust the control signals in each level to adapt the body to the environment.

The purpose of Ph.D. dissertation is to establish, based on Neuro-synergy model, the robot motion generation method to automatically generate the detail control signals from the symbolized action purposes and the human motion support method to enhance the motion of human beings, especially post-stroke patient. By focusing on a scheme of Neuro-synergy model, that is, the top-down process and the bottom-up process, we address it from both the robot side and the patient side.

From the robot side, by designing feedback control loops by a biological learning method and the symbolized action purpose designed by a physical feature of the robot, a controller imitating Neuro-synergy model is developed. The designed controller is applied to a balance control of a two DoF inverted pendulum, as the result, the pendulum become robust against huge disturbance adjusting the control signals by the feedback control loops. The controller is applied to a walking control of a humanoid robot, as the result, the robot can walk forward/backward and turn left/right adjusting the symbolized action purpose with maintaining the balance by the feedback control loops. These results show that it is important for the robot to generate the motion by simultaneous activation of the feedback control loop and the symbolized action purpose.

From the post-stroke patient side, it is established that the support method that promotes patient motions by intervening the feedback control loops of the post-stroke patient. At first, a rehabilitation robot is designed to promote a grasping motion of the patients by intervening the feedback control loops and inducing a grasping reflex. As the result, the robot succeeds in promoting the patient's grasping motion by intervening the feedback control loops. Next, the support method is extended for more general motion, and a robot control scheme for the support is established theoretically. As a result, designed controller can control a walking motion of a lower limb exoskeleton robot to promote the motion of a subject without disturbing the subject's motion. These results indicate that it is important to intervene the feedback control loops when supporting the motion of the patient.

Finally, from the results of the motion generation study and the motion support study, it is confirmed that simple functional actions can be realized by intervening the feedback control loops in both robots and post-stroke patients. Furthermore, it can be expected that more complex functional actions can be realized by integrating multiple simple functional actions with top-down processes. If the robots and human beings share the symbolized action purpose and can generate appropriate motions not only according to the environment but also each other's motions, the robots will achieve better support in their interactions.

Acknowledgements

This work could never be accomplished without the support from many contributors. I wish to give my utmost gratitude to them for various supports to this work.

First of all, I would like to thank Dr. Shingo Shimoda unit leader in Intelligent Behavior Control Unit at RIKEN BSI-TOYOTA Collaboration Center and Professor Yasuhisa Hasegawa of Department of Micro-Nano Mechanical Science and Engineering at Nagoya University, instruction and encouragement to make this work possible.

I am grateful to the members of my Ph.D. thesis committee, Professor Seiichi Hata of Department of Micro-Nano Mechanical Science and Engineering at Nagoya University, Professor Masahiro Ohka of Department of Complex Systems Science at Nagoya university, and Professor Kosuke Sekiyama of Department of Mechatronics Engineering at Meijo University for their help.

I wish to express my appreciation to all of the previous and present faculty and staff members, secretaries and colleagues of Hasegawa lab at Nagoya University and Shimoda lab at RIKEN. My special thanks to Associate Professor Jun Nakanishi, Assistant Professor Tadayoshi Aoyama, Designated Assistant Professor Masaru Takeuchi, Dr. Fady Shibata-Alnajjar, Dr. Hiroshi Yamasaki, Dr. Álvaro Costa-García, Dr. Sayako Ueda, Mr. Matti Itkonen, and Ms. Sonoo Moeka for their support and discussion.

Finally, I wish to express my deep appreciation to my family for their understanding and support throughout my life.

2019/8/22

Shotaro Okajima

Contents

List of Figures

List of Tables

Chapter 1

INTRODUCTION

1.1 Abstract history of robotic

Current robot is a good partner for helping people?

There is not so long history in a robotics compared with sciences such as astronomy or mathematics that exist before christ. At least, a word "robot" does not exist until 1920. It is said that "robot" was firstly used in a play called R.U.R.(Rossum's Universal Robots) written by Karel Čapek in 1920. Robots in this play had been written as human-like objects without emotions that work instead of human beings. About 50 years after this play, automatic machines working instead of human beings started to be used in factories. Especially in Japan, Kawasaki Heavy Industries Ltd. made first industrial robot in 1968 [1], which had a five degree of freedom arm and could move objects below 12 [kg](see Fig. 1.1(a)). While the industrial robots had achieved commercial success, many researchers tried to develop humanoid robots to enrich human life.

In 1973, first full-scale humanoid robot is completed in the world. Waseda university launched WABOT project in 1967, and through researches on bipedal walking robot and arm robot, WABOT-1 was completed in 1973(see Fig. 1.1(b)), which could realize bipedal walking, object recognition, and object grasping. After succeeding the walking by WABOT-1, researches about the bipedal walking robot increased in the world [2–11], but those robots had not achieved smooth and stable bipedal walking. It was considered

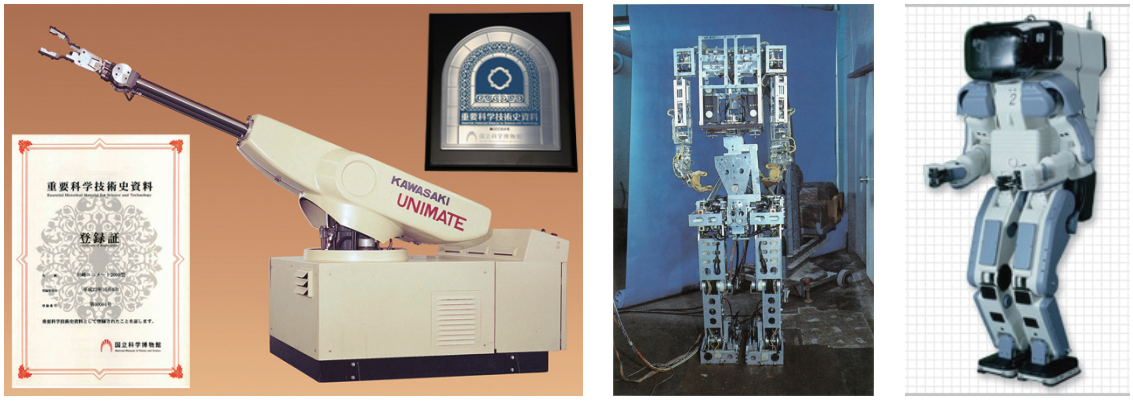

(a) Kawasaki-Unimate 2000(1968) (b) WABOT-1(1973) (c) P2(1996)

Fig. 1.1: Robots at the dawn of Japanese robotics. (a) Kawasaki-Unimate 2000 in 1968(`https://www.khi.co.jp/news/detail/20101020-1.html`). (b) WABOT-1 in 1973(`http://www.humanoid.waseda.ac.jp/booklet/kato_2-j.html`). (c) P2 in 1996(`https://www.honda.co.jp/ASIMO/kids/iam/ayumi/p2/`).

to be impossible for the robot to smoothly and stably walk for a long time. In 1996, a humanoid robot P2 impacted robotic researchers.

P2 [12] was developed by Honda Motor Co., Ltd. without any publishing in 1996(see Fig. 1.1(c)). P2 firstly accomplished smooth and stable bipedal walking and surprise researchers and the public. It is thought that the reason why P2 could realize the smooth and stable walking is that a project could reach a certain level of maturity within a project team. In terms of academic novelty, it is difficult for researchers to keep doing the same thing at universities. From that point of view, the humanoid robot like P2 could only be created by a company, we consider. In fact, regardless of software, hardware configuration of P2 was different from past humanoid robots.

First, actuators with a strain wave gear mechanism were used in P2's joins instead of a planetary gear mechanism used in academic humanoid robots. The actuators with the strain wave gear mechanism have a few backlashes compared with the actuators with the planetary gear mechanism that were used in the humanoid robot before P2. In addition to that, it is said that Honda ordered custom-made strain wave gear mechanisms that could generate high torque output. Second, accelerometers and gyroscopes were used to detect the change of the posture. In addition to that, six-axis force sensors were used in foots of the robot to detect the ground reaction force. It is said that

the sensors were also custom-made force sensors that could withstand landing impact during walking. After succeeding P2, even though the design drawing was not distributed, similar robots were developed one after another, and these two elements, the actuator with the strain wave gear mechanism and multiple sensors, became standard configurations of the humanoid robot now.

There are many research institutes and laboratories around the world developing robots including semi-humanoid robots. National Institute of Advanced Industrial Science and Technology(AIST) has developed humanoid robots(HRP series [13–21]) for working at construction sites and danger places alternative to human beings. Honda continued to improve P2 and produced that famous ASIMO [22](see Fig. 1.2(b)). Toyota Motor Corporation also has developed a humanoid robot and semi-humanoid robots that are able to play wind instruments [23], be able to follow the action of human beings [24], and aim at wide support for assistance, independence, and daily life [25]. In university laboratories also, humanoid robots about 30 [cm] in total height have been developed for verifying gait algorithms, communicate algorithm, or so on. As for the production of robots, it is considered that the ripening period has been reached, but the ability of robots to perform tasks like human beings is not as high as the public expected. It was showed in DARPA robotics challenge.

Reflecting the 2011 Tohoku earthquake and tsunami, Defense Advanced Research Projects Agency(DARPA) organized a robotics challenge in 2015. DARPA Robotics Challenge(DRC) was a competition in which robotics researcher around the world could participate. Each team had to prepare a humanoid robot that could autonomously perform a part of tasks when the robot could not get control commands from an operator because of jamming. There were eight tasks that robots performed, which were (1)driving a car, (2)getting out of the car, (3)opening a door and entering a building, (4)opening a valve, (5)drilling a hole on a wall with an electric saw, (6)getting over a rubble, (7)going up a stairs, and (8)a task not notified in advance. These tasks were not so difficult, which take from one minute to five minutes if human beings performed these. However, almost robots had taken over 40 minutes to accomplish the tasks [26]. Main reason of it is that the robots needed to measure around environment to update the environmental model before moving, and it took about 15 min between

actions. You can see it in a video [26]. In addition to that, some robots had been unable to act because of lost balance or wrong movements [27]. These robot's behaviors and fails in DRC indicate that current robots are good at following pre-decided actions and not good at generating and modifying actions in the interaction with the environment like living things.

1.2 Research motivation

It is no exaggeration to say that the 2011 Tohoku earthquake and DRC drive the development of robots that could be used in real environment. Atlas [28](see Fig. 1.2(a)) is a humanoid robot developed by Boston dynamics, and it had been developed to rescue in the disaster sites and work in damaged nuclear power plants. At the time of this writing, Atlas has realized running and continuously jumping to a step of 40 [cm] height by one foot. In addition to that, Atlas can do back-flip like gymnasts, and a vibration absorbing structure and control is astounding. These findings lead to develop a mobile box handling robot called Handle [29] that has one arm, two legs, and wheels to pick up and move under 15 [kg] box. Boston dynamics has developed also a quadruped walking robot called BigDog and SpotMini [30], and these have extremely high stability against disturbance and the motor function to go up/down stairs. At the time of this writing, demonstration experiments have been conducted by using SpotMini in the building sites in Japan.

Honda finished developing ASIMO series and has developed new humanoid robot called E2-DR [31–36]. E2-DR has been developed in order to work on the disaster site, which can switch biped walking and quadruped walking like a gorilla respond to the extent of stability and can climb the ladder. AIST has developed HRP-5P [19–21] that is the latest version of the HRP series and has been developed to conduct the heavy-duty work and working in a dangerous place instead of human beings. HRP-5P not only has superior hardware but also advanced robot control method consisting of object recognition and whole-body motion plan and could realize construction of gypsum board without help from human beings. These robots achieved multi tasks thanks to high objective recognition technology and machine learning technology, however these

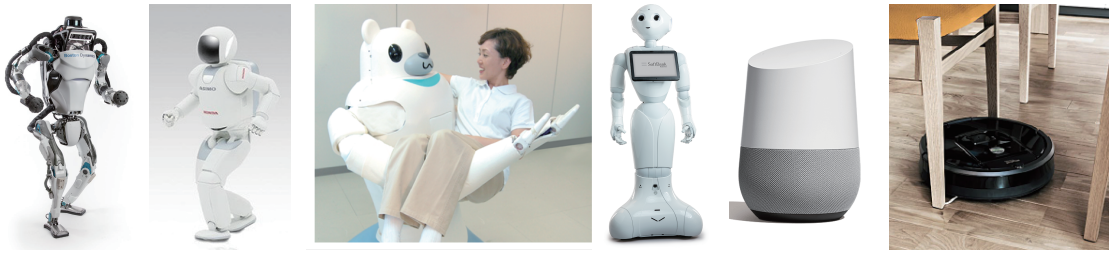

(a) Atlas (b) ASIMO (c) RIBA (d) Pepper (e) Google Home (f) Roomba

Fig. 1.2: Examples of utilitarian robot, symbiosis robot, and household robot. (a) Atlas(`https://www.bostondynamics.com/atlas`). (b) ASIMO(`https://www.honda.co.jp/ASIMO/history/asimo/index.html`). (c) Pepper(`https://www.softbankrobotics.com/us/pepper`). (d) RIBA(`http://rtc.nagoya.riken.jp/RIBA/`). (e) Google Home(`https://store.google.com/jp/product/google_home`). (f) Roomba(`http://www.irobot-jp.com/roomba/980/`).

"utilitarian" robots do not enrich our daily life drastically because these robots are not designed to live with human beings.

On the other hand, there are robots designed on the assumption that the robots have been used in the environment with human beings. We will call these robots as "symbiosis robot". LBR iiwa [37] is seven degree of freedom arm robot developed by KUKA. LBR iiwa has joint torque sensors in each joint that can detect abnormal contact and immediately reduce arm's speed and force, making it possible that human-robot collaboration work in a workspace. FRANKA EMIKA also has developed a similar seven DoF arm robot called Panda [38] that can sensitively detect abnormal contact force and stop its motion. Human Support Robot(HSR) [25] developed by TOYOTA is a single arm robot, and this robot also has good force control system achieving transferring and exchanging objects like PET bottles. RIBA [39](see Fig. 1.2(c)) is a care support robot developed by RIKEN. RIBA was developed to transfer care receivers between a bed and a wheelchair instead of care givers. By using soft control, distributed information processing, and back drivability of actuators, it can flexibly respond to the changes of the position, the posture and environment of the care receivers. PARO [40–43] developed by AIST is a therapy robot imitating a baby seal, and it is said that using PARO can achieve a same effect as an animal therapy. In the United States, PARO is recognized as a medical equipment for a neurological therapy. TOYOTA has developed a robot called Pocobee [44] that monitors a healthy of aged people and encourages a daily conversation. Pepper [45–47](see Fig. 1.2(d))

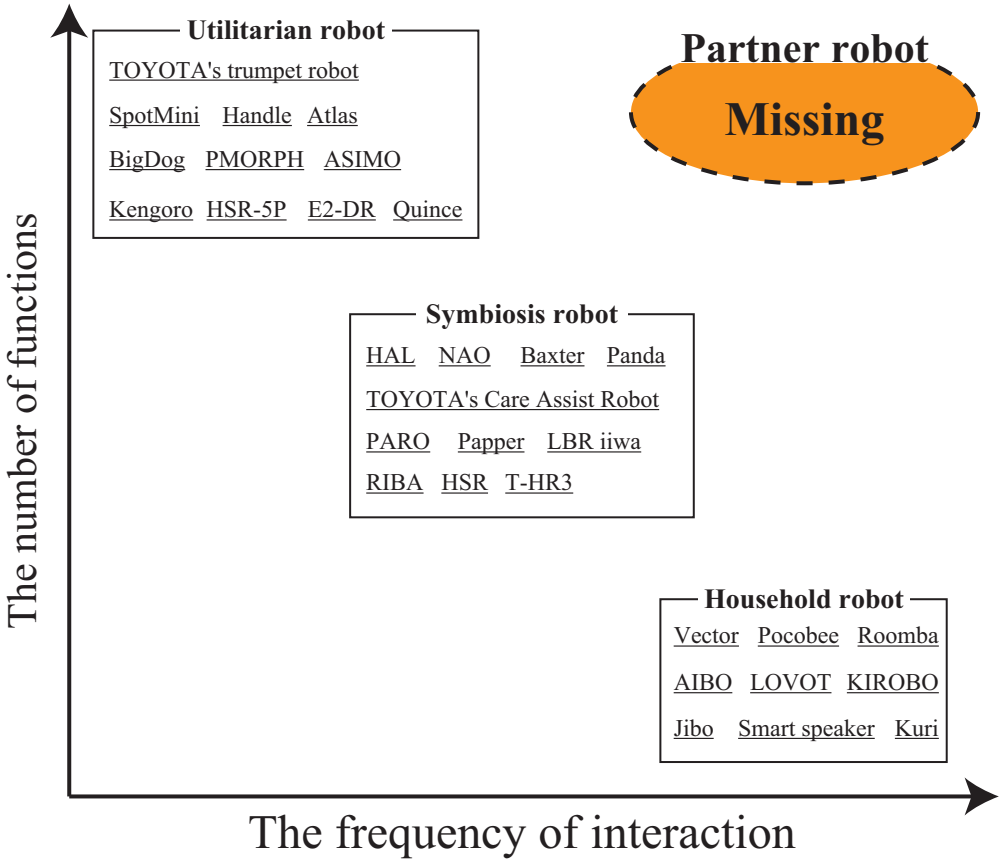

Fig. 1.3: The frequency of interaction versus the number of functions between human and several types of robots. Current utilitarian robots have multi functions but interact less frequency with human beings. Current symbiosis robots have a less functions than the utilitarian robots but interact more frequency with human beings than the utilitarian robots. Current household robots interact have a less functions than the utilitarian robots but often interact with human beings, but these functions are limited. The partner robot should interact with human being so often and have multi functions.

is a semi-humanoid robot developed by SoftBank Robotics, and it is said that Pepper has an ability to estimate an emotion of people by using voice tones and expressions of people. Pepper is used for mainly dealing with customers in restaurants, car shops, and so on. The feature of these robots is that their functions are narrowed down than the utilitarian robot instead of working close to human beings.

The function of robots interacting with human beings with higher frequency than the symbiosis robot, such as household robot, is more limited than the symbiosis robot. Smart speakers [48–51](see Fig. 1.2(e)) are, simply speaking, personal computers

that can be operated by conversation. Significant improvements in speech recognition and speech synthesis technology by the development of machine learning technology have made it possible for smart speakers to withstand everyday use. Roomba [52](see Fig. 1.2(f)) may be the most famous robot vacuum cleaner in the world. It realizes efficient cleaning with a map of a living room made by SLAM technique. The more people attempt to develop the robot that can work closer to human beings, the more limited the function of the robot.

The robots working for enriching the human life should have the ability to perform various tasks, especially to share same objective and to help human beings in order to achieve the objective. When the robot acquires the ability to share same objective and help human beings, that robot will be called as "partner robot". The relationship of each robot we consider is shown in Fig. 1.3. From the fact that there is no robot that can share the objective and help us, the partner robot is considered to be missing. Our research motivation is to develop the robot can be a good partner for helping people.

In case of human beings, we can naturally help people unlike robots. For instance, when a human being takes a heavy object, other people may help him/her when they see that scene or when he/she asks for help. The reason why we can help people is that we can share a task and create each motion when given an objective such as "Taking a heavy object". We do not need to specify a motion direction and joint trajectories to the other like a robot. Furthermore, it is unique to human beings to act in a way that encourages the other's action without disturbing the other's action, which is such as arranging the object in a place where the other is easy to hold. From the viewpoint of these examples, in this study, we focus on two important functions missing from current robotic systems in order to develop the robot can be the partner, which are (1) robot motion generation method and (2) human motion support method.

1.3 Two important functions to be robot helping human: Motion generation and Motion support

1.3.1 Motion generation

First, it is a method to create robot behaviors from symbolized action purposes such as “Walk faster” and “Turn right” or more symbolic forms such as “go to the station”. For instance, we can walk by only being conscious of “Walking” without taking care of the movement of each joint angle.

Generating the action from “Walking” or “Turning” seems to have a strong connection with linguistic function of the brain, and it is true. However, this does not mean that the language directory generates the motion. It can be understood from that walking motion itself can be generated by a baby who does not acquire a word “Walking”.

As the result of teaching from parents, the connection between the word and a network consisting of a few neurons that well represents the walking motion becomes stronger, so it seems that the language produces the action. From that point of view, the essential of the symbolized action purpose can be defined as low-dimensional control signals than the number of actuators well representing the action. Generating the action from the symbolized action purpose essentially indicates that low-dimensional control signals generate high-dimensional control signals for actuators.

As it is written before, when a human being takes a heavy object, other people may help him/her when they see that scene or when he/she asks for help. In addition to that, each person changes him/her action according to instructions or seeing what task each person is doing. Figure 1.5(b) shows an overview of a control scheme to generate the action from the symbolized action purpose, that is, to generate high-dimensional control signals from low-dimensional control signals. In sharing the symbolized action purpose, each person takes a part of the work with or without verbal communication and starts to generate the detailed control signals through several control functions such as making joint trajectories and muscle activities. At that time, the person takes care of not joint trajectories or muscle activities but the symbolized action purpose. It is because feedback control loops in each level adjust the signals to adapt an action output to the environment. The detailed control signals that create such motion, such as joint trajectories and muscle activities, are then generated automatically by hierarchical functions and the interaction between the environment and the body.

(a) Exoskeleton robot and motion patterns for each joint

(b) Walking results with healthy subjects

Fig. 1.4: (a) Photograph of an exoskeleton robot and motion patterns for each joint. Motion patterns are applied to each joint of the exoskeleton robot in conventional motion control. The robot faithfully reproduces these patterns to walk. (b) Walking results with healthy subjects. Three healthy subjects participated in the experiment willingly and their safety was guaranteed. They could not walk properly following the walking pattern.

They have said that as the complexity of the environment and the dynamics of the robot change, a task becomes more complex, and it is difficult for the robot to perform the task. However, if motion control can be conducted using symbolized information, the task does not become complex even if the environment around the robot changes, and the robot performs the task. They designed robot motions as skills in advance, and then let the robots learn the relationships between the skills and the symbols for the robot to perform a task based on the symbol. However, since the robot should generate motions under the constraint of own dynamics, the robot should generate the motions reflecting own dynamics and not generate given motions from symbolized information. We aim to develop a method to generate motions reflecting the physical features of the robot from the symbolized action purpose.

1.3.2 Motion support

It is difficult for the robot to support the motion of the human beings without disturbing the human behaviors. For instance, Fig. 1.4(b) shows a walking experiment we conducted, which is that healthy subjects walk with motion support from a lower

limb exoskeleton robot. The exoskeleton robot is controlled to follow pre-defined joint trajectories(see Fig. 1.4(a)). In this experiment, all subjects could not walk properly because of losing balance when they started to walk with the exoskeleton.

We thought, before the experiment, as the robot supported our walking motion, we could walk in comfort. However, an opposite result was obtained. The subjects could not walk properly, and one subject fell down at the early stage of the experiment. The reason why losing the balance is the robot motion is quite difference from the human motion, and the robot motion becomes a disturbance for the human beings.

The problem that the human beings cannot achieve a task because of the robot support can be occurred on all robots that support the human beings. In order to achieve the task, the subjects need to be aware of following the motion of the robot, and they will feel bothersome to use the robot. Therefore, in order to solve the problem, it is necessary to develop a motion support method of the robot based on the human motion, furthermore, a control scheme that generate the human motions.

In our daily live, we focus on not each muscle activities but symbolized action purposes that are highly specialized. It is said that control signals to the muscles are automatically created and adjusted by the activities of local neural systems including the cerebellum and spinal cord. The appropriate behavior and detailed control signals to achieve action purposes are chosen according to the environment including situations. If we could share such symbolized action purposes with robots, and if the robots could create the appropriate behavior independently according to not only the environment but also the features of our respective functions, then we would feel that the robots are our partners. Therefore, generating robot behavior from the symbolized action purpose and the supporting method to enhance human behavior could be an important way to assess the extent to which robots could be our partners with human-like behavior.

1.4 Important foundation for motion generation and motion support

It is no exaggeration to say that the biological control principle, that is, a biological information processing structure is a basis of human activity. Of course, there is dynamics-based skillful motions such as passive walking, but the biological information processing structure is a key factor to generate the actions depending on the environment and the situation. This is no exception for the motion generation and the motion support. Therefore, it is reasonable to establish there two methods by referring to the biological information processing structure.

Simply speaking, in order for the robot to generate the action from the symbolized action purpose like human beings, it is natural to develop the method by imitating the biological information processing structure. In addition to that, in order to develop the support method to promote the human action, it is necessary to understand what kind of reaction human beings do based on the biological information processing structure. From that point of view, current robots miss the functions that the biological information processing structure generates. We need to know the biological information processing structure, then establish techniques generating robot behavior from the symbolized action purpose and enhancing human behavior in the interaction based on the biological information processing structure.

The information processing structure of living things is discussed from the aspect of physiological approach and model-based approach. In current physiological approach, Takei et al. [55] reported the existence of neurons in the spinal cords of monkeys that commonly activate in association with various hand actions, suggesting that a small control signal, with dimensionality lower than the number of muscles, can encode complicated hand motion. The muscle synergy [56–64] and joint synergy [65–67] represent cooperative movement patterns of muscles and joints, and the muscle and the joint are controlled by a few control signals than the number of muscles and joints. The sensory synergy has been discussed regarding estimating sensor signals from the environment [68–70]. These research results suggest that there are a part integrating sensory inputs into low dimension and a part dividing the integrated information into

high dimensional action outputs in the biological information processing structure.

Model-based approaches provide the conceptual basis for the aforementioned physiological approach. There is the structure called bow-tie structure well representing the biological information processing structure. We develop new structure called Neuro-synergy model based on bow-tie structure in this study. The details will be shown in Chapter 2, but the features of bow-tie structure and Neuro-synergy model are briefly described here. The shape of bow-tie structure is similar to a bow tie. Sensory signals from the environment are input to high-dimensional sensory system in bow-tie structure, and sensory signals are gradually integrated into symbolized information, then the part of the symbolized information is selected and adjusted. The adjusted information is gradually divided into high-dimensional concrete control signals, and the concrete signals control muscles, then the action is generated. Signals flowing in bow-tie structure should pass through the part of the symbolized information, therefore bow-tie structure misses feedback control loops generating such as reflex motions that human beings naturally have. Neuro-synergy model being an extended model of bow-tie structure takes the feedback control loops in bow-tie structure. When we walk, we can reach a destination without thinking road conditions, and this is thought to be because the feedback control loops automatically control the body to adapt to environmental changes.

Another important approach to clarifying the mechanisms that generate automatic motor commands is the development of artificial controllers that have the same features as those of biological controllers. The autoencoders discussed in artificial intelligence [71] [72] share the same idea as the bow-tie structure. Recently, there have been various discussions about using autoencoders to control robots [73–76]. Kullback-Leibler control [77] is an interesting task-dependent approach to control robot [78] [79] with combination of control policies.

These computational approaches clarified that small control signals, with dimensional lower than the number of motors, can represent behavioral features, suggesting that lower-dimensional control signals play the role of symbolized action purposes. Shimoda et al. proposed a bio-mimetic behavior-adaptation architecture known as tacit learning [80–82] and have used it to generate bipedal walking from a roughly defined

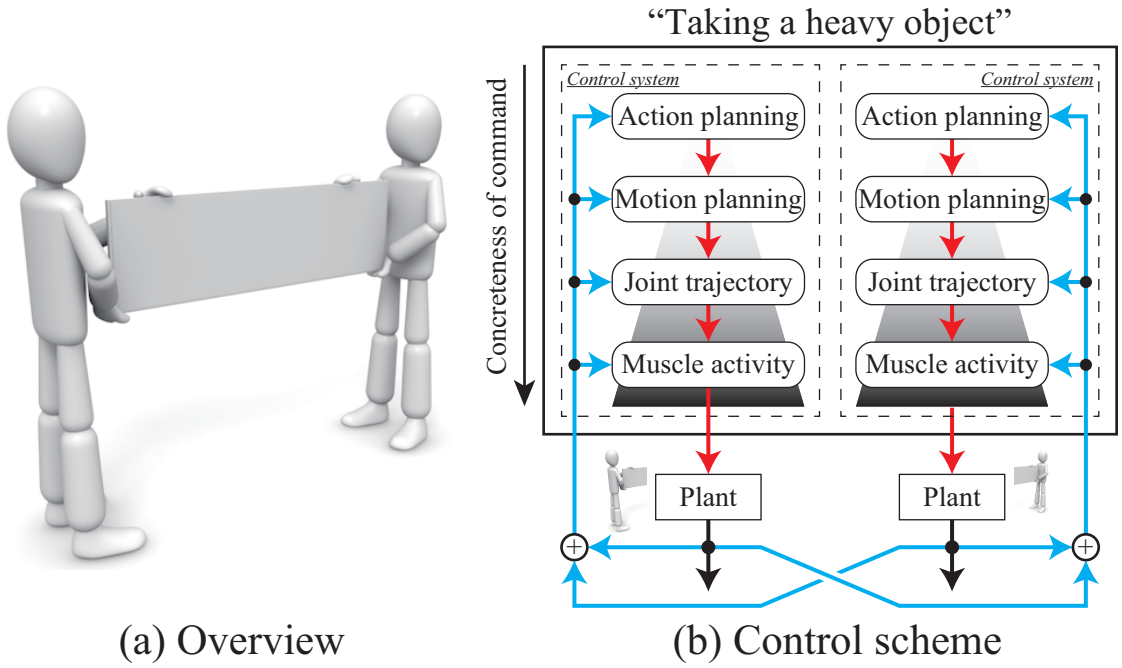

Fig. 1.5: Example of collaborative work and control scheme at it; (a) Example condition: "Taking a heavy object". (b) Overview of control scheme. Human can make action planning according to circumstances. From the action command, human being generates concrete control commands step by step, then generates driving stimulus to each muscle at the last. Action outputs affect not only its own control but also the control of others, whereby the control of each step is appropriately corrected for achieving the objective.

walking gait [81], to control the wrist joint of a forearm prosthesis in response to the wearer's shoulder movements [83], and to control a lower-limb exoskeleton robot in response to the wearer's movements [84]. Through experiments on this tacit learning adaptation, they established that two types of adaptation process could work simultaneously to adapt the behavior to an unorganized environment. One of these processes is selecting appropriate behavior and the other is adapting reactive behavior to unpredictable disturbances and small changes in body parameters and environment without changing the action purpose.

1.5 Purpose of doctoral dissertation

Our research policy is to develop necessary technologies through advanced machine intelligence researches to enable a robot to be a partner of human beings in our life.

As it was written in background, realization of generating robot behavior from the symbolized action purpose and the support to enhance human behavior in the interaction is essential for the robot to be the partner robot. In this research, we aim to establish these two important technologies based on Neuro-synergy model, which are a motion generation of the robot and a motion support for the human being. First, we attempt to develop a technology for the robot to automatically generate the detailed control signals from the symbolized action purposes by imitating the Neuro-synergy model. Second, we attempt to develop a technology for the robot to support and enhance the motion of human beings based on the Neuro-synergy model. Especially in second target, we narrow the person getting the support down to post-stroke patients in this dissertation.

1.6 Outline of doctoral dissertation

In this doctoral dissertation, we conduct the discussion along an outline in Fig. 1.6. In Chapter 2, one of biological information processing structures called bow-tie structure is introduced, and a model that extends bow-tie structure called Neuro-synergy model is proposed. In Chapter 3, components are discussed for robots to achieve automatically generating the detailed control signals from the symbolized action purposes through results of simulations and experiments: standing balance control of two DoF inverted pendulum and bipedal walking control of humanoid robot by using controllers with imitating Neuro-synergy model. Chapters 4 and 5 are focused on generating and enhancing the action of the post-stroke patient. In Chapter 4, a scheme and technologies are discussed to enhance the motion of the post-stroke patient, especially grasping motion, through the results of Chapter 3 and design a grasping-training robot based on the discussion, then the effect of the grasping-training robot is verified with clinical experiment. In Chapter 5, the scheme in Chapter 4 is extended to general exercise and

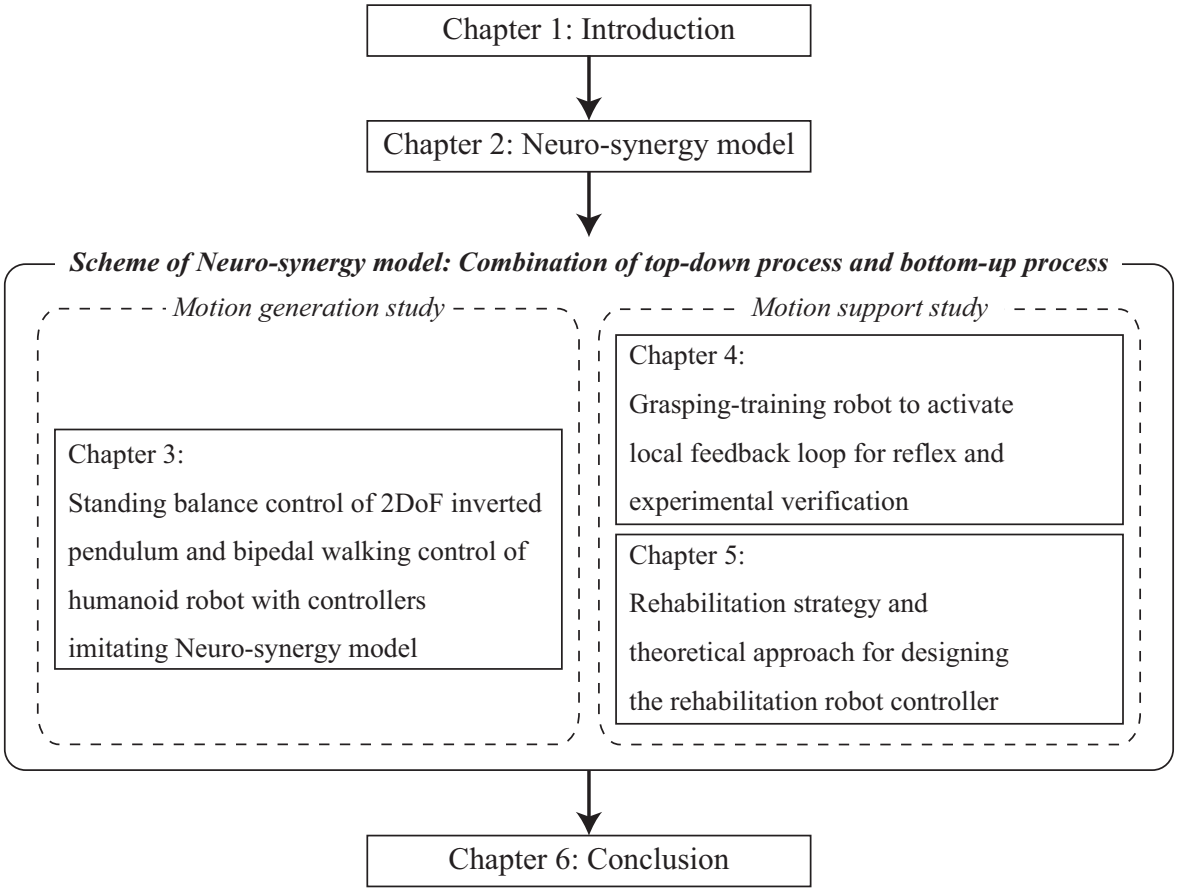

Fig. 1.6: Outline of doctoral dissertation. Chapter 1 is Introduction. Chapter 2 shows the biological information processing structure. Chapter 3 shows important factors for robots to realize automatically generating the detailed control signals from the symbolized action purposes: standing balance control of two DoF inverted pendulum and bipedal walking control of humanoid robot. Chapter 4 shows technologies to enhance the motion of the post-stroke patient and a grasping-training robot based on the technologies, then we verify the effect of the grasping-training robot with clinical experiment. Chapter 5 shows an extended scheme in Chapter 4 to general exercises and design a control system including the robot and the post-stroke patient with modeling the patient's recovery, then we show that the designed robot controller achieves the support way. Chapter 6 shows conclusion.

establish a support method of the rehabilitation training for the post-stroke patient. A controller of a rehabilitation robot is designed based on established support way with modeling the robot and the post-stroke patient. Then, the validity of the robot controller is verified through simulations and an experiment. In Chapter 6, what is the important role for establishing the partnership between the robot and human being is discussed through the whole results.

Chapter 2

Neuro-synergy model

2.1 Bow-tie structure

Living things move around the environment and work on the environment, and surrounding environment changes so often. In order for living things to survive in the environment, a wide variety of actions are needed to deal with environmental changes. However, the controllers of living things, such as the brain, have limitation on computational speed and amount of computation, so living things would be extinct by the environmental changes if they generated the action by processing feedback signals from sensory receptors such as vision or tactile sense one by one. In order to solve this problem, there is a hypothesis that living things have an information processing structure called Bow-tie structure(see Fig. 2.1).

Bow-tie structure has a sensory input side and an action output side. Signals are passed through from the sensory input side to the action output side in bow-tie structure. On the sensory input side, high-dimensional sensory signals are input from the sensory receptors in the body, for instance, human beings have over 17,000 sensory receptive nerve fibers in hand. On the action output side, high-dimensional muscle activities make the action, for instance, human beings have over 400 controllable muscles in the body, and one muscle consists of countless myofibers.

High-dimensional sensory signals are gradually integrated into the symbolized information and reduce its dimension as passing through the bow-tie structure. The part

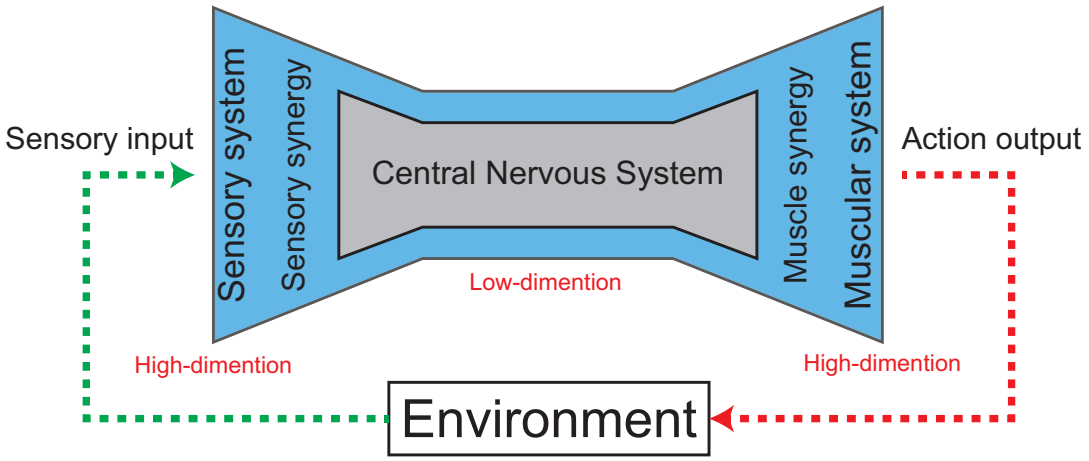

Fig. 2.1: Bow-tie structure. Bow-tie structure represents the biological information processing structure. High-dimensional sensory signals are gradually integrated into the symbolized information and reduce its dimension as passing through the bow-tie structure. The symbolized action purposes are gradually divided into high-dimensional concrete motor commands for muscles as passing through the bow-tie structure, in some sense, this process can be defined as the control.

of the symbolized information is used for the cognition, in some sense, this process can be defined as the cognition process. Based on the symbolized information, the symbolized action purposes like “Walk fast” or “Turn right” are generated, in some sense, this process can be defined as the decision making. The symbolized action purposes are gradually divided into high-dimensional concrete motor commands for muscles as passing through the bow-tie structure, in some sense, this process can be defined as the control.

The middle part of bow-tie structure is considered to be a central nerve system in human beings and is responsible for the symbolized action purposes like “Walk fast” or “Turn right”. An important role of the middle part is to avoid the frame rate problem. In addition to that, when human beings work together, people explicitly or implicitly share the symbolized action purposes each other. This means sharing the middle part of bow-tie structure each other. We can make the appropriate action and concrete motor commands for muscles according to the surrounding environment and each action.

The notions of muscle synergy [56–64] and joint synergy [65–67] that represent

the output side of this bow-tie structure are prominent examples of estimating lower-dimensional signals from observable signals such as electromyographic signals. The sensor synergy representing the input side of the bow-tie structure has been discussed regarding estimating sensor signals from the environment [68–70].

Bow-tie structure has well represented the symbolization of the biological control principle, but this structure is highly conceptual structure. Therefore, it is difficult to apply it to a robot controller directory. In addition to that, the signal in bow-tie structure is passed through from the left side to the right side, so the signal needs to go through the symbolized action purpose once. However, the action of human beings has been adjusted by feedback controls without passing through symbolized action purposes. Bow-tie structure cannot represent these features of human beings' motion control. In order to solve these problems, the concept of bow-tie structure is needed to be extended, and an extended model called Neuro-synergy model is proposed.

2.2 Neuro-synergy model

New model is developed by introducing feedback control loops and a hierarchical structure to bow-tie structure. The hierarchical structure has been well used to explain functions of a brain and in the field of machine learning imitating a method of living things. Paul D. MacLean proposed a concept called "triune brain" that the human brain evolved with maintaining three basic layers: a primitive reptile brain, old mammalian brain, and new mammalian brain manage an emotion adjusting the emotion, and learning respectively [85]. The concept affected many brain scientists, but this concept is denied in recent because this concept assumed a linear evolution from primitive living things to higher living things and human beings. Many other researches [86–89] have also proposed hierarchical model of the brain. You can see that each layer plays a role of a specific function, making it easy to understand the information processing of the brain but difficult to mathematically represent it in research on the brain model.

In the field of machine learning imitating living things, the most famous hierarchical structure is considered to be neural network. It is no doubt, nowadays, that the neural network is a hot topic thanks to an artificial intelligent bubble. The neural network is

designed by connecting layers that artificial neurons called perceptrons are arranged in parallel. The perceptron has an input side and an output side. It outputs 0.0 until the summation of input values exceeds a certain threshold and outputs 1.0 when the summation exceeds the certain threshold. Since a lot of models has been proposed, the detail is no described here, but recently, a neural network with several thousand to several millions of layers has appeared: Convolutional Neural Network(CNN) [90–94], Recurrent Neural Network(RNN) [95–99], Deep Q-Network(DQN) [100–105], Generative Adversarial Network(GAN) [106–110], Long short-term memory(LSTM) [111–115], Asynchronous Advantage Actor-Critic(A3C) [116], Auto encoder [71–76]. These networks, basically, acquire a specific function after end-to-end learning with evaluation functions or reference data sets, and the functions are diverse: controlling the robot, object recognition, voice recognition, voice synthesis, bio-signal analysis, and so on. However, because of the feature of the end-to-end learning, researchers cannot understand the mean of each layer after learning.

A conceptual biological information processing structure "Neuro-synergy model" is proposed by introducing feedback control loops and a hierarchical structure to bow-tie structure(see Fig. 2.2). In bow-tie structure, the signal is passed through from the left side to the right side. Neuro-synergy model has a hierarchical structure, and signals are flowed from the bottom to the bottom via the top. Neuro-synergy model has two structural features as below.

First, Neuro-synergy model has structures integrating input signals and dividing the symbolized action purpose. Plants on a bottom layer have the role of sensors and actuators, and the high-dimensional sensory inputs from the environment are received by the plants. The high-dimensional sensory inputs are gradually integrated into the symbolized signals to reduce its dimension like bow-tie structure as going to the top layer. The symbolized signal is adjusted by a controller, and the adjusted signals are gradually divided into high-dimensional concrete control commands for actuators as going to the bottom layer. The muscle synergy representing the output side in the lower layer is a well-known example of controlling a high-dimensional musculoskeletal system with low-dimensional abstracted signals [56–62]. The sensory synergy representing the input side in the lower layer is a well-known example of integrating high-dimensional

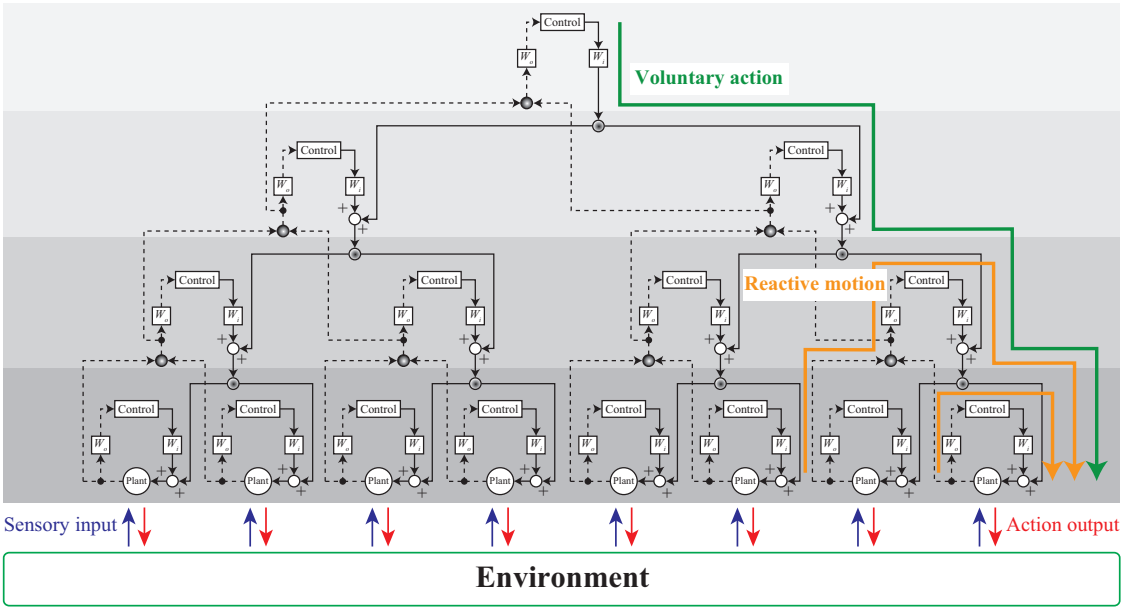

Fig. 2.2: Neuro-synergy model. Neuro-synergy model is a hierarchical structure based on a bow tie structure [117] [118]. The structure consists of several control loops. Each loop has a plant and a controller. The plant functions as a sensor and an actuator and receives high-dimensional sensory inputs from the environment. The inputs are gradually integrated into abstract information to reduce their dimensions, and the actual control signals for the high-dimensional musculoskeletal system are generated by dividing the low-dimensional abstract information.

sensory inputs into low-dimensional abstracted signals [68–70]. This signal processing can be defined as a process of making a voluntary action.

Second, Neuro-synergy model has structures feedback control loops to adjust the signals in each layer. In each layer, the signals going up and down are connected via controller, and these form local feedback control loops that are not represented in bow-tie structure. Each local feedback control loop has different function respond to each layer, in other word, symbolized levels. For instance, simple loops in the bottom layer play the role of generating reflex motion like stretch reflex, on the other hand, complex loops in the upper layer play the role of generating functional motion like an adjustment of acceleration in driving. These loops automatically adjust the action to adapt it to the environmental changes. The action generated from these feedback control loops can be defined as a reactive motion.

Neuro-synergy model looks similar to subsumption architecture [119, 120] from the

view point of the hierarchical structure. Subsumption architecture is considered to be a kind of a primitive artificial intelligent. It has some functional modules in its structure like “making a map”, “exploring”, “walking”, “moving legs”, and so on. An upper module subsumes and interfere in lower modules, and the lower module carries out its function without taking care about interfering. Subsumption architecture and Neuro-synergy model share a concept about the relationship of the upper layer and the lower layer, but it is because they are both inspired by living things. However, the design of modules of subsumption architecture is left to designers, and it is difficult to express mathematically. Therefore, in many cases, subsumption architecture does not necessarily represent the control principle of living things.

Neuro-synergy model in Fig. 2.2 has only four layers, but it does not mean that the four layers are enough to represent the biological information processing structure, and each layer performs specific functions like the subsumption architecture. It is considered that the biological information processing structure is like a fractal structure, and Fig. 2.2 is just a part in a whole Neuro-synergy model.

Neuro-synergy model has innumerable layers, and each layer does not play the role of a specific function like motion planning. In the brain, each neuron does not have a specific function like motion planning. Viewing it macroscopically with fMRI or NIRS, it can be seen that a cluster of some neurons plays the role of the function. However, viewing it microscopically, clear boundaries cannot be identified in it. Like the brain, a cluster of some layers plays the role of the specific function in Neuro-synergy model, but there are not clear boundaries.

Sharing the symbolized action purpose meant sharing the middle part of bow-tie structure each other. In the case of Neuro-synergy model, it means sharing the upper part of Neuro-synergy model each other. In order to verify components for robots to realize automatically generating the detailed control signals from the symbolized action purposes, controllers are needed to be designed by imitating Neuro-synergy model and using a biological learning method called tacit learning as the adjustment method of feedback control loops.

The rest of this chapter is showing a mathematical representation of Neuro-synergy model. $\boldsymbol{x}_i$ is a vector representing state variables of a i-th layer, and the bottom layer

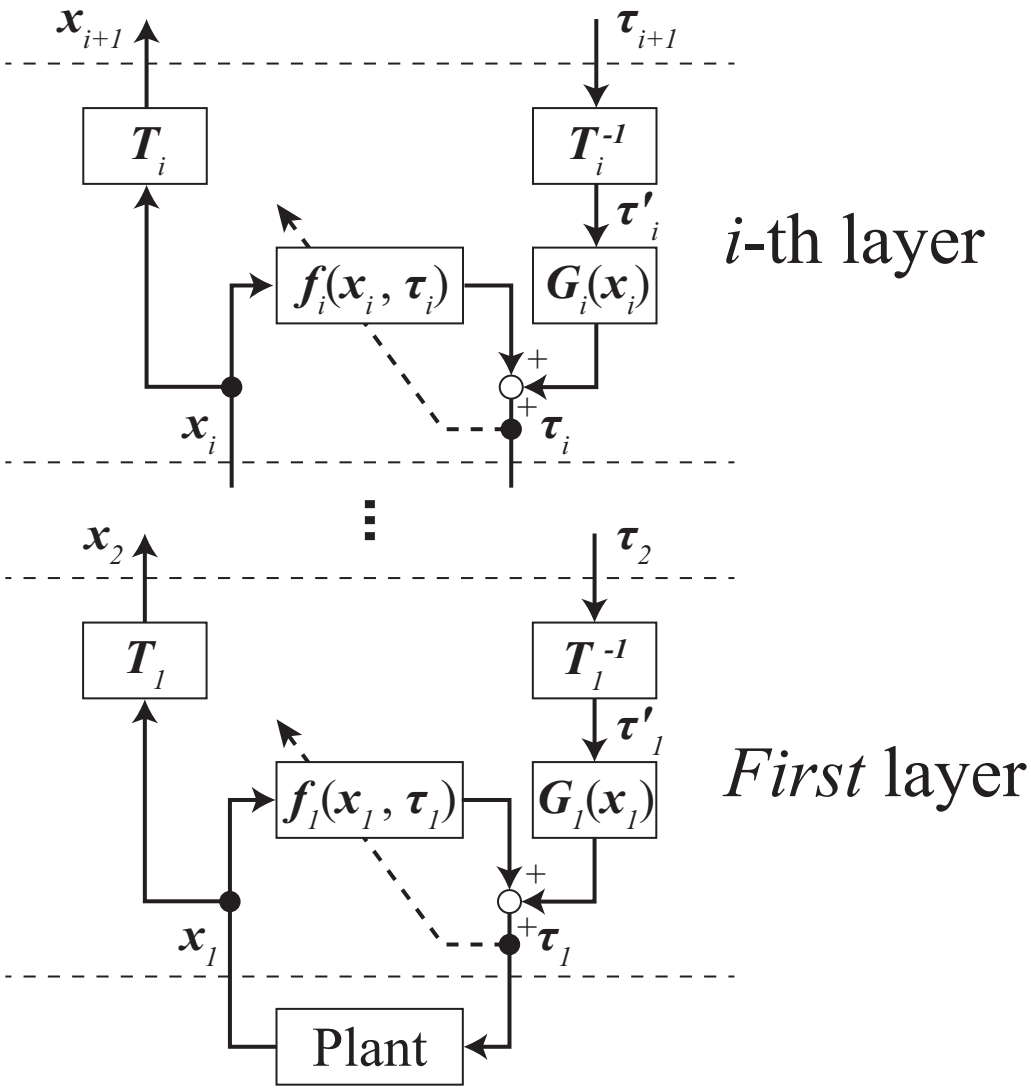

Fig. 2.3: Mathematical representation of Neuro-synergy model. Please see the detail shown in the last of this chapter.

is defined as first layer($i = 1$). $\boldsymbol{\tau}_i$ is a vector representing control signals of a i-th layer, and $\boldsymbol{\tau}'_i$ is a vector representing control signals after transferring the control signals of a $i+1$-th layer by a transfer matrix. The control system of the i-th layer of Neuro-synergy model is represented as

$$\boldsymbol{\tau}_i = \boldsymbol{f}_i(\boldsymbol{x}_i, \boldsymbol{\tau}_i) + \boldsymbol{G}_i(\boldsymbol{x}_i)\boldsymbol{\tau}'_i \tag{2.1}$$

$$\boldsymbol{x}_i = \left[\begin{array}{cccccc} {}^i x_1 & \cdots & {}^i x_{\frac{m}{2}} & {}^i \dot{x}_1 & \cdots & {}^i \dot{x}_{\frac{m}{2}} \end{array} \right]^T, \tag{2.2}$$

where $\boldsymbol{f}_i(\bullet) \in \boldsymbol{R}^m$ is a non-linear vector, $\boldsymbol{G}_i(\bullet) \in \boldsymbol{R}^{m\times m}$ is a non-linear matrix, and $\boldsymbol{\tau}_i, \boldsymbol{x}_i, \boldsymbol{\tau}'_i \in \boldsymbol{R}^m$. It is considered that a control system in living things is not a liner control system, making it difficult to represent the control system distinguishing the lower control loop and the top-down signal. In this study, the control system is represented like a symmetric affine system and distinguish the lower control loop and the top-down signal. The first term of right side of Eq. (2.1) represents the control loop for the reactive motion in Fig. 2.2, and it represents simple reflex loops when $i = 1$. The second term of right side of Eq. (2.1) represents the top-down signal of the voluntary action in Fig. 2.2.

The first term of right side of Eq. (2.1) works for adjusting the motion by the interaction with the environment. As it is written above, tacit learning is used for the adjustment. Please see [80–82] for the detail about tacit learning. Tacit learning works with the control output from the controller, so the control output in included in the first term of right side of Eq. (2.1).

The signals in Neuro-synergy model are gradually integrated into the symbolized information as the layer going up, and the symbolized information is gradually divided into the control signals as the layer going down. It indicates that a state space of i-th layer and the state space of $i+1$-th layer are switched by a transfer matrix respectively. In this dissertation, the transfer matrix is defined as

$$\boldsymbol{x}_{i+1} = \boldsymbol{T}_i \boldsymbol{x}_i, \tag{2.3}$$

where $\boldsymbol{x}_i \in \boldsymbol{R}^m$ and $\boldsymbol{x}_{i+1} \in \boldsymbol{R}^n$ $(n \leq m)$. By an inverse of the transfer matrix, the space can be switched from $i+1$-th layer to i-th layer:

$$\begin{cases} \boldsymbol{\tau}'_i = \boldsymbol{T}_i^{-1} \boldsymbol{\tau}_{i+1} & (n = m) \\ \boldsymbol{\tau}'_i = \boldsymbol{T}_i^{+} \boldsymbol{\tau}_{i+1} & (n < m) \end{cases}, \tag{2.4}$$

where $\boldsymbol{T}_i^+$ is called pseudoinverse matrix, and $\boldsymbol{T}_i \boldsymbol{T}_i^+ = \boldsymbol{I}$. The transfer matrix should reflect physical characteristics of the living things. In case of the human, $\boldsymbol{T}^{-1}$ corresponds to the muscle synergy.

From these equations, the control signal that is input into the plant can be represented when there is one layer as

$$\boldsymbol{\tau}_1 \;=\; \boldsymbol{f}_1(\boldsymbol{x}_1, \boldsymbol{\tau}_1) + \boldsymbol{G}_1(\boldsymbol{x}_1) \boldsymbol{T}_1^{-1} \boldsymbol{\tau}_2. \tag{2.5}$$

$\boldsymbol{\tau}_2$ can be represent as same form as Eq. (2.5) as follow:

$$\boldsymbol{\tau}_2 = \boldsymbol{f}_2(\boldsymbol{x}_2, \boldsymbol{\tau}_2) + \boldsymbol{G}_2(\boldsymbol{x}_2)\boldsymbol{T}_2^{-1}\boldsymbol{\tau}_3. \tag{2.6}$$

Therefore, the control signal that is input into the plant can be represented when there is two layers as

$$\boldsymbol{\tau}_1 = \boldsymbol{f}_1(\boldsymbol{x}_1, \boldsymbol{\tau}_1) + \boldsymbol{G}_1(\boldsymbol{x}_1)\boldsymbol{T}_1^{-1}\boldsymbol{f}_2(\boldsymbol{x}_2, \boldsymbol{\tau}_2) + \boldsymbol{G}_1(\boldsymbol{x}_1)\boldsymbol{T}_1^{-1}\boldsymbol{G}_2(\boldsymbol{x}_2)\boldsymbol{T}_2^{-1}\boldsymbol{\tau}_3. \tag{2.7}$$

By arranging this equation, the equation is written as

$$\boldsymbol{\tau}_1 = \sum_{i=1}^{2}\left\{\left(\prod_{q=0}^{i-1}\boldsymbol{G}_q(\boldsymbol{x}_q)\boldsymbol{T}_q^{-1}\right)\boldsymbol{f}_i(\boldsymbol{x}_i, \boldsymbol{\tau}_i)\right\} + \left(\prod_{i=1}^{2}\boldsymbol{G}_i(\boldsymbol{x}_i)\boldsymbol{T}_i^{-1}\right)\boldsymbol{\tau}_3 \tag{2.8}$$

$$\boldsymbol{G}_0(\boldsymbol{x}_0)\boldsymbol{T}_0^{-1} = \boldsymbol{I}, \tag{2.9}$$

Equation (2.9) is an equation to establish Eq. (2.8), and there is no physical meaning.

From above example, when there are n layers, the control signal that is input into the plant can be represented as

$$\begin{aligned}\boldsymbol{\tau}_1 = {} & \boldsymbol{f}_1(\boldsymbol{x}_1, \boldsymbol{\tau}_1) + \boldsymbol{G}_1(\boldsymbol{x}_1)\boldsymbol{T}_1^{-1}\boldsymbol{f}_2(\boldsymbol{x}_2, \boldsymbol{\tau}_2) \\ & + \boldsymbol{G}_1(\boldsymbol{x}_1)\boldsymbol{T}_1^{-1}\boldsymbol{G}_2(\boldsymbol{x}_2)\boldsymbol{T}_2^{-1}\boldsymbol{f}_3(\boldsymbol{x}_3, \boldsymbol{\tau}_3) + \cdots \\ & + \boldsymbol{G}_1(\boldsymbol{x}_1)\boldsymbol{T}_1^{-1}\cdots\boldsymbol{G}_{n-1}(\boldsymbol{x}_{n-1})\boldsymbol{T}_{n-1}^{-1}\boldsymbol{f}_n(\boldsymbol{x}_n, \boldsymbol{\tau}_n) \\ & + \boldsymbol{G}_1(\boldsymbol{x}_1)\boldsymbol{T}_1^{-1}\cdots\boldsymbol{G}_n(\boldsymbol{x}_n)\boldsymbol{T}_n^{-1}\boldsymbol{\tau}_{n+1}.\end{aligned} \tag{2.10}$$

By arranging this equation, the equation is written as

$$\boldsymbol{\tau}_1 = \sum_{i=1}^{n}\left\{\left(\prod_{q=0}^{i-1}\boldsymbol{G}_q(\boldsymbol{x}_q)\boldsymbol{T}_q^{-1}\right)\boldsymbol{f}_i(\boldsymbol{x}_i, \boldsymbol{\tau}_i)\right\} + \left(\prod_{i=1}^{n}\boldsymbol{G}_i(\boldsymbol{x}_i)\boldsymbol{T}_i^{-1}\right)\boldsymbol{\tau}_{n+1} \tag{2.11}$$

$$\boldsymbol{G}_0(\boldsymbol{x}_0)\boldsymbol{T}_0^{-1} = \boldsymbol{I}. \tag{2.12}$$

The role of Eq. (2.12) is as same as that of Eq. (2.9).

Chapter 3

Action Generation from Symbolized Action Purpose with Controllers Imitating Neuro-synergy Model

3.1 Purpose in chapter 3

In this chapter, as said before, it is aimed to clarify the mechanisms of generating automatic motor commands from the symbolized action purpose like human beings. Bow tie structure was extended to Neuro-synergy model, which is one of model-based approaches providing the conceptual basis for the aforementioned physiological approach. In Neuro-synergy model, symbolized information is divided by methods based on physical characteristics such as muscle synergy, automatically generating concrete control commands for muscles. The voluntary action generated from the symbolized information is automatically adjusted by each feedback control loop with biological learning method.

Shimoda et al. proposed a bio-mimetic behavior-adaptation architecture known as tacit learning [80–82] and have used it to generate bipedal walking from a roughly defined walking gait [81], to control the wrist joint of a forearm prosthesis in response to the wearer's shoulder movements [83], and to control a lower-limb exoskeleton robot in response to the wearer's movements [84]. Through experiments on this tacit learning

adaptation, they established that two types of adaptation process could work simultaneously to adapt the behavior to an unorganized environment. One of these processes is selecting appropriate behavior and the other is adapting reactive behavior to unpredictable disturbances and small changes in body parameters and environment without changing the action purpose.

Even though it has been established that it is important for these two processes to operate in parallel, the conditions of the controllers needed to realize such adaptation remain under discussion. Herein, this discussion is advanced by using an artificial controller that can adapt the motor commands to real-time changes in the symbolized action purpose, and the conditions for adapting in real time to both the environment and the symbolized action purpose are clarified. Chapter 3.2 is begun from designing a controller with tacit learning and a method transferring the control signals into a different control space know as mechanical resonance mode space (MRM-space). The mechanical resonance mode of the robot corresponds to the muscle synergy of human beings. In MRM-space, the signals are used to control the mechanical resonance modes of the robot. This makes it easy to understand how the robot behavior changes when the control signal is changed in MRM-space. In Chapter 3.3 and Chapter 3.4, an adaptation method in MRM-space is proposed using a two-degree-of-freedom (two DoF) inverted pendulum, 27 DoF humanoid robot, and the NAO humanoid robot [121], respectively. It is shown that this controller can adapt the motion to the environment through simulation and experiment. In Chapter 3.5, it is discussed that the importance of body mechanisms in the process of simultaneous adaptation and how that process can be used to evaluate the human-like motion of a robot. In Chapter 3.6, it is concluded that this chapter with summarizing our simulation and experiment results.

3.2 Methods Used to Design a Control Structure

Transfer to MRM-space and behavior adaptation by tacit learning are the key analytical methods of the present study. Because both methods are discussed in detail elsewhere (mechanical resonance mode [122]; tacit learning [80–82]), their essential points are briefly explained herein.

3.2.1 Mechanical Resonance Mode

A mechanical resonance mode is defined by the position and the condition of the robot joints. For instance, a two DoF inverted pendulum has two mechanical resonance modes as shown in Fig. 3.1(a)(b). A mechanical resonance mode is characterized mathematically by mode vectors and singular values. Writing the equation of motion of a two DoF inverted pendulum as

$$\begin{aligned} \boldsymbol{M}\ddot{\boldsymbol{\theta}} + \boldsymbol{K}\boldsymbol{\theta} &= \boldsymbol{0} && (3.1) \\ \Leftrightarrow \quad \ddot{\boldsymbol{\theta}} &= -\boldsymbol{M}^{-1}\boldsymbol{K}\boldsymbol{\theta}, && (3.2) \end{aligned}$$

where $\boldsymbol{\theta} \in \boldsymbol{R}^{2\times 1}$ implies the angles of the joints, the mode vectors and eigenvalues are calculated by a singular-value decomposition (SVD) of $\boldsymbol{M}^{-1}\boldsymbol{K}$:

$$\boldsymbol{M}^{-1}\boldsymbol{K} \xrightarrow[SVD]{} \begin{cases} \boldsymbol{v}_1, \boldsymbol{v}_2 & (mode\ vectors) \\ \lambda_1, \lambda_2 & (singular\ values) \end{cases}, \tag{3.3}$$

where $\boldsymbol{M} \in \boldsymbol{R}^{2\times 2}$ is the inertia matrix of the pendulum linearized around $\boldsymbol{\theta} = \boldsymbol{0}$ and $\boldsymbol{K} \in \boldsymbol{R}^{2\times 2}$ is a stiffness matrix that has the spring coefficients of the joints on its main diagonal. The first mode ($\boldsymbol{v}_1$) corresponds to the smallest eigenvalue (λ_1) and the second mode ($\boldsymbol{v}_2$) corresponds to the next-largest eigenvalue (λ_2). The mode vector represents the shape of the pendulum oscillation.

The state variable $\boldsymbol{\theta}$ of the pendulum can be represented as a superposition of the mode vectors as follows:

$$\begin{aligned} \boldsymbol{\theta} &= \boldsymbol{v}_1 w_1 + \boldsymbol{v}_2 w_2 = \begin{bmatrix} \boldsymbol{v}_1 & \boldsymbol{v}_2 \end{bmatrix} \begin{bmatrix} w_1 & w_2 \end{bmatrix}^T \\ \therefore \boldsymbol{\theta} &= \boldsymbol{T}\boldsymbol{w}\ (\Leftrightarrow\ \boldsymbol{w} = \boldsymbol{T}^{-1}\boldsymbol{\theta}), && (3.4) \end{aligned}$$

where w_1, w_2 represent the weights of each mode vector and $\boldsymbol{T}$ can be defined as a transfer matrix. The weights of the mode vectors can be defined as state variables in MRM-space.

The adjustment of the state variables is reflected in the movement of individual joints by the transfer matrix. This is much like the top-down process in people, namely changing one's behavior by means of symbolized information without having to attend to the actions of individual joints.

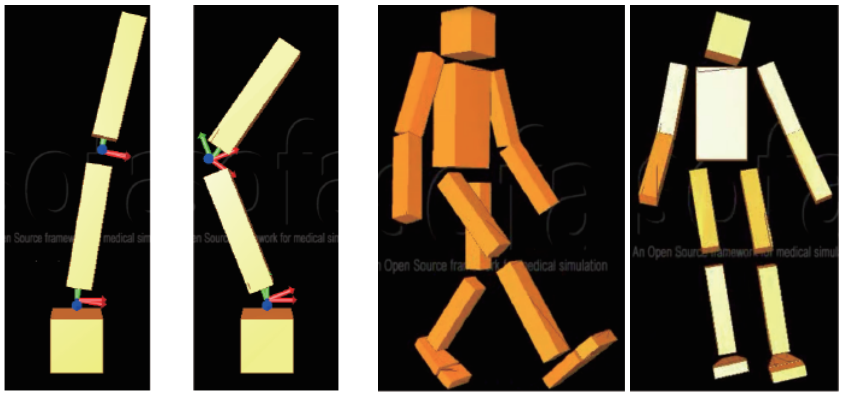

Fig. 3.1: Modes of two-degree-of-freedom (two DoF) inverted pendulum and 27 DoF humanoid robot: (a) first mode of pendulum (same-phase posture); (b) second mode of pendulum (anti-phase posture); (c) first mode of robot (bipedal leg swinging); (d) eighth mode (leg swinging on frontal plane).

3.2.2 Tacit Learning

Tacit learning is an adaptive learning method inspired by two features of living beings. First, living beings can perform adaptive behavior globally even though control is realized by only a summation of local nerve-cell firings. Second, adaptive learning and behavioral control are calculated in parallel; this is unlike machine learning, whose calculation is divided into a learning phase and an action phase.

To apply these features to artificial controller, action targets and the concept of "reflex" are used in tacit learning. The reflex plays a role in directing the movement of the controlled system toward a state in situations in which the system does not receive many environmental stimuli from a global perspective. By enhancing the reflex by accumulating reflex commands, the system can acquire a state autonomously through system–environment interactions, where there are fewer environmental stimuli without having to distinguish between the learning phase and the action phase.

Other learning methods use behavioral functions or teaching signals to adjust the controlled system behavior and achieve adaptive behavior in a top-down manner. In that sense, tacit learning can be defined as a bottom-up learning process, adjusting the behavior through system–environment interactions. However, it can control the system to achieve adaptive behavior from a global perspective. Herein, tacit learning

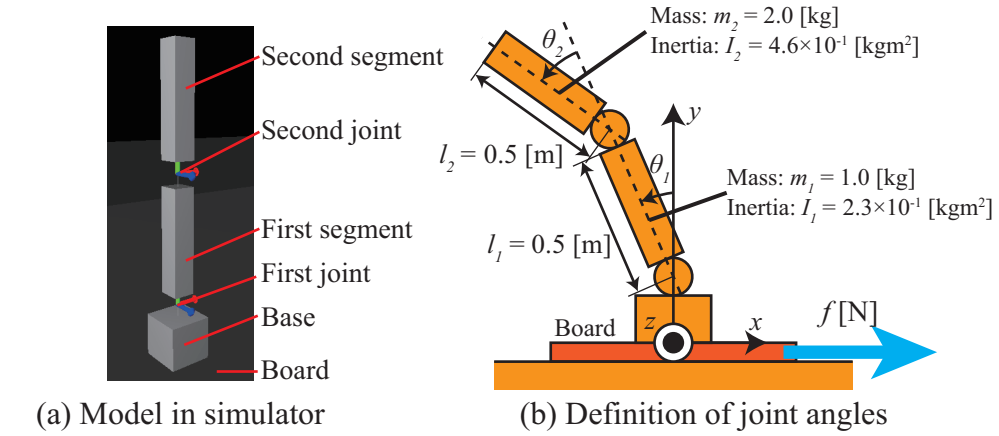

Fig. 3.2: Model of two DoF inverted pendulum: (a) pendulum model in simulator; (b) definitions of joint angles and system parameters. The pendulum sits on a board that is moved horizontally by a force f [N], thereby imparting disturbances to the pendulum.

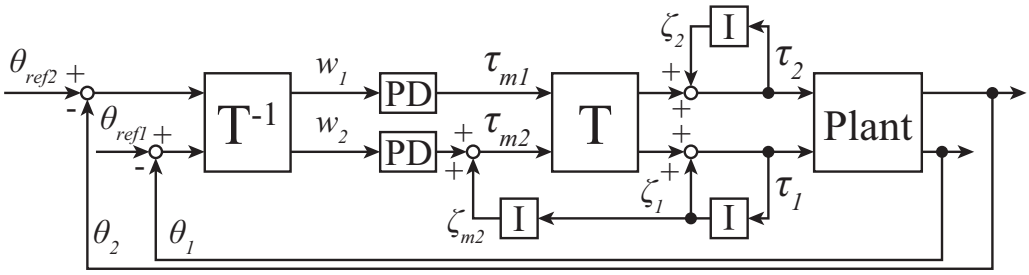

Fig. 3.3: Block diagram for standing balance control of two DoF inverted pendulum; see Chapter 3.3.2 for details.

is used to develop a bio-mimetic adaptation process.

3.3 Standing Balance Control with two DoF Inverted Pendulum

In this chapter, the controller with tacit learning in MRM-space is introduced and is applied to standing balance control of a two DoF inverted pendulum. It is shown that the tacit learning controller can maintain balance against larger disturbances than the case without learning.

3.3.1 Model of two DoF Inverted Pendulum

Figure 3.2 shows the two DoF inverted pendulum model used in this simulation. Its equation of motion is

$$\boldsymbol{M}(\boldsymbol{\theta})\ddot{\boldsymbol{\theta}} + \boldsymbol{\omega}(\boldsymbol{\theta}, \dot{\boldsymbol{\theta}}) = \boldsymbol{\tau}, \tag{3.5}$$

where $\boldsymbol{\theta}$ is a 2×1 vector consisting of the joint angles, $\boldsymbol{\tau}$ is a 2×1 torque vector that affects each joint, and $\boldsymbol{M}(\boldsymbol{\theta})$ is a 2×2 inertia matrix given by

$$\boldsymbol{M}(\boldsymbol{\theta}) = \begin{bmatrix} I_1 + m_1 a_1^2 + l_1^2 m_2 + \eta + 2\xi \cos\theta_2 & \eta + \xi \cos\theta_2 \\ \eta + \xi \cos\theta_2 & \eta \end{bmatrix}, \tag{3.6}$$

where $a_1 = l_1/2$, $a_2 = l_2/2$, $\eta = I_2 + m_2 a_2^2$, $\xi = l_1 m_2 a_2$, and $\boldsymbol{\omega}(\boldsymbol{\theta}, \dot{\boldsymbol{\theta}})$ is

$$\boldsymbol{\omega}(\boldsymbol{\theta}, \dot{\boldsymbol{\theta}}) = \begin{bmatrix} -\xi(2\dot{\theta}_1 + \dot{\theta}_2)\dot{\theta}_2 \sin\theta_2 - g_1 \sin\theta_1 - g_2 \sin(\theta_1 + \theta_2) \\ \xi \dot{\theta}_1^2 \sin\theta_2 - g_2 \sin(\theta_1 + \theta_2) \end{bmatrix}, \tag{3.7}$$

where $g_1 = (m_1 a_1 + m_2 l_1) g$, $g_2 = m_2 a_2 g$, and $g = 9.81$ m/s^2.

3.3.2 Standing Balance Control Structure

Figure 3.3 shows a standing balance controller designed by using the transfer matrix $\boldsymbol{T}$ described in Eq. (3.4) and tacit learning. Terms θ_i and τ_i are the angle and torque, respectively, of joint i. The torque vector $\boldsymbol{\tau}$ for each joint is

$$\boldsymbol{\tau} = \boldsymbol{T}\boldsymbol{A}\boldsymbol{T}^{-1}\Delta\boldsymbol{\theta} + \boldsymbol{T}\boldsymbol{B}\boldsymbol{T}^{-1}\Delta\dot{\boldsymbol{\theta}} + \boldsymbol{T}\boldsymbol{\zeta}_m + \boldsymbol{\zeta}, \tag{3.8}$$

$$\boldsymbol{\tau} = \begin{bmatrix} \tau_1 & \tau_2 \end{bmatrix}^T. \tag{3.9}$$

$\Delta\boldsymbol{\theta}$ and $\Delta\dot{\boldsymbol{\theta}}$ are

$$\Delta\boldsymbol{\theta} = \begin{bmatrix} \boldsymbol{\theta}_{ref} - \boldsymbol{\theta} \end{bmatrix}, \Delta\dot{\boldsymbol{\theta}} = -\dot{\boldsymbol{\theta}}, \tag{3.10}$$

where $\boldsymbol{\theta}$ and $\dot{\boldsymbol{\theta}}$ are state variables:

$$\boldsymbol{\theta} = \begin{bmatrix} \theta_1 & \theta_2 \end{bmatrix}^T, \quad \dot{\boldsymbol{\theta}} = \begin{bmatrix} \dot{\theta}_1 & \dot{\theta}_2 \end{bmatrix}^T. \tag{3.11}$$

$\boldsymbol{\theta}_{ref}$ is a reference for each joint:

$$\boldsymbol{\theta}_{ref} = \begin{bmatrix} \theta_{ref1} & \theta_{ref2} \end{bmatrix}^T. \tag{3.12}$$

Terms $\boldsymbol{A}$ and $\boldsymbol{B}$ are diagonal matrices:

$$\boldsymbol{A} = \begin{bmatrix} k_{p1} & 0 \\ 0 & k_{p2} \end{bmatrix}, \quad \boldsymbol{B} = \begin{bmatrix} k_{d1} & 0 \\ 0 & k_{d2} \end{bmatrix}, \tag{3.13}$$

where k_{p1} and k_{p2} are proportional(P) gains of the proportional-derivative(PD) controller in MRM-space, k_{d1} and k_{d2} are derivative gains of the PD controller in MRM-space, and $\boldsymbol{T}^{-1}$ is the transfer matrix from joint space to MRM-space.

Term $\boldsymbol{\zeta}$ is a vector that consists of the integration of $\boldsymbol{\tau}$ as follows:

$$\boldsymbol{\zeta} = \begin{bmatrix} \zeta_1 \\ \zeta_2 \end{bmatrix} = \begin{bmatrix} k_1 & 0 \\ 0 & k_2 \end{bmatrix} \begin{bmatrix} \int \tau_1 dt \\ \int \tau_2 dt \end{bmatrix}, \tag{3.14}$$

where k_1 and k_2 are the coefficients of the integrators that accumulate the joint torques and output the integrated values. These accumulations correspond to tacit learning, and these integrators adjust the individual joint torques and work to keep the pendulum upright after disturbance through pendulum–environment interaction, as in [81]. This tacit learning corresponds to the adjusting function of the feedback control loops in Neuro-synergy model.

Term $\boldsymbol{\zeta}_m$ a vector that consists of the integration of $\boldsymbol{\zeta}$ as follows:

$$\boldsymbol{\zeta}_m = \begin{bmatrix} \zeta_{m1} \\ \zeta_{m2} \end{bmatrix} = \begin{bmatrix} 0 & 0 \\ k_{m2} & 0 \end{bmatrix} \begin{bmatrix} \int \zeta_1 dt \\ 0 \end{bmatrix}, \tag{3.15}$$

where k_{m2} is the coefficient of the integrator in MRM-space that accumulates ζ_1 and outputs the integrated values. k_{m2} can change the level of learning in standing balance control. $k_{m2} = 0$ is defined as "without learning", and $k_{m2} > 0$ is defined as "with learning." $\boldsymbol{\zeta}_m$ adjusts the movement of the second mode, which it was selected based on visual inspection of the movement of all modes. Because any disturbance has a pronounced effect on joint 1, the torque of the second mode is adjusted based on the torque of joint 1.

The whole system can be expressed by combining Eqs. (3.5) and (3.8) as follows:

$$\boldsymbol{M}(\boldsymbol{\theta})\ddot{\boldsymbol{\theta}} + \boldsymbol{\omega}(\boldsymbol{\theta}, \dot{\boldsymbol{\theta}}) = \boldsymbol{T}\boldsymbol{A}\boldsymbol{T}^{-1}\Delta\boldsymbol{\theta} + \boldsymbol{T}\boldsymbol{B}\boldsymbol{T}^{-1}\Delta\dot{\boldsymbol{\theta}} + \boldsymbol{T}\boldsymbol{\zeta}_m + \boldsymbol{\zeta}. \tag{3.16}$$

Table 3.1: Stability changes due to different coefficients

Disturbance	Without learning $k_{m2} = 0.0$	With learning $k_{m2} = 5.0 \times 10^{-4}$
$170 \leq f \leq 184$ [N]	Stable	Stable
$185 \leq f \leq 204$ [N]	Fallen	Stable
$205 \leq f$ [N]	Fallen	Fallen

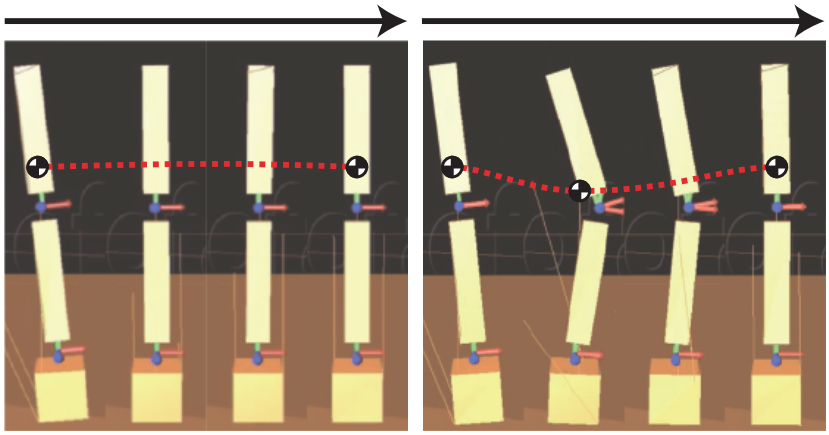

Fig. 3.4: Overview of standing balance control simulation: (a) without learning; (b) with learning. "Without learning" means that tacit learning is applied to only joint space, and "With learning" means that tacit learning is applied to joint space and MRM-space. The red dotted line is the general trajectory of the center of mass (CoM) of the pendulum in the process of regaining balance after a disturbance. The CoM falls lower while regaining balance with tacit learning in MRM-space.

3.3.3 Standing Balance Control Simulation and Results

The two mode vectors $\boldsymbol{v}_1, \boldsymbol{v}_2$ of the pendulum defined in Fig. 3.2 are given as

$$\boldsymbol{v}_1 = \begin{bmatrix} \text{-0.9} \\ \text{-0.3} \end{bmatrix}, \quad \boldsymbol{v}_2 = \begin{bmatrix} 0.3 \\ \text{-0.9} \end{bmatrix}. \tag{3.17}$$

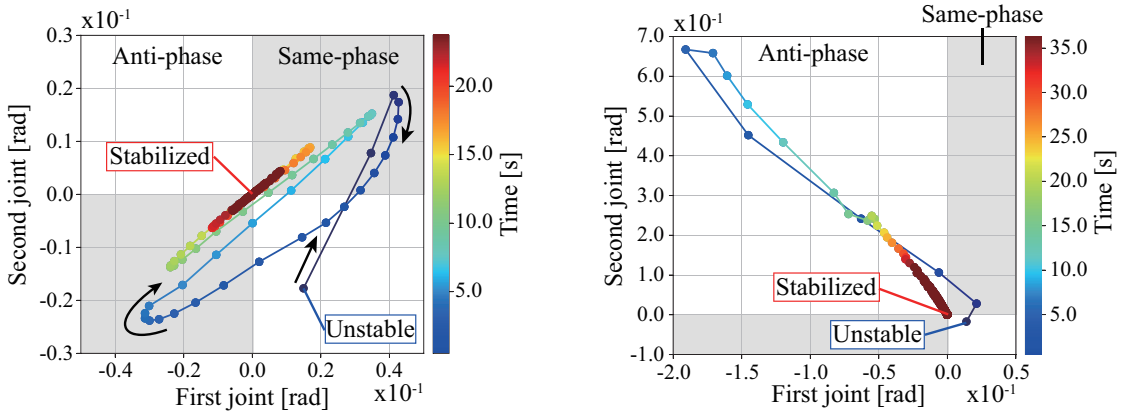

(a) Without learning (b) With learning

Fig. 3.5: Trajectories of joints 1 and 2 while regaining balance in the simulation: (a) without learning; (b) with learning. The gray areas are where the joints move in phase, the white areas are where they move in anti-phase. Joints 1 and 2 move in phase while regaining balance without tacit learning in MRM-space. Joints 1 and 2 move in anti-phase while regaining balance with tacit learning in MRM-space. The disturbance is $f = 184$ N. The gain of tacit learning in MRM-space is $k_{m2} = 5.0 \times 10^{-4}$.

As shown in Fig. 3.1(a)(b), the first mode $\boldsymbol{v}_1$ represents same-phase posture and the second mode $\boldsymbol{v}_2$ represents anti-phase posture. The transfer matrix $\boldsymbol{T}$ is

$$\boldsymbol{T} = \begin{bmatrix} -0.9 & 0.3 \\ -0.3 & -0.9 \end{bmatrix}. \tag{3.18}$$

Standing balance control simulations are conducted as follows.

1. The pendulum is placed upright on a board that can move horizontally.
2. The board is moved for 0.2 [s] with the disturbance f [N].
3. A simulation is ended once the height of the center of mass(CoM) of the pendulum falls below 0.2 [m] or the pendulum become upright.

simulations are conducted with each of $f = 170, \cdots, 210$ [N]. The gains are $k_{p1} = 22.0, k_{d1} = 21.0, k_{p2} = 22.0, k_{d2} = 21.0, k_1 = 1.0 \times 10^{-3}$, and $k_2 = 1.0 \times 10^{-3}$. The references are $\theta_{ref1} = \theta_{ref2} = 0.0$.

Table 3.1 gives the results of whether the pendulum falls down in the process of trying to maintain standing balance. The pendulum is clearly more stable with tacit learning in MRM-space than without tacit learning in MRM-space.

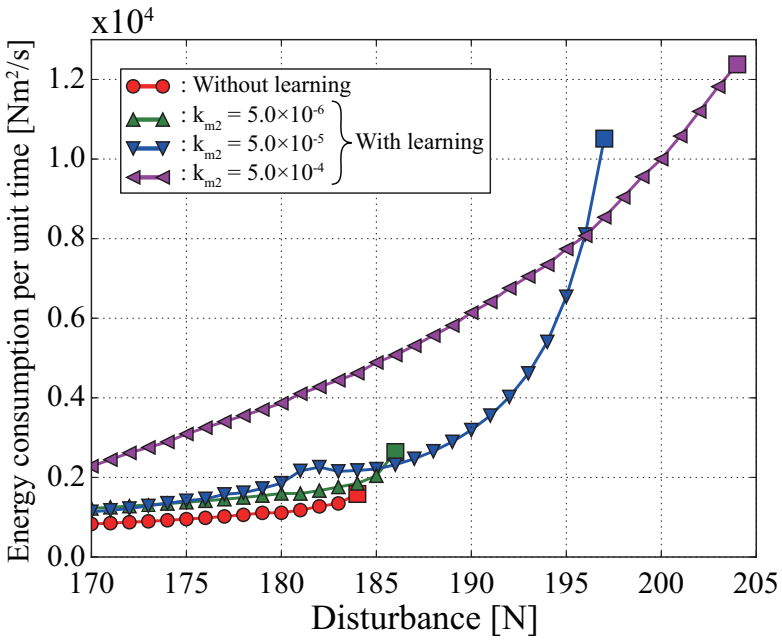

Fig. 3.6: Relationship between energy consumption per unit time and disturbance in the simulation. Each square represents the maximum disturbance for which the pendulum can become upright. For instance, the pendulum cannot become upright against a disturbance of 185 N or more without learning in MRM-space. Both the energy consumption per unit time and the stability against disturbance increase with the coefficient of tacit learning in MRM-space.

In this simulation, the motion of the pendulum is automatically generated by the feedback control loops of tacit learning in MRM-space. It means that the time taken for one control cycle is the time required for automatic motion generation. A computer we use has 3.7 GB memory and Intel® Core™ i5 CPU M550 @ 2.67 GHz×4, and python2.7 is installed. In this case, the mean value of the time required for automatic motion generation is calculated, and it is 1.7×10^{-2} [s]. This result is strongly related to the performance of the computer and how to write a program code, therefore the time will be fast if these bottle necks are improved.

Figure 3.4 shows an overview of standing balance control simulations without and with learning in MRM-space. The pendulum CoM falls lower in the process of regaining balance when tacit learning is applied in MRM-space. Figure 3.5 shows the trajectories of joints 1 and 2 in the process of regaining balance. Figure 3.5(a) shows the case without learning in MRM-space, and the pendulum becomes upright after the

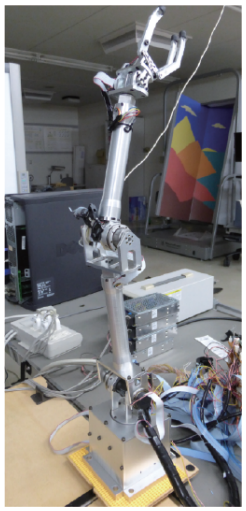

(a) Two DoF inverted pendulum.

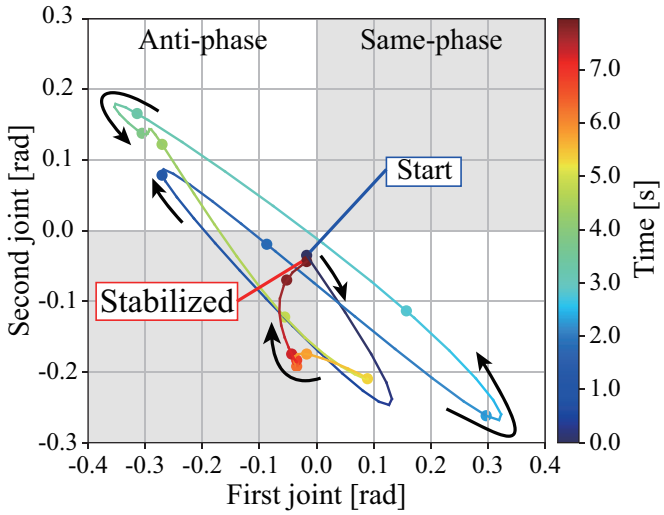

(b) Trajectories of joints 1 and 2 in the process of regaining balance in the experiment.

Fig. 3.7: (a) Two DoF inverted pendulum. (b) Trajectories of joints 1 and 2 in the process of regaining balance in the experiment. Each point is supplemented with a spline curve. The gray areas are where the joints move in phase, the white areas are where they move in anti-phase. Joints 1 and 2 move in anti-phase in the process of regaining balance, as in the simulation with tacit learning.

disturbance by moving joints 1 and 2 in phase. By contrast, Fig. 3.5(b) shows the case with learning in MRM-space, and joints 1 and 2 move in anti-phase.

Figure 3.6 shows the relationship between the disturbance and the energy consumption E per unit time, which is calculated from

$$E = \frac{1}{T}\sum_{t=0}^{T}({\tau_1}^2 + {\tau_2}^2), \tag{3.19}$$

where T is the time until the pendulum becomes upright. E is also calculated when the simulation is conducted with tacit learning in MRM-space by using different integral coefficients, namely $k_{m2} = 5.0 \times 10^{-6}$ and 5.0×10^{-5}.

The pendulum can become upright against a larger disturbance with learning in MRM-space than without learning in MRM-space. The size of disturbance that the pendulum can withstand without falling over increases with the integral coefficient k_{m2} for tacit learning. However, E also increases with k_{m2}.

(a) Ankle strategy (b) Hip strategy

Fig. 3.8: Standing balance control strategies of a person. (a) Ankle strategy: the person mainly moves the ankle joints and can balance against small disturbances only. (b) Hip strategy: the person moves the hip and ankle joints in anti-phase and can balance against larger disturbances. The participant of this figure gave informed consent to appear on the current work.

3.3.4 Standing Balance Control Experiment and Results

An experiment on a real two DoF inverted pendulum with the same block diagram as in the simulation was conducted. The transfer matrix was calculated based on the physical parameters of the pendulum, whereas the gains in the block diagram were determined by trial and error.

In this experiment, the mean value of the time required for automatic motion generation could not be calculated. After conducting the experiment and measuring the motion of the pendulum, the real two DoF inverted pendulum was broken. Therefore, the experiment could not be conducted for calculating the mean value of the time.

Figure 3.7(a) shows the actual two DoF inverted pendulum. Figure 3.7(b) shows the trajectories of joints 1 and 2 in the process of regaining balance. The pendulum becomes upright by moving joints 1 and 2 in anti-phase, as in the simulation with tacit learning in MRM-space.

3.3.5 Discussion of Standing Balance Control

The pendulum can remain upright against larger disturbances as the coefficient of tacit learning in MRM-space is increased (see Fig. 3.6). However, a problem is that the energy consumption per unit time in same disturbance also increases as the coefficient is increased. Another problem is that, although the stability of this system was not analyzed, too large an integral tacit learning coefficient makes the system unstable (see [123]). To regain balance efficiently after a disturbance, it is necessary to change the tacit learning coefficient according to the disturbance.

It is well-known that people change their standing balance strategies between ankle and hip strategies [124–126] according to the prevailing disturbances. Each strategy is shown in Fig. 3.8. The ankle strategy is a standing balance control method in which the person mainly moves the ankle joints in response to a relatively small disturbance, whereas the hip strategy is a standing balance control method in which the person moves the hip and ankle joints in anti-phase in response to a larger disturbance. The movements involved in the hip strategy are similar to those of the two DoF pendulum when tacit learning is applied in MRM-space. It is interesting that our method of adjusting signals in MRM-space with tacit learning has something in common with a human strategy.

3.4 Bipedal Walking Control on Flat Plane with 27 DoF Humanoid Robot

In Chapter 3.3, it was discussed that the validity of well designing the feedback control loop by using standing balance control of the two DoF pendulum against disturbances. In this chapter, a "top-down" signal is added to include intentional behavioral changes. The same control strategies are applied to a 27 DoF humanoid robot walking control with the added top-down signal. The weight and the length of segments of the robot is decided based on the Nasa biometric research [127]. It is shown through simulation and experiment that the signal added to the controller in MRM-space plays the role of behavioral intentions to change walking direction while maintaining walking balance.

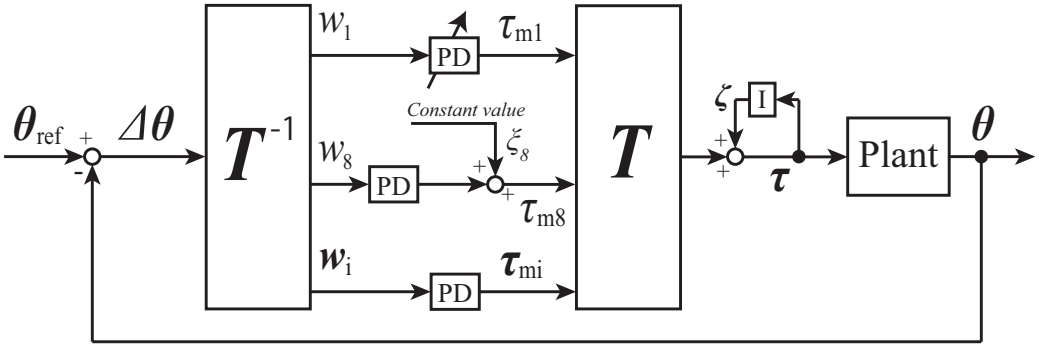

Fig. 3.9: Block diagram for bipedal walking control of 27 DoF robot; see Chapter 3.4.1 for details.

Table 3.2: Target set for bipedal walking control simulation

Step	Description	Target angle [rad] $\times 10^{-1}$	
		left leg	right leg
Step 0	Standing posture	-	-
Step 1	Balance on left leg	hip (−0.1)	hip (0.1)
Step 2	Right leg up	-	hip knee (−9.0) (9.0)
Step 3	Right leg down	-	hip knee (−4.5) (4.5)
Step 4	Balance on both leg	-	-
Step 5	Balance on right leg	hip (0.1)	hip (−0.1)
Step 6	Left leg up	hip knee (−9.0) (9.0)	-
Step 7	Left leg down	hip knee (−4.5) (4.5)	-
Step 8	Balance on both leg	-	-

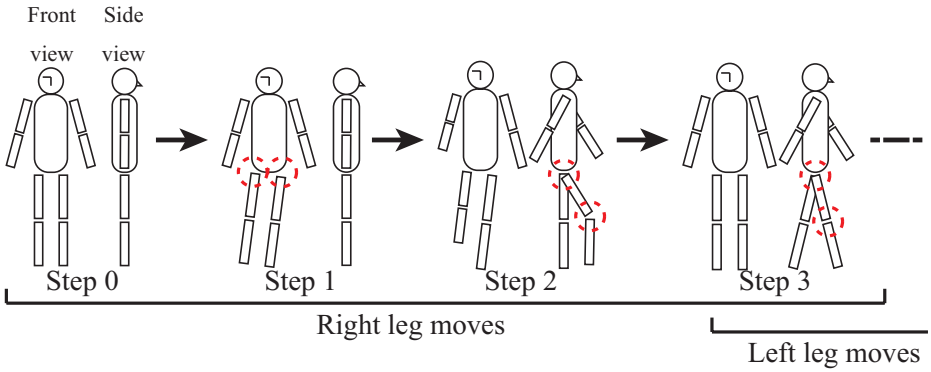

(a) Posture of each target set, for which the joints enclosed by dashed circles are controlled

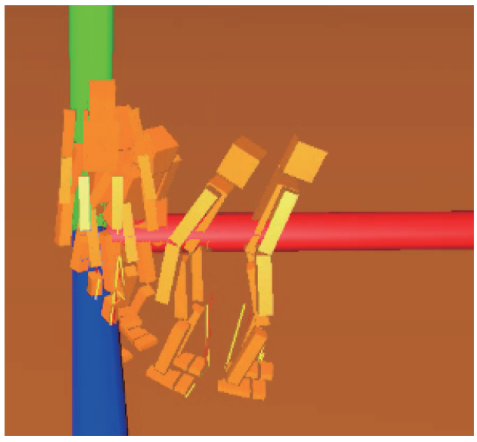

(b) Overview of walking simulation for adjusting the eighth mode

Fig. 3.10: (a) Posture of each target set, for which the joints enclosed by dashed circles are controlled. Steps 5–7 (not shown) are the bifrontally symmetric postures of steps 1–3. Steps 4 and 8 (not shown) involve waiting for a time while holding the posture of the corresponding previous target set. References for joints are given in Table 3.2. (b) Overview of walking simulation for adjusting the eighth mode. By adding positive constant values to the eighth mode, the robot can turn left.

3.4.1 Bipedal Walking Control Structure

Figure 3.9 shows a bipedal walking controller designed by using the transfer matrix $\boldsymbol{T}$ and tacit learning. Terms $\boldsymbol{\theta}$, $\dot{\boldsymbol{\theta}} \in \boldsymbol{R}^{27}$ are vectors of state variables. Terms $\boldsymbol{\theta}_{ref} \in \boldsymbol{R}^{27}$ is a vector of angle references. The torque vector $\boldsymbol{\tau} \in \boldsymbol{R}^{27}$ for each joint is represented

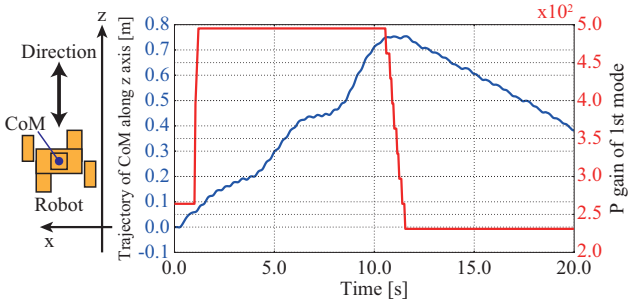

(a) Walking forward and backward

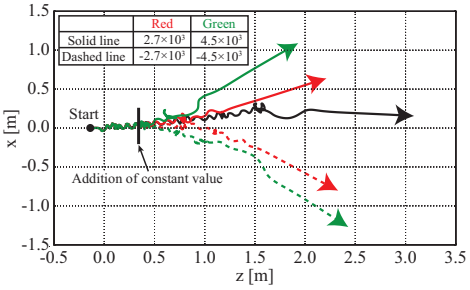

(b) Turning left and right

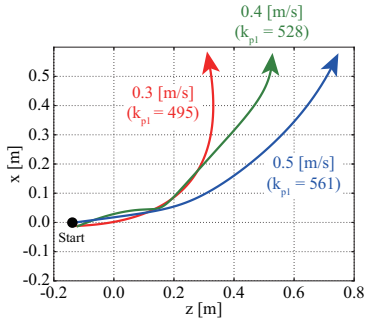

(c) Direction with different walking speed

Fig. 3.11: Trajectory and time series of CoM position in turning and walking forward and backward in simulation: (a) Time series of CoM position in the direction in which the robot walks and the P gain of the first mode in the simulation. In the early stage of walking, the P gain is set as $k_{p1} = 270.0$. The robot walks forward and backward according to changes in the P gain of the first mode. (b) Trajectories of robot CoM in walking simulation with adjusting the movement of the eighth mode. The robot walks from the left to the right of the figure. The black line is a trajectory of the robot walking forward without adjusting the movement of the eighth mode. The walking direction is changed depending on the constant value. The robot turns more as the constant value is increased. (c) Directions of robot CoM in turning with different walking velocities. Solid lines represent walking directions. The constant value is set as $\xi_8 = 4.5 \times 10^3$. Walking velocity can be changed in turning behavior with different P gain k_{p1}, and the walking direction is affected by walking velocity.

as

$$\boldsymbol{\tau} = \boldsymbol{T}\boldsymbol{A}\boldsymbol{T}^{-1}\Delta\boldsymbol{\theta} + \boldsymbol{T}\boldsymbol{B}\boldsymbol{T}^{-1}\Delta\dot{\boldsymbol{\theta}} + \boldsymbol{T}\boldsymbol{c} + \boldsymbol{\zeta}, \tag{3.20}$$

$$\boldsymbol{\tau} = \begin{bmatrix} \tau_1 & \cdots & \tau_{27} \end{bmatrix}^T, \tag{3.21}$$

$$\boldsymbol{\zeta} = diag(\begin{bmatrix} 0 & \cdots & k_{lankle} & k_{rankle} & \cdots & 0 \end{bmatrix}) \int \boldsymbol{\tau} dt, \tag{3.22}$$

where $\boldsymbol{\zeta}$ is a vector that consists of the integral values of tacit learning, and tacit learning is applied to joints of the legs. The balance in the sagittal plane is maintained

by tacit leaning, as in [81]. Terms k_{lankle} and k_{rankle} are the integral coefficients for the left and right ankle joints, respectively. Terms $\Delta\boldsymbol{\theta}$ and $\Delta\dot{\boldsymbol{\theta}}$ are

$$\Delta\boldsymbol{\theta} = \left[\begin{array}{c} \boldsymbol{\theta}_{ref} - \boldsymbol{\theta} \end{array} \right], \quad \Delta\dot{\boldsymbol{\theta}} = -\dot{\boldsymbol{\theta}}. \tag{3.23}$$

Terms $\boldsymbol{A}$ and $\boldsymbol{B}$ are diagonal matrices:

$$\boldsymbol{A} = diag(\left[\begin{array}{cccc} k_{p1} & k_{p2} & \cdots & k_{p27} \end{array} \right]), \tag{3.24}$$

$$\boldsymbol{B} = diag(\left[\begin{array}{cccc} k_{d1} & k_{d2} & \cdots & k_{d27} \end{array} \right]), \tag{3.25}$$

where $k_{p1}, \cdots, k_{p27}$ are values obtained by multiplying the eigenvalues of each mode by 10, and $k_{d1}, \cdots, k_{d27}$ are values obtained by multiplying the eigenvalues of each mode by 0.1. The eigenvalues are given by the mechanical resonance mode of the robot.

Term $\boldsymbol{c}$ is a vector that consists of the constant value of the torque of the eighth mode and is given by

$$\boldsymbol{c} = \left[\begin{array}{ccccc} 0 & \cdots & \xi_8 & \cdots & 0 \end{array} \right]^T, \tag{3.26}$$

where ξ_8 is a constant that can be adjusted manually.

The transfer matrix $\boldsymbol{T} \in \boldsymbol{R}^{27\times 27}$ of the 27 DoF robot can be calculated using the method given in Chapter 3.2. In controlling the robot behavior, two specific modes from all the modes are focused on, namely the first and eighth modes (see Figs. 3.1(c) and (d)). Two specific types of walking is expected to be achieved. Adjusting only the signal of the first mode while changing the P gain k_{p1} can make the robot change its walking velocity on a flat plane. Adjusting the signal of the eighth mode with the constant value $\boldsymbol{c}$ can make the robot turn left and right on a flat plane with fixing k_{p1} for the robot to walk forward.

3.4.2 Bipedal Walking Simulation and Results

Bipedal walking is performed as shown in Fig. 3.10(a), with one cycle of walking consisting of eight steps. The integral coefficients for the left and right ankle joints are $k_{lankle} = k_{rankle} = 1.0 \times 10^{-4}$. The references for each joint at each step in the simulation are described in Table 3.2. After finishing one cycle, the reference returns to the beginning of the cycle.

Each step shifts to the next step under specific conditions. When the robot raises a foot, that step shifts to the next step when a knee joint angle of the robot equals the reference of the knee joint angle. When the robot puts a foot down, that step shifts to the next step when the sole of the foot touches the ground. If the robot falls down while walking, the robot is moved to the initial position while holding the integral values of tacit learning.

In this simulation, the walking motion of the robot is changed by adjusting the coefficient values in MRM space in each trial, and the walking motion in response to adjusted values is automatically generated through the transfer matrix. In addition to that, the robot maintains the balance by the feedback control of tacit learning. Therefore, the time required for automatic motion generation is the time taken for one control cycle as same as the case of the pendulum. A computer we use has 3.7 GB memory and Intel® Core™ i5 CPU M550 @ 2.67 GHz×4, and python2.7 is installed. In this case, the mean value of the time required for automatic motion generation is 4.2×10^{-2} [s], and the time is almost same in each condition. This result is strongly related to the performance of the computer and how to write a program code, therefore the time will be fast if these bottle necks are improved.

(i) Walking forward and backward

Figure 3.11(a) shows time series of the CoM position in the direction in which the robot walks and the P gain k_{p1} used to adjust the movement of the first mode. In the early stage of walking, the P gain is set as $k_{p1} = 270.0$. It can be seen that the robot walks forward and backward according to the adjustment of the P gain.

(ii) Turning left and right

Figure 3.10(b) shows an overview of the walking simulation adjust the movement of the eighth mode by adding positive constant values to the signal of the eighth mode with an appropriate P gain k_{p1} to walk forward. The robot can be seen turning left.

Figure 3.11(b) shows the trajectories of the CoM of the robot from the top view;

Table 3.3: Target set for bipedal walking control experiment

Step	Description	Target angle [rad]	
		left leg	right leg
Step 0	Standing posture	-	-
Step 1	Balance on left leg	hip (-0.1×10^{-1})	hip (0.1×10^{-1})
Step 2	Right leg up	-	hip knee (-0.8) (1.0)
Step 3	Right leg down	-	hip knee (-0.4) (0.7)
Step 4	Balance on both leg	-	-
Step 5	Balance on right leg	hip (0.1×10^{-1})	hip (-0.1×10^{-1})
Step 6	Left leg up	hip knee (-0.8) (1.0)	-
Step 7	Left leg down	hip knee (-0.4) (0.7)	-
Step 8	Balance on both leg	-	-

the robot walks from the left of the figure to the right with the appropriate P gain k_{p1}. From Fig. 3.11(b), it can be seen that the walking direction is changed depending on the constant value used to adjust the movement of the eighth mode. The robot turns more as the constant value is increased.

Figure 3.11(c) shows the trajectories of the CoM of the robot from the top view; the robot walks from the left of the figure to the right with a fixed constant value $\xi_8 = 4.5 \times 10^3$. From Fig. 3.11(c), it can be seen that P gain k_{p1} is a key factor that affects the velocity in turning behaviors, and the walking direction is changed.

3.4.3 Bipedal Walking Experiment and Results

Not only simulations but also walking experiments were conducted by using an actual robot, namely the humanoid robot NAO made by Aldebaran. This has 25DoF, and the angle of each of its joints can be controlled. NAO is controlled by angle inputs rather than torque inputs. A control structure that generates reference joint angles was designed by using the transfer matrix $\boldsymbol{T}$.

The reference joint angle for a wide variety of walking can be described as

$$\boldsymbol{\phi}' = \boldsymbol{T}^{\dagger} \left[\begin{bmatrix} k_{p1} & & & 0 \\ & 1.0 & & \\ & & \ddots & \\ 0 & & & 1.0 \end{bmatrix} \boldsymbol{T}^{\dagger -1} \phi + \begin{bmatrix} 0.0 \\ \vdots \\ \alpha_8 \\ \vdots \\ 0.0 \end{bmatrix} \right] \tag{3.27}$$

$$if\ k_{p1} = 1.0\ and\ \alpha_8 = 0.0,\ \phi' = \phi,$$

where $\boldsymbol{\phi} \in \boldsymbol{R}^{25}$ is a vector that consists of joint-angle references for walking, and $\boldsymbol{\phi}' \in \boldsymbol{R}^{25}$ is an adjusted vector. Term $\boldsymbol{T}^{\dagger}$ is a transfer matrix modified from the transfer matrix $\boldsymbol{T}$ to fit the DoF of NAO. Term k_{p1} works like the P gain in the simulation of walking forward and backward. Term α_8 works like the constant value in the simulation of turning. Walking balance is acquired by applying tacit learning to joint space in the same way as two DoF inverted pendulum postural control.

Experiments are conducted using the same scheme as that shown in Fig. 3.10(a). The target joint angles at each step in the simulation are described in Table 3.3. Each step shifts to the next step under specific conditions. When NAO raises a foot, a step that raising the foot shifts to the next step in case that the knee joint angle of the robot equals the reference knee joint angle. When NAO puts a foot down, a step that putting the foot down shifts to the next step in case that the sole of the foot touches the ground.

In this experiment, a computer is used which has 4 GB memory and Intel® Core™ i3-4005U CPU @ 1.7 GHz, and C++ is installed. In this case, the mean value of the time required for automatic motion generation is 2.0 [s], and the time is almost same in

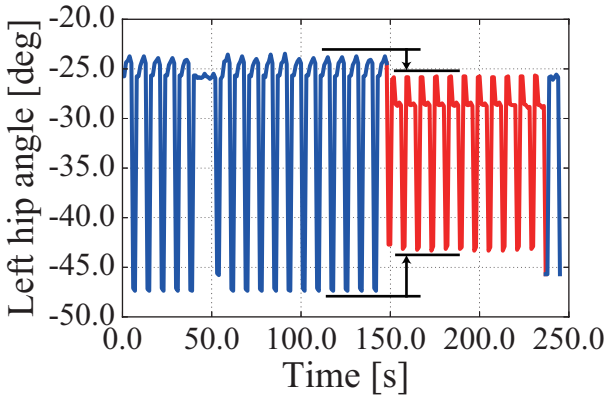

(a) Left hip angle

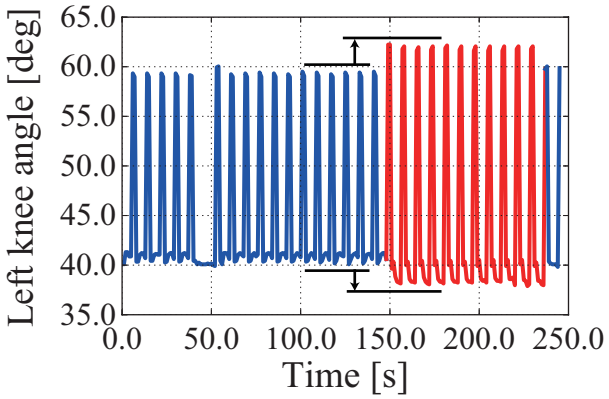

(b) Left knee angle

Fig. 3.12: Time series of left hip and left knee joint angles in an experiment involving walking forward and backward. The P gain k_{p1} for adjusting the movement of the first mode changes as follows: $k_{p1} = 1.0$ for 0.0–150.0 [s], $k_{p1} = 1.1$ for 150.0–240.0 s, and $k_{p1} = 1.0$ for 240.0–250.0 [s]. NAO walks forward for 0.0–150.0 [s] and backward for 150.0–240.0 [s]. When walking is switched from forward to backward by adjusting the movement of the first mode, the hip joint angle decreases and the knee joint angle increases.

each condition. This required time may be slow, but it is thought that wi-fi is used to communicate with NAO, and the conditions for transferring to the next leg movement are severe. This issue will be solved by using the computer having high-performance, a wired communication, and improving the programing code.

(i) Walking forward and backward

NAO can walk forward and backward when only the movement of the first mode is adjusted by changing its gain. Figure 3.12 shows time series of the left hip joint and left knee joint angles while walking forward and backward. When walking is switched from forward to backward by adjusting the movement of the first mode, the hip joint angle decreases and the knee joint angle increases (see around 150.0 [s] in Fig. 3.12).

(ii) Turning left and right

Figure 3.13(a) shows NAO turning left adjust the movement of the eighth mode by adding a positive constant value to the signal of the eighth mode with an appropriate P gain k_{p1} to walk forward. Figure 3.13(b)(c) shows the trajectories of the CoM and feet when the movement of the eighth mode is adjusted with positive and negative constant values. Figure 3.14 shows time series of the knee angles when NAO turns left and right.

NAO can turn left and right by adjusting the movement of the eighth mode, as in the simulation. As shown in Fig. 3.14(a), the amplitude of the left knee joint angle is bigger than that of the right knee joint angle in adjusting the movement of the eighth mode by the constant value $\alpha_8 = -25.0$, whereupon NAO turns left. The converse holds in Fig. 3.14(b).

3.4.4 Discussion of Bipedal Walking Control

The robot NAO could turn left and right by adjusting the movement of the eighth mode, that is, adjusting the bending of the robot and NAO at the waist on the frontal plane by adjusting the constant value. Adjusting the movement of the eighth mode deflected the CoM to the left-hand or right-hand side of the body, whereupon one foot took a larger step than did the other foot. This phenomenon can be confirmed from the fact that the amplitude of the left knee joint angle was bigger than that of the right knee joint angle (see Fig. 3.14(a)).

The robot and NAO could walk forward and backward by adjusting the movement

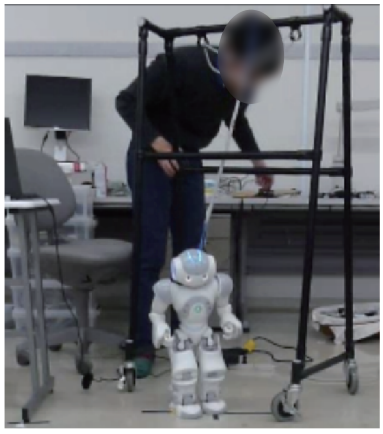

(a) Overview of walking experiment with NAO

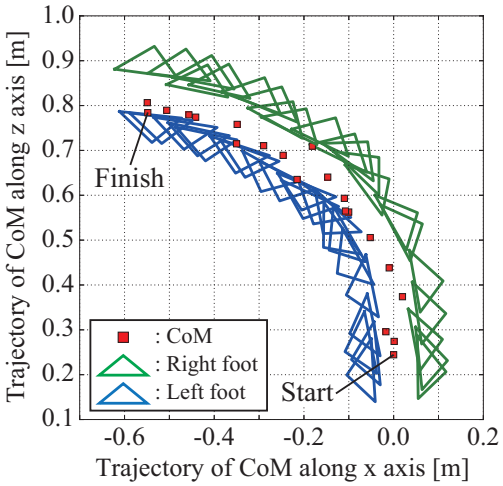

(b) Turning left.

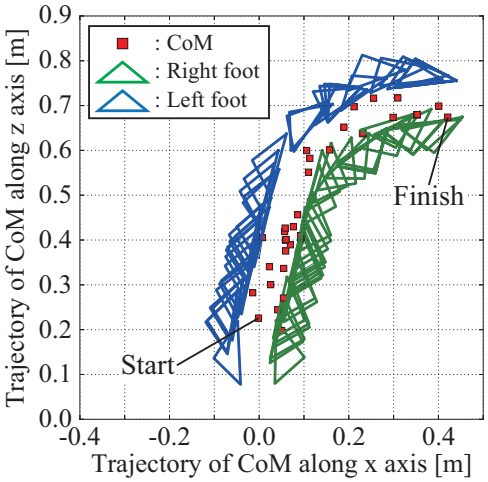

(c) Turning right

Fig. 3.13: Overview of walking experiment with NAO, and CoM and foot trajectories when NAO turns left and right in the experiment. (a) Overview of walking experiment with NAO. (b) Turning left: NAO can turn left when the constant value α_8 for adjusting the movement of the eighth mode is positive. (c) Turning right: NAO can turn right when the constant value α_8 for adjusting the movement of the eighth mode is negative. The participant of this figure gave informed consent to appear on the current work.

of the first mode. The robot and NAO differed in how the gain was adjusted, but we consider this to be because the gains of the other modes differed between the robot and NAO. When the movement of the first mode is adjusted, the degree to which the legs are opened is adjusted, whereupon the position at which the foot touches the ground

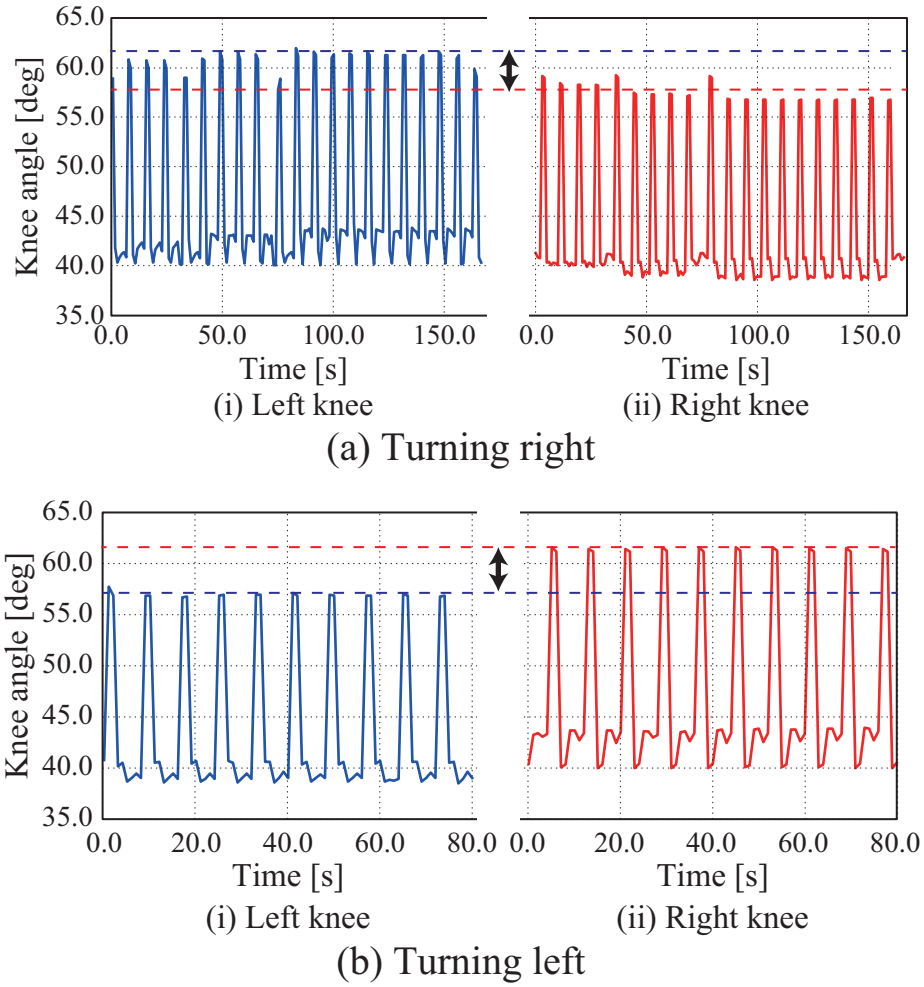

Fig. 3.14: Time series of knee joint angle in turning experiment: (a) turning right; (b) turning left. When NAO turns right, the amplitude of the left knee joint angle is bigger than that of the right knee joint angle in adjusting the movement of the eighth mode by the constant value $\alpha_8 = -25.0$. When the constant value is negative, NAO turns left.

can be adjusted. This can be confirmed from the fact that the hip joint angle decreases and the knee joint angle increases when walking switches from forward to backward (see Fig. 3.12).

It is normally difficult to make a robot walk in a wide variety of ways because that necessitates designing a plurality of controllers and preparing references concerning each combination of individual joints. Instead, our method realizes turning and walking forward and backward smoothly by adjusting a few parameters in MRM-space without

having to care about each combination of 27 joints and switching controllers. This is because there is a pattern of movements according to the mode, and the pattern to adjust is easy to understand visually.

A person can change behavior while caring intentionally only about "turn left and right" or "forward and backward." Likewise, our method can adjust signals and realize behavior without caring about each joint, which is important in considering human-like movement in the robot under consideration.

3.5 Discussion

In this study, it was reasoned that the key problem in developing a controller with mechanisms generating automatic motor commands from the symbolized action purpose would be realizing bio-mimetic adaptation with two-way action adaptation. The first way is selecting the appropriate behavior that progresses in a top-down manner, and the second is adjusting the behavior according to the environment, which is a bottom-up process that progresses through body–environment interactions.

In the preliminary study, it was discussed that the standing balance control of a two DoF inverted pendulum to introduce our control strategies, focusing only on the bottom-up adaptation process. The simulation and experimental results showed that the standing balance control capability was increased when the two DoF inverted pendulum was controlled using MRM-space, suggesting that the simple adaptation mechanism is enough to improve the action performance of standing balance when behavior control is conducted in a space where the direction of behavior can be set by adjusting to the change of the disturbance. The similarities between the mechanical resonance modes used in this system and the hip and ankle motion strategies of people must be another indication of the importance of reacting to a wide range of disturbances in a space in which the body parameters are well represented.

In the bipedal walking study using NAO, two-way adaptation was discussed. In the simulation and the experiments, it was succeeded that changing the behavior to turn left/right and go forward/backward by stimulating different mechanical resonance modes.

It is considered that the signals added to the specified mode control can be treated as generating the action from symbolized action purpose in our study from the viewpoint of generating high-dimensional joint movements from the low-dimensional signals. The detailed commands to the joint control were created in two processes, namely, transferring the control signal from MRM-space to joint space, and tacit learning for maintaining walking balance while reacting to environmental inputs. Therefore, these results suggest that one-dimensional signal change can create the complicated combinations of the 25DoF of NAO required to change the behavior when the appropriate mode is stimulated.

Joint control is much more complicated in people than it is in robots because complicated combinations of muscles are required in the former. The notion of muscle synergy introduced in Chapter 1.1 shares the same features as those of the mechanical resonance mode used in our method for robot control because the muscle-synergy space represents the action features of body mechanisms and contributes to adjusting behavior in our case by using lower-dimensional signals.

These results and discussion suggest that transferring the signals to the appropriate control space is the key process for reducing the complexity of the signals from the environment. In addition to that, by using tacit learning as the feedback control loops, the feedback control loops can work as the adjustment function without the action phase and the learning phase, realizing the action generation with the interaction between the robot and the environment. Discussing muscle synergy in a human controller and the mechanical resonance mode is only one step to the final output. If such steps were to be more accumulated to form a larger network as Neuro-synergy model, various behaviors could be formed from the more-symbolized action target such as “Go to the station”.

3.6 Conclusion

As discussed in Chapter 3.1, the aim of this research was to clarify the mechanisms of automatically generating motor commands from the symbolized action purpose, that is, generating each joint movement from the low-dimensional signals. Our approach

was to develop an artificial controller that embodies those mechanisms and derive the important features of that function to assess the extent to which the robot behavior is human-like.

The artificial controller was designed by using the mechanical resonance mode and tacit learning and applied it to the standing balance control of the two DoF inverted pendulum as a preliminary study. In our control strategy, the control signals to each joint are transferred to another space computed by using the mechanical resonance modes, whereby it can be easily understood that the action pattern created from each control signal. Tacit learning was applied in MRM-space and developed the controller to maintain standing against various levels of disturbance. The simulation results showed that as the coefficient value increased, the two DoF inverted pendulum could withstand huge disturbance, and the experimental results showed that the actual two DoF inverted pendulum could also get withstand huge disturbance when applying tacit learning in MRM-space. On the other hand, it was showed that the energy consumption per unit time became large as the coefficient value increases. This result indicates that by switching the controllers in response to the disturbance, the control making the standing balance capability and the energy efficiency will be possible.

The controller designed by the mechanical resonance mode and tacit learning was applied to walking control of 27 DoF humanoid robot and NAO and conducted walking simulation and experiment. In the simulation and experiment, it was focused on not only the bottom-up adaptation process but also the top-down process that is related to the symbolized action purpose. To represent the top-down process, the appropriate resonance mode was chosen to adjust the behavior to the desired one. When adjusting the coefficient value of the first mode, the robot changed the walking velocity to walk forward and backward with maintaining walking balance. When adjusting the parameter of the eighth mode, the robot turned left and right with maintaining walking balance. These adjustments were strongly related to the top-down process from the viewpoint of adjusting low diverse signals in high diverse integrated signals. Walking balance was maintained by tacit learning applying the method in [81] to joint space in the same way as the two DoF inverted pendulum control as the bottom-up process.

By designing the artificial controller based on Neuro-synergy model, it was achieved

that a motion control changing motions by adjusting a few parameters in the higher layer without caring the state of the lower layer. However, the bottom-up adaptation process cannot deal with all environmental changes, and living things is consider to adapt the environmental changes by adjusting or learning in the higher layer. Therefore, it is important to design a learning method in higher layer well so that the learning methods in the higher layer and the lower layer cooperate each other.

Chapter 4

Grasp-training Robot to Activate Feedback Control Loop for Reflex and Experimental Verification

4.1 Purpose in chapter 4

From this chapter, the motion support method to enhance the human motion is aimed to be developed. Especially, target subjects getting the support are post-stroke patients in this study, because the post-stroke patient will greatly improve their quality of life through the support.

The post-stroke patient is the patient who cannot make the voluntary actions. The previous robotic research suggested that the combination of the feedback control loops and the symbolized action purpose is a key factor to generation the action. However, the patients have a damage in the part of a primary motor cortex and cannot generate the detailed control signals from symbolized action purpose even though they think "Grasp" or "Walk". This means that the top-down process does not works well, and the signal from the top cannot reach the muscles properly, therefore the patients cannot generate the action.

In order for the patients to recover from a motion paralysis, they need to conduct a rehabilitation training with an external physical support from a therapist. The reason

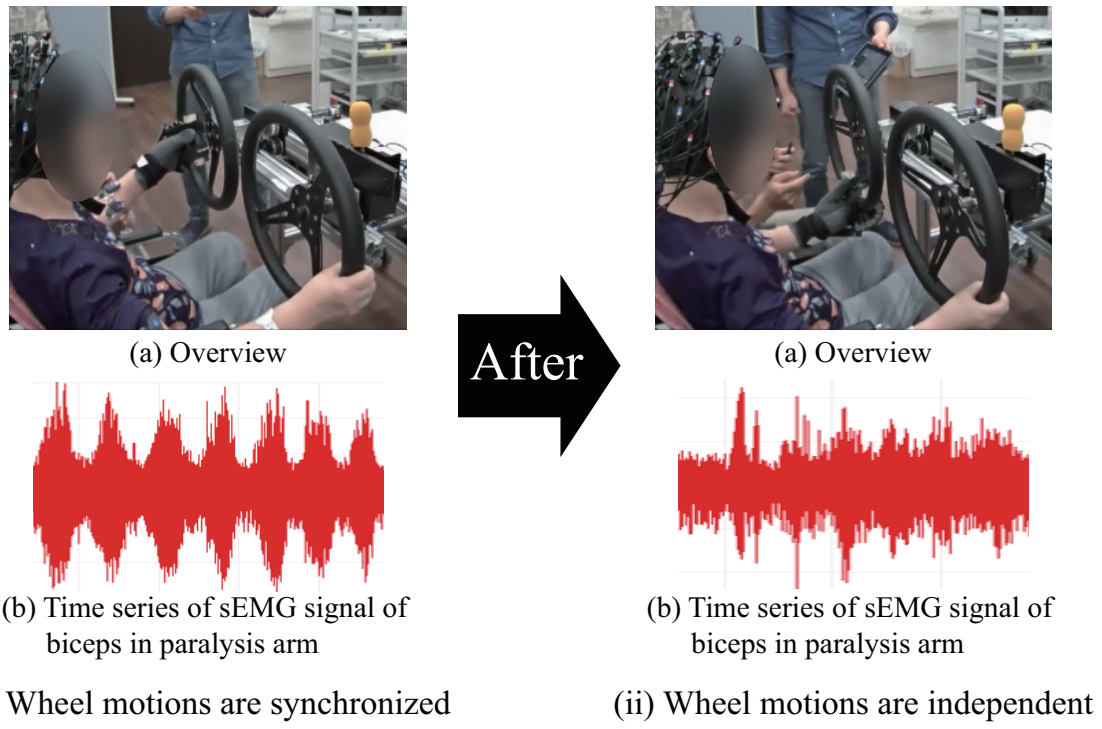

Fig. 4.1: Effect of interpreting the feedback control loops on muscle activities of the post-stroke patient by using a dual-wheel rehabilitation system. (i) Motion of wheels are synchronized. The post-stroke patient in this figure has a healthy right arm and a completely paralysis left arm. A left hand of the patient is fixed on a left wheel, and when the patient moves a right wheel by her hand, the left arm is moved due to the wheels are connected. By activating the feedback control loops using this system, a completely paralyzed biceps could be activated(Fig. 4.1(i)(b)). (ii) Motion of wheels is independent. After an experiment of (i), the patient could create the muscle activity in paralyzed biceps muscle by him/herself in a few seconds(Fig. 4.1(ii)(b)).

why the patient recovers from the paralysis is considered that the training encourages a brain plasticity among a sensory area, a part surrounding damaged motor area, and a part playing the role of the intention by the training. The brain plasticity is getting higher when these three activities are occurred at the same time: muscles outputting sensory signals after muscle activities, the patient intentionally trying to move the paralysis part, and the part surrounding damaged motor area activating by chance. Especially, the rehabilitation aiming the recovery by encouraging the brain plasticity is called as neuro-rehabilitation.

However, by only moving the body by an external physical support, the sensory signals from the muscles are so weak than when human beings intentionally activate

the muscles. There are methods to increase the activation in the sensory area, for instance, inducing muscle activities by electrical stimulation or by Transcranial Magnetic Stimulation(TMS) in the motor area. However, these methods cannot induce specific action, so there may be a doubt that un-functional neural network is formed by these methods.

From the view point of a scheme of Neuro-synergy model in the patients, it is considered that the feedback control loops of lower layers does not get the damage. If the feedback control loops can be intervened to promote the action by an external physical support, it will lead to better neuro-rehabilitation. It can be thought that the un-functional neural network may not be formed by activating the muscles with the intervention to original feedback control loops. Based on Neuro-synergy model, the support method of neuro-rehabilitation is studied to promote the motion of the post-stroke patient and leading the recovery from the motion paralysis by intervening in the feedback control loops.

Neuro-synergy model has not only simple feedback control loop but also complex loops such as including the cerebellum or the cortex in feedback control loops. The simple feedback control loops, for instance, provide reflex motions such as a stretch reflex. Some rehabilitation methods use the reflex motion in the rehabilitation training. Kawahira method [128] and Bobath approach are rehabilitation methods using activating the feedback control loops such as reflex loops. In Kawahira method, the therapist aims to recover the function of the patient's finger extension by they quickly flexing the patient's finger to induce a stretch reflex with synchronized with the patient's intention to extend. In Bobath approach, the therapists stimulate muscle spindles and touch the skin to activate the feedback control loops. These approaches show that the synchronization of activating the motion intention and the feedback control loops is important to promote the connection of an appropriate neural network among the sensory area, the part playing the role of the intention, and the motor area to bypass the damaged motor area.

The effect of intervening the complex feedback control loops on promoting the patients' motion is shown by using an on-going research in our laboratory. This study is conducted based on self-support phenomenon. Self-support phenomenon was discov-

ered by our laboratory. It is that surface electromyography(sEMG) could be measured in the paralysis arm when the patient conducted an elbow bending of the paralysis arm by using a healthy arm. By measuring a brain activity in that exercise by using NIRS, it was confirmed that area around the damaged motor area more activated than the paralysis arm was supported the others. It shows the control loops including more upper neural system is activated.

Figure 4.1 shows a dual-wheel rehabilitation system designed based on self-support phenomenon to promote the motion of the paralysis arm. The motion of the wheels can be chosen to be synchronized or be independent, and the patient move the paralysis arm connected to the wheel by moving the other wheel with the healthy arm when the motions of the wheels are synchronized. Figure 4.1(i)(b) shows the time series of sEMG of the biceps muscle in the paralysis arm, suggesting that the muscles in the paralysis arm could activate as same as self-support phenomenon. After this experiment, we made the wheels moving independently, but the patient could create a little muscle activity in paralyzed biceps muscle by him/herself in a few seconds. Figure 4.1(ii)(b)) shows that result, suggesting that the support method based on patient's own motion contributes to the intervention in the complex feedback control loops in more complex motion.

In this chapter, as a first step of realization of neuro-rehabilitation method based on Neuro-synergy model, a rehabilitation robot promoting the patients' motion is developed by intervening in the simple feedback control loop. Robotic rehabilitation is now recognized as an important approach for effective recovery from motion paralysis. Robots such as the reach-training robots InMotion ARM [129] [130] and ReoGo [131] [132] and the exoskeleton robot HAL [133] [134] have been developed and used in clinical practice, leading to effective recovery.

One of the most important aims of robotic rehabilitation is grasp training, in which it is difficult for therapists to support patients in making precise and repetitive movements. To date, several types of robot have been proposed for supporting grasp training [135–143]. The power-assisted hand designed by LAP Co., Ltd. [135] is a "glove-type" robot controlled by air pressure for grasp therapy. This robot automatically supports the extension and flexion of the fingers. The Hand of Hope system

designed by Rehab-Robotics Co. [136] is an exoskeleton robot that is controlled by linear actuators using sEMG signals from the user. HEXORR designed by Schabowsky et al. [137] is an exoskeleton robot controlled by two motors. It can compensate for gravity in finger movements and can provide assistive forces according to the finger movements of its wearer. The Exo-Glove PM device [138] is an exoskeleton robot made of polymer and controlled by air pressure. This robot is fixed by polymer belts to the distal phalanges and palm of its wearer. It is created by three-dimensional printing and can be adapted to individual hands.

Many grasp-training robots move their user's fingers in response to his or her motion intentions as decoded from motion triggers or sEMG or electroencephalogram (EEG) signals, for instance. However, the mechanical motion supported by a grasping-training robot is not enough to promote neural activity in the feedback control loops.

In this chapter, therefore, a grasping-training robot is proposed which can stimulate the feedback control loops. In addition to the function for stimulating the feedback control loops, it is aimed to develop a grasping-training robot that is suitable for use in clinical practice in relation to its usability and wearability.

In Chapter 4.2, the problems with using conventional grasping-training robots in clinical practice are listed, and a grasping-training robot with the ability to stimulate the feedback control loops is proposed. In Chapter 4.3, experimental results from healthy subjects are used to show that a finger extension/flexion mechanism can move the subject's fingers in the same way that a therapist can. In Chapter 4.4, experimental results from clinical tests are used to show that the proposed robot can activate reflex motion in the paralyzed hand of a post-stroke patient. sEMG signals were detected from the patient's arm only when reflex motion was stimulated by our robot. In Chapter 4.5, it is concluded by summarizing our experimental results and describing future work toward the use of our robot in clinical practice.

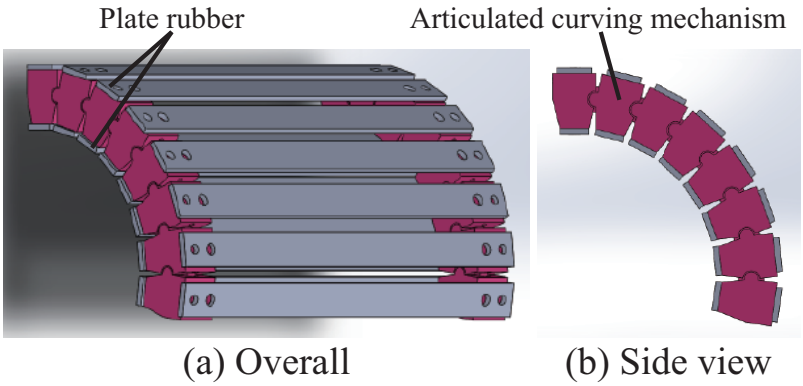

Fig. 4.2: Design of device to move fingers: (a) overall; (b) side view. This device is referred to herein as a "four-finger glove". The side of the four-finger glove consists of two articulated curving mechanisms (red), and the top and bottom consist of 16 rubber plates (gray). To use the four-finger glove, the user inserts his or her hand between the rubber plates.

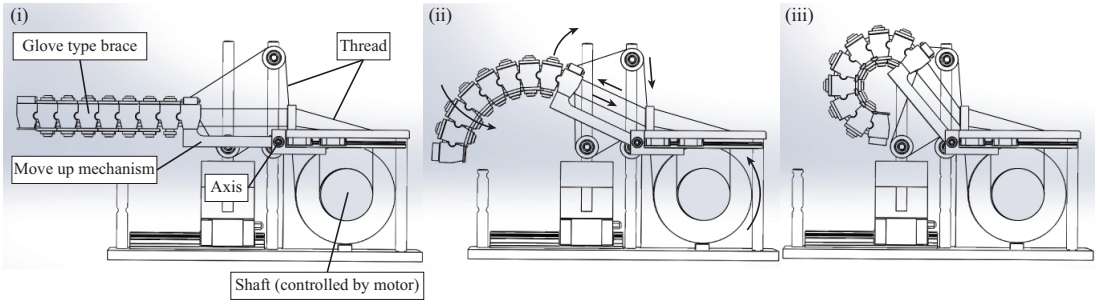

Fig. 4.3: Design of device to move wrist. This device is referred to herein as a "bascule bridge mechanism". This mechanism has single link and axis. The four-finger glove is set on the edge of the mechanism. (i) Initial position. (ii) When the threads are pulled by the rotation of the shaft, the mechanism is pulled up, and at the same time, the four-finger glove is flexed. (iii) At finishing the rotation of the shaft, the extension of the mechanism and the flexion of the glove is accomplished.

4.2 Grasping-training Robot

4.2.1 Problems with Conventional Grasping Robots in Clinical Practice

Human beings can grasp objects with just taking care of the motor intention "Grasp" and the finger tips. However, careful observation shows that wrist extension and thumb opposition are also conducted at the same time. This can be said to be due to the

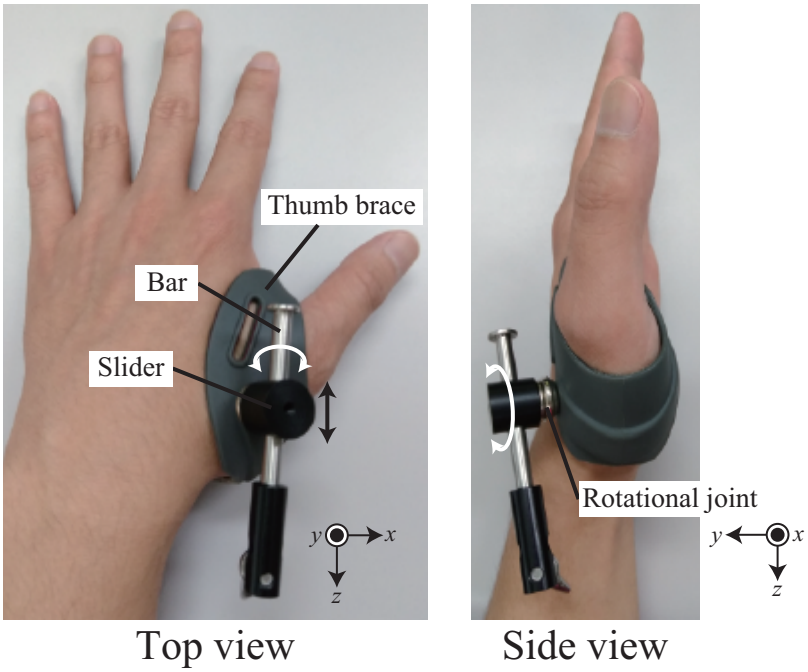

Fig. 4.4: Design of device to move thumb: This device is referred to herein as a "thumb fixer". The thumb fixer consists of a thumb brace, a bar, and a rotational joint. By extending the wrist with setting the thumb fixer on the robot, the thumb will oppose with restraining the bone of the thumb on a flat surface. Two rotational joints and one slider works to absorb changes in position and angle of the thumb during the thumb opposition.

work of the feedback control loops. However, current grasping-training robots do not pay attention to the wrist extension and the thumb opposition, and those robots fix the wrist and the thumb during grasping training.

There is a mechanical constraint called tenodesis action in human being, which is a phenomenon that the muscles of the fingers are pulled by the wrist extension, and the fingers are flexed naturally. It can be considered that human being uses the tenodesis action for easy to grasp. The feedback control loops are tried to be intervened by supporting the tenodesis action and thumb opposition from the outside.

In addition to that, a grasping reflex is used, in this research, for activating the feedback control loops from the neural system side. The grasping reflex is one of primitive reflexes, and the grasping motion is induced by stimulating the palm of hand. It is considered that high rehabilitation effect can be obtained by inducing the grasping reflex after making easy state of grasping by supporting the tenodesis action

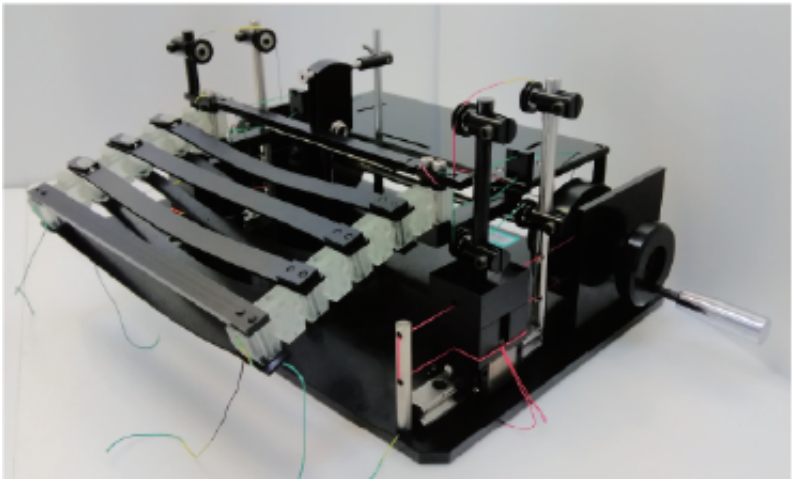

Fig. 4.5: Design of grasp-training robot: This robot consists mainly of the four-finger glove, the bascule bridge mechanism, the thumb fixer, a wrist rest, an actuator, and a shaft. In use, the subject puts his/her wrist on the wrist rest, inserts the fingers into the four-finger glove, and sets the thumb fixer on the wrist rest. This robot is controlled by one motor. The four-finger glove is extended and bent, the bascule bridge mechanism is down and up, and the thumb fixer with the thumb is opened and opposed by the rotation of the shaft controlled by the motor.

and the thumb opposition.

The most important step in recovering from grasping paralysis is the intentional initiation of movement, thereby overcoming complete paralysis. For the early stage of training to recover intentional motion, to move the fingers separately is considered unnecessary. Rather than using such complicated motion support in clinical practice, it is better to have a device in which it is easy to place completely paralyzed fingers and that requires little training time. Also, robots that are complicated to control are not suitable in clinical practice because of the lack of highly skilled engineers.

Based on these discussions and the mechanism for stimulating the grasping reflex, a grasping-training robot is proposed with the following features:

1. The glove-type device illustrated in Fig. 4.2, into which all the fingers except the thumb are inserted together and moved at the same time.

2. The bascule bridge mechanism in Fig. 4.3, which the glove-type device is moved up.

3. The thumb fixer in Fig. 4.4, which has the brace part and the rod part.

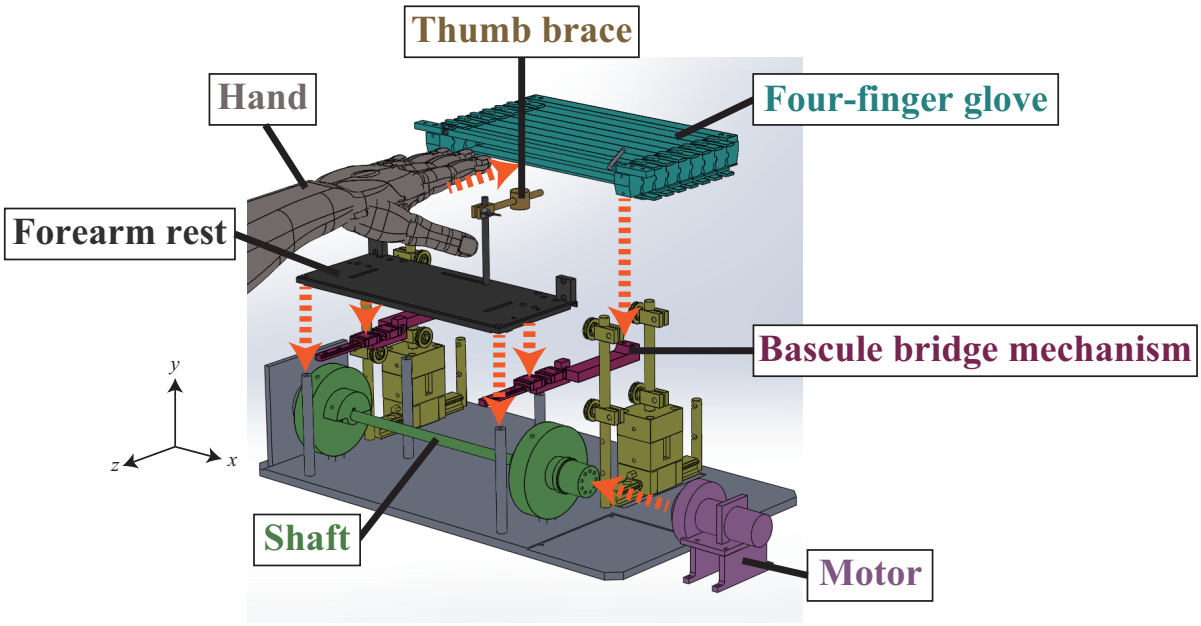

Fig. 4.6: Connection among the parts of the robot. The four-finger glove is attached to the bascule bridge mechanism. The bascule bridge mechanism is attached on the wrist rest. The thumb fixer is attached on the wrist rest. The motor is attached to the shaft. Four threads are passed through the four-finger glove, and the other four threads are attached on the edge of the bascule bridge mechanism. The threads are fixed on the shaft.

4. One motor is used to help extend and bend the fingers.

5. The grasping reflex is stimulated by grasping a bar set on the robot.

4.2.2 Mechanism of Proposed Robot

In this chapter, a robot mechanism is shown, which was designed taking the aforementioned problems into account. Figure 4.5 shows an overview of the proposed robot, which consists of a four-finger glove, the bascule bridge mechanism, and the thumb fixer. Figure 4.6 shows the connection of each part. The four-finger glove and the bascule bridge mechanism are driven by threads attached to a shaft. The threads made by ultra-high molecular weight polyethylene is used in this research, and Young's modulus of this thread is 79 [GPa].

The four-finger glove consists of an articulated curving mechanism to which are attached upper and lower rubber plates as illustrated Fig. 4.2. Young's modulus of

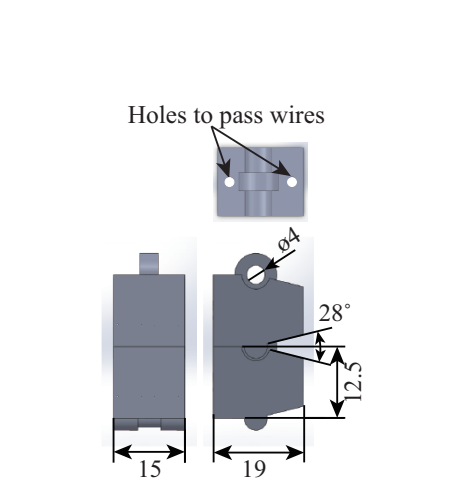

(a) Design of articulated curving mechanism of two segments

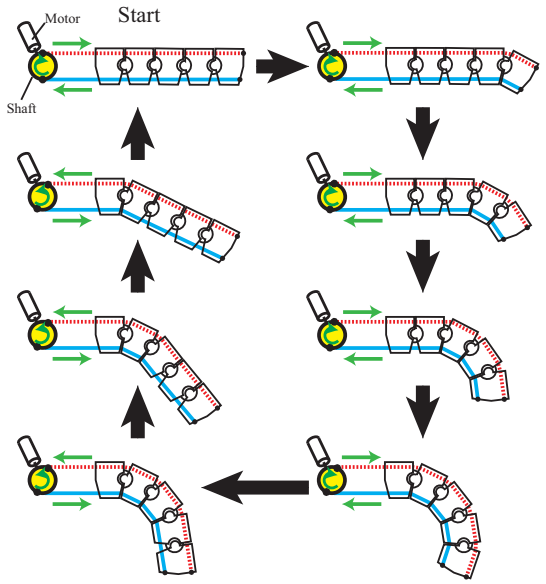

(b) Mechanism of articulated curving mechanism of five segments

Fig. 4.7: Articulated curving mechanism and movement: (a) size of a segment of the curving mechanism; (b) movement of a five-segment mechanism. When the bottom thread is pulled, bending begins from the distal segment to the proximal segment. By fixing threads to the shaft, the rotation of the segments can be controlled by one action.

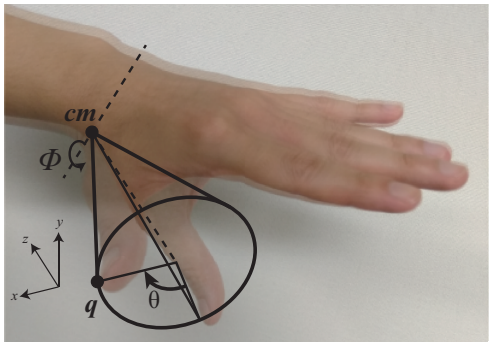

(i) Motion of thumb opposition

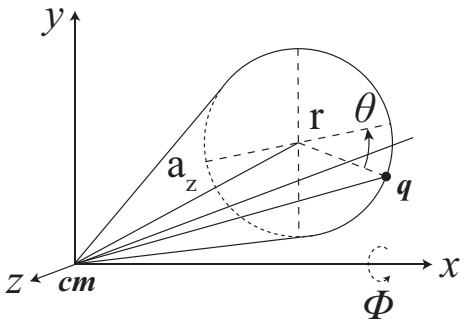

(ii) Cone model

Fig. 4.8: Cone model of thumb opposition motion: (a) motion of thumb opposition. a thumb bone moves on the side surface of a cone shape with a carpometacarpal joint(cm joint) of the thumb as an apex. (b) cone model of thumb opposition motion. $\boldsymbol{q}$ is the point on the bone of the thumb. r is a radius of bottom of cone shape, a_z is a distance from apex to bottom. θ represents the rotation of the thumb opposition. ϕ represents the rotation of the wrist movement.

the rubber is 12.7 [MPa]. Each segment of the curving mechanism has two holes in it and is connected to the next segment by a rotational joint (see Fig. 4.7(a)). The angle between the segments, namely 28°, was determined by trial and error according to the

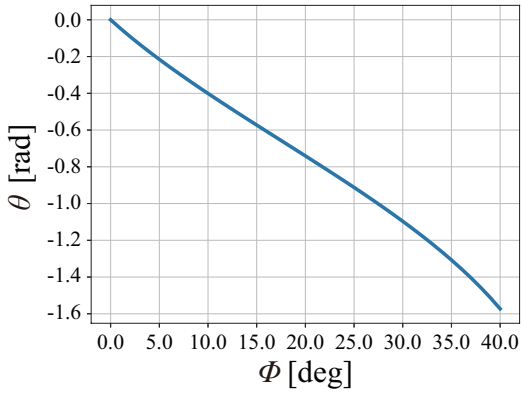

Fig. 4.9: Example of the relationship of the thumb opposition θ and the wrist movement ϕ. When substituting an appropriate value for r and a_z, in this case $r = 1$ and $a_z = 1$, and changing ϕ from 0 to 40 degrees, there is a trend that θ changes from zero to negative value like Fig. 4.9. As you can see Fig. 4.8, the positive value of ϕ represents the wrist extension, and the negative value of ϕ represents the thumb opposition.

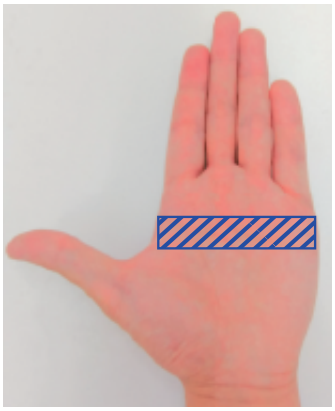

Fig. 4.10: Region for stimulating grasping reflex. Pushing a bar on a paralyzed hand can improve grasping by activating the grasping reflex. The grasping reflex is aimed to be induced by locating the bar on this region.

support motions discussed in the next chapters. The sizes of the other parts of the four-finger glove were determined with reference to the average hand size summarized in Table 4.1.

The threads pass through the curving mechanism as illustrated in Fig. 4.7(b). When the thread of the bottom side in Fig. 4.7(b) is pulled, the mechanism starts to bend from end to end. When the upper side thread is pulled, the mechanism straightens out again.

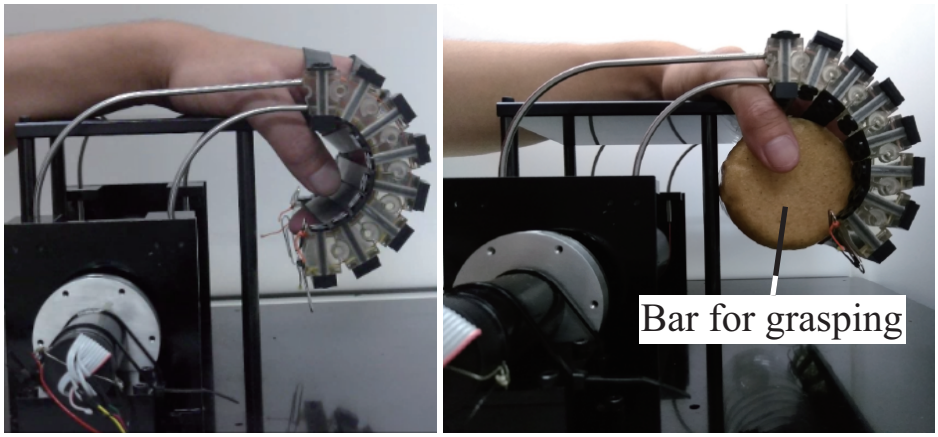

(a) Without bar (b) With bar

Fig. 4.11: Location of elastic bar: (a) without bar; (b) with bar. The bar (brown) for grasping is attached under the hand rest so that the inside diameter of the four-finger-glove can contact the bar. The bar applies stimulation to the fingers.

The bascule bridge mechanism consists of simple one link. One segment can be rotated around one joint, the other segment is connected on the wrist rest. The threads are connected on the edge of rotatable segment, and the amount of rotation can be adjusted by pulling the amount of the threads.

The four-finger glove is set on the bascule bridge mechanism, and the threads are connected to the shaft in Fig. 4.6. A DC motor is used to rotate the shaft in opposite directions, causing the four-finger glove to either extend or flex and the bascule bridge mechanism to either down or up. Figure 4.3 shows a motion of the four-finger glove and the bascule bridge mechanism when the threads are pulled by the rotation of the shaft.

The four-finger glove and the bascule bridge mechanism have simple mechanisms, on the other hand, since the mechanism of the thumb is complicated, a robot mechanism will become complicated to oppose the thumb by external force. The thumb opposition is tried to be modeled, and the support method is considered based on the model. Figure 4.8(i) shows the motion of the thumb opposition, suggesting that a thumb bone moves on the side surface of a cone shape with a carpometacarpal joint of the thumb as an apex. The thumb opposition can be modeled with the cone shape like Fig. 4.8(ii).

A point $\boldsymbol{q}$ represents a point on the bone of the thumb. The point $\boldsymbol{q}$ is written by using rotation matrices as follows:

$$\boldsymbol{q} = \begin{bmatrix} q_x & q_y & q_z \end{bmatrix}^T = \boldsymbol{R}_x(\phi)\boldsymbol{R}_z(\theta)\boldsymbol{s}_q, \tag{4.1}$$

$$\boldsymbol{q}_s = \begin{bmatrix} r & 0 & -a_z \end{bmatrix}^T, \tag{4.2}$$

$$\boldsymbol{R}_z(\theta) = \begin{bmatrix} \cos\theta & -\sin\theta & 0 \\ \sin\theta & \cos\theta & 0 \\ 0 & 0 & 1 \end{bmatrix}, \boldsymbol{R}_x(\phi) = \begin{bmatrix} 1 & 0 & 0 \\ 0 & \cos\phi & -\sin\phi \\ 0 & \sin\phi & \cos\phi \end{bmatrix}, \tag{4.3}$$

where $\boldsymbol{q}_s$ is an initial position of $\boldsymbol{q}$, r is a radius of bottom of cone shape, a_z is a distance from apex to bottom. $\boldsymbol{R}_z(\theta)$ and $\boldsymbol{R}_x(\phi)$ are rotation matrices around the z axis and around the x axis, respectively. θ represents the rotation of the thumb opposition. ϕ represents the rotation of the wrist movement.

From Eqs. (4.2), (4.3), and (4.3), y component of $\boldsymbol{q}$ is

$$q_y = r\cos\phi\sin\theta + a_z\sin\phi. \tag{4.4}$$

When q_y will be zero,

$$0 = r\cos\phi\sin\theta + a_z\sin\phi \tag{4.5}$$

$$\theta = \sin^{-1}\left(\frac{-a_z\sin\phi}{r\cos\phi}\right). \tag{4.6}$$

Equation (4.6) represents the relationship of the thumb opposition θ and the wrist movement ϕ. When substituting an appropriate value for r and a_z, in this case $r = 1$ and $a_z = 1$, and changing ϕ from 0 to 40 degrees, there is a trend that θ changes from zero to negative value like Fig. 4.9. As you can see Fig. 4.8, the positive value of ϕ represents the wrist extension, and the negative value of ϕ represents the thumb opposition. These results show that the thumb will oppose when the wrist extends with restraining the bone of the thumb on a flat surface without extra motor for the thumb opposition.

Figure 4.4 is the brace working to constrain the thumb on the flat surface when the wrist extension. The brace has two rotational joints, one slider, and one bar. The bar will be fixed on the wrist rest of the robot and works to constrain the thumb. Two

Table 4.1: Average hand-size data and robot dimensions

		M	F	
Middle finger length, dorsal [mm]	Mean	93.4	86.5	Glove length < 120 [mm]
	S.D.	4.5	4.2	
Hand breadth, diagonal [mm]	Mean	83.3	74.0	Glove breadth < 160 [mm]
	S.D.	3.6	3.0	Hand-rest breadth < 100 [mm]
Hand thickness at metacarpal-3 head [mm]	Mean	32.1	27.8	Glove thickness > 19 [mm]
	S.D.	2.1	1.8	

rotational joints and one slider works to absorb changes in position and angle of the thumb during the thumb opposition.

It is known that the grasping reflex appears most strongly when the hand region shown in Fig. 4.10 is stimulated. Hence, the elastic bar is located at the position shown in Fig. 4.11, and set out to confirm its influence experimentally.

4.3 Grasping Experiment and Results of Clinical Experiment

In this chapter, it is shown that the proposed robot can induce the grasping reflex, that is, activate the feedback control loops through experiments on a post-stroke patient. In this experiment, the function of the four-finger glove is focused on, and the functions for the wrist and the thumb are not used. Also, for the convenience of the experiment, the four-finger glove is used with a setting in 4.1. It is said that primitive reflexes are observed in the post-stroke patient with motion paralysis. It was tested that the stimulation of the grasping reflex and the usability of the proposed robot clinically by asking five post-stroke patients to participate in our experiments. With four of the patients, we merely placed their hands in the four-finger glove. The fifth patient, who

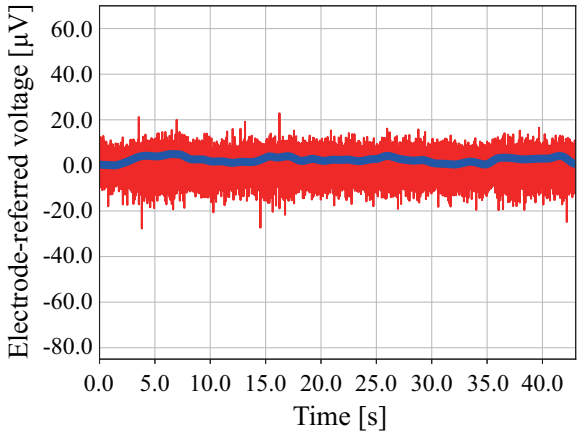

Fig. 4.12: Surface Electromyography (sEMG) time series of main flexor muscle group in grasping and opening without the elastic bar. Red line is the measured sEMG signal of the main flexor muscle group. Blue line is the signal after being low-pass filtered with a cutoff of 0.1 Hz. In this case, the robot extended and bent five times at a frequency of roughly 0.1 Hz. The absence of peaks indicates that grasping was not promoted without the bar.

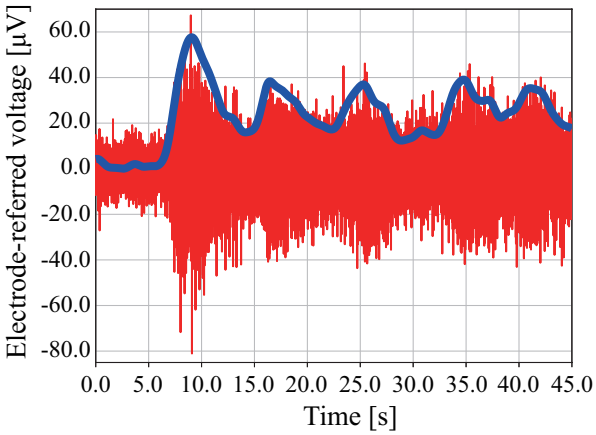

Fig. 4.13: Electromyography time series of main flexor muscle group in grasping and opening with the elastic bar. The conditions are the same as those in Fig. 4.12. The five peaks show that the flexor muscle was activated when the four-finger glove and fingers grasped the bar. This result indicates that grasping is promoted with the bar. This is similar to the way that post-stroke patients with grasping paralysis can grasp more easily when bars are pressed on their hands.

could not intentionally activate the muscles required for grasping, attended the grasp-training experiments. Permission to participate in the grasp-training experiments could not be obtained from other patients.

Regarding placing a paralyzed hand in the four-finger glove, it is succeeded that less than 5 min in all four tests, with the average time being 2.5 min. No patient felt

any pain during the test.

In the experiments for stimulating the grasping reflex, the patient was asked to relax during the supported motion. The shaft was manually rotated at a velocity that the patient did not feel pain because the motor could not be used due to wire breakage. the sEMG of the main flexor muscle were measured while the robot bent and extended the patient's hand at a frequency of about 0.1 Hz with and without the elastic bar.

Figures 4.12 and 4.13 describe the sEMG time series without and with the elastic bar, respectively. The blue lines in the figure represent the sEMG signal after it was low-pass filtered with a cutoff of 1.0 Hz. The robot began extending the fingers at 0.0 s, proceeding to extend and bend the fingers repeatedly five times.

The results show a recognizable sEMG response to grasping when the elastic bar was present and none when the bar was absent. Five peaks are visible in Fig. 4.13 at around 9.0, 17.0, 25.0, 35.0, and 42.0 [s]. The appearance of the peaks coincides with the robot grasping the elastic bar fully. In this experiment, even though the patient was asked to relax while the experiment was conducted, the flexor muscle activated unintentionally (on the part of the patient) because of flexion by the robot. This phenomenon indicates that the robot can stimulate the grasping reflex if it is equipped with an elastic bar.

As it was written above, it was attempted to promote the motion of the patient by stimulating the feedback control loop, that is, the grasping reflex. In this case, the motion of the patient is automatically generated by inducing the grasping reflex. In general, it is said that the time from stimulating to starting simple reflex motion is 10.0-20.0 [ms] because the reflex motion is generated by sensory stimulation reaching a muscle via the spine [144–146]. In this experiment, only sEMG signal was measured from flexor muscles, therefore the time of automatically generating the motion by stimulating the feedback control loop could not be got. However, since the change of the grasping motion is slow, it is necessary to verify in detail what elements and which neural pathways are contributing to induce the grasping motion by using fMRI.

4.4 Conclusion

Activation the feedback control loops during rehabilitation from grasping paralysis is a key factor for effective recovery. In this study, the grasping-training robot was proposed, which can activate the feedback control loops by mechanical motion support for the finger flexion, the wrist extension, the thumb opposition, and the grasping reflex induced by stimulating the palm of the hand with the elastic bar. The proposed robot consists of the four-finger glove with a curving mechanism, the bascule bridge mechanism, the thumb fixer, the shaft, and threads. The threads are connected to the curving mechanism of the glove and the edge of the bascule bridge mechanism. The glove can extend and bend, and the bascule bridge mechanism can down and up repeatedly by pulling the threads with the shaft. Respond to the wrist extension, the thumb is opposed by the constraint with the thumb fixer.

There are important features of the proposed robot. It allows stimulation of the grasping reflex in hands paralyzed by strokes. When the motion support by the robot was applied to a post-stroke patient, the sEMG signals were detected from the completely paralyzed hand. These results suggest that appropriate motion support and the grasping of an elastic bar could stimulate the grasping reflex of patients.

The results presented here can be taken collectively as a case study of stimulating the grasping reflex. Next, experiments with several patients should be conducted with different materials and sizes of the grasping object and other functions of the robot to be sure that the proposed robot can stimulate the grasping reflex.

Chapter 5

Theoretical Approach for Designing the Rehabilitation Robot Controller

5.1 Purpose in chapter 5

In previous chapter, a concept was proposed that activating the feedback control loops realized the effective rehabilitation from motion paralysis. From that point of view, the grasping-training robot consisting of the four-finger glove, the bascule bridge mechanism, the thumb fixer, and the grasping reflex was designed to activate the feedback control loops. This robot could induce the grasping reflex by stimulating the palm of the hand with the elastic bar, and one of the merits of rehabilitation robots is to conduct these kinds of motion support repetitively. However, the potential of robot rehabilitation should not be limited to repetitive grasping support, and it is necessary to extend the concept to general actions and establish a new robot rehabilitation strategy.

In the European Commission project of the Seventh Framework Programme (FP7) called "Smart Wearable Robots with Bioinspired Sensory-Motor Skills (BioMot)" [147], the robot rehabilitation strategy was examined through clinical tests and concluded that the robot should first adapt to the patient's motions, and then gradually improve the patient's motion [84]. The robot rehabilitation strategy is shown in detail in Chapter 5.2.

To create the robot controller to achieve the proposed strategy, tacit learning was used [80–84, 123, 148]. Tacit learning has been used to generate bipedal walking from a roughly defined walking gait [81], to create behaviors from a symbolized purpose [148], and to control the wrist joint of a forearm prosthesis in response to the wearer's shoulder movements [83]. In the BioMot Project, tacit learning was used to control an exoskeleton robot and adapted the joint trajectories to the wearer's motions by tuning the stiffness of the joints as the first stage in the proposed robot rehabilitation strategy [84].

Next, it is needed to extend the discussion and propose a control system that can improve the motion of the patient. The most important problem in proposing the control system is to deal with differences between patient's recovery potential and recovery speed in each patient. In particular, defining the fully recovered state is a critical problem for designing the controller. If all patients could recover their motion to the same state as before the disease, the fully recovered state could be set as the ideal state. However, the fully recovered state cannot always be defined in this way because the recovery potential is different in each patient. Many patients live with paralysis even though perfect rehabilitation is provided. In cases where patients cannot make a full recovery, a state that can maximize the quality of life should be aimed, even if the patient is still paralyzed. For the control system, the problem of setting the ideal state is the difficulty in setting the reference for the controller. To overcome this problem, a controller is designed to improve the patient's state without defining the ideal state. The controller reference is changed when the patient's state is improved by rehabilitation.

In this research, it is described that the theoretical basis of the rehabilitation strategy discussed above. A controller is proposed, which can improve the patient's state according to their recovery and analyze the recovery process theoretically using the controller. To design the controller, several assumptions are made based on the biological control principle.

In Chapter 5.2, the concept of designing the controller is explained based on Neurosynergy model. In Chapter 5.3, the mathematical model of the controller is explained, and the assumptions for the recovery are also explained. In Chapter 5.4, the controller

that can dealing with differences between patients is shown through simulations. In Chapter 5.5, a method how to apply the proposed system for controlling a lower limb exoskeleton robot is described. In Chapter 5.6, it is the discussion.

5.2 Robot rehabilitation strategy and patient model including recovery

5.2.1 Problems with robot motion support

To clear the problems with robot rehabilitation, the failure in motion support using the exoskeleton robot is shown again(Fig. 1.4). In the experiments, healthy young subjects were asked to walk wearing an exoskeleton robot that was controlled with a fine-tuned bipedal walking trajectory. Figure 1.4(b) shows an overview of the experiments when the subjects tried to walk for the first time wearing the exoskeleton robot. The subjects could not walk with the robot motion support. The exoskeleton robot appeared to disturb the motion of the subjects rather than supporting the walking. The subjects finally lost their balance and could not keep walking.

There is the reason why subjects were not able walk, even though they were young healthy people who can walk with no difficulty. This reason can be explained by using Neuro-synergy model. This model demonstrates that our motions are created with a combination of voluntary actions and reactive motions. Voluntary actions are created by the symbolized action purpose described in the higher layer, whereas reactive motions are created by the feedback control loops as a response to unexpected inputs from the environment to the controller. In the case of the exoskeleton robot support in Fig. 1.4, the activation of the feedback control loops by an excessive support force causes the inhibition of walking and the loss of balance. One of the causes of the excessive support force is a discrepancy between the movements of the robot and the subjects.

5.2.2 Robot rehabilitation strategy

Losing balance through an unexpected external support force is the extreme case of non-ideal motion support. In any rehabilitation, however, consistency between motion intention and motion support is an important factor in efficient recovery from paralysis. Even though the feedback control loops of the subjects are working properly, there is a possibility that the robot may hinder a target action by supporting the motion. Therefore, unexpected inputs by rehabilitation robots may have a negative effect on recovery. The robot should not provide the unexpected inputs to keep activating the feedback control loops properly and secure a period during which the subject gets used to the robot motion at first.

The following steps are proposed for the robot rehabilitation:

1. Robot motions are controlled to adapt to patient motions without creating discrepancies.

2. Robot motions are gradually tuned to improve patient motions with small external forces.

3. Patient motions converge to the full recovery state possible for the patient.

If paralysis is so severe that the patients cannot move the paralyzed limbs at all, Step 1. may be unnecessary. In many cases, however, patients move in abnormal ways with activating the feedback control loops. In the proposed rehabilitation process, the robot should be controlled to follow the abnormal movements in Step 1. In Step 2, the robot should improve the movements of the paralyzed limbs with a small difference between the patient's abnormal motions and the supported motions. In Step 3, the limits of recovery are identified. Many patients cannot make a recovery to their previous condition. The limits of recovery should be detected and the robot support should converge its motion to this state.

5.2.3 Mathematical expression for rehabilitation

In this research, the theoretical basis of the rehabilitation robot control is created with two assumptions in the patient paralysis and recovery model, which are the expressions

of motion paralysis and the recovery.

One method for describing paralysis in a mathematical model is to describe the source of the paralysis and the motion controller separately. The method shown in Fig. 5.2 is used, where the reference for the abnormal motion is created by the summation of the source of paralysis and the normal motion reference,

$$x_P = x_{1ref} + \mu, \tag{5.1}$$

where x_P, x_{1ref}, and μ are the reference for the abnormal movement, the reference for the normal motion, and the suppression from the source of the paralysis, respectively.

In this model, μ represents the suppression of the normal motion reference by the source of the paralysis, and the reduction of μ expresses the reduction of the suppression. That is, the reduction of μ by the rehabilitation training means that the patient can generate the muscle activity again due to decreasing the influence of the damaged motor area by constructing the neural network among the sensory area, a part surrounding the damaged motor area, and a part playing the role of the intention. μ is described as

$$\mu = h(x_1), \tag{5.2}$$

$$\frac{\mathrm{d}\dot{\mu}}{\mathrm{d}x_1} = \frac{\mathrm{d}^2 h(x_1)}{\mathrm{d}x_1 \mathrm{d}t} < 0, \tag{5.3}$$

where x_1 represents the position of the patient, and $h(x_1)$ is a function. The function is called as recovery function. Equation (5.3) represents a property where the suppression is reduced by the change of the position of the patient.

Figure 5.1 visualizes the property of Eq. (5.3). In Fig. 5.1, it is assumed that x_1 does not reach the reference for the normal motion because of the paralysis $-C$ and becomes $x_1(0)$ at the early stage of the rehabilitation training. For easy to understand, x_1 is described discretely in this figure. When the rehabilitation training makes x_1 close to the reference for the normal motion x_{1ref},

$$\{x_1(i+1) - x_{1ref}\} - \{x_1(i) - x_{1ref}\} = x_1(i+1) - x_1(i) > 0. \tag{5.4}$$

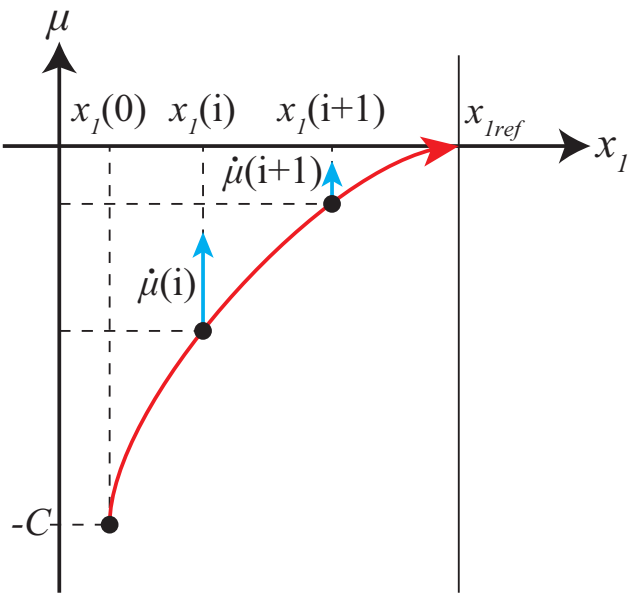

Fig. 5.1: Property of μ. it is assumed that x_1 does not reach the reference for the normal motion x_{1ref} because of the paralysis $-C$ and becomes $x_1(0)$ at the early stage of the rehabilitation training.

At that time, from Eqs. (5.3) and (5.4), the time derivative of μ is written as

$$\begin{aligned} &\frac{\mathrm{d}\dot{\mu}}{\mathrm{d}x_1} < 0 \\ \Leftrightarrow\ &\frac{\dot{\mu}(i+1) - \dot{\mu}(i)}{x_1(i+1) - x_1(i)} < 0 \\ \Rightarrow\ &\dot{\mu}(i+1) - \dot{\mu}(i) < 0 \\ &\dot{\mu}(i+1) < \dot{\mu}(i). \end{aligned} \tag{5.5}$$

This can be interpreted in two ways; As the patient performs well, the paralysis increases, or as the patient performs well, the paralysis gradually decreases. From the viewpoint of Eq. 5.1, the performance does not improve despite the paralysis increase, the condition of Eq. (5.3) represents the property that the paralysis is reduced by the rehabilitation training that extends, in this study, the position of the patient x_1. This function corresponds to the blue part in Fig. 5.2.

In the next chapter, it is discussed that the rehabilitation robot controller and the rehabilitation process using the controller based on the above assumptions.

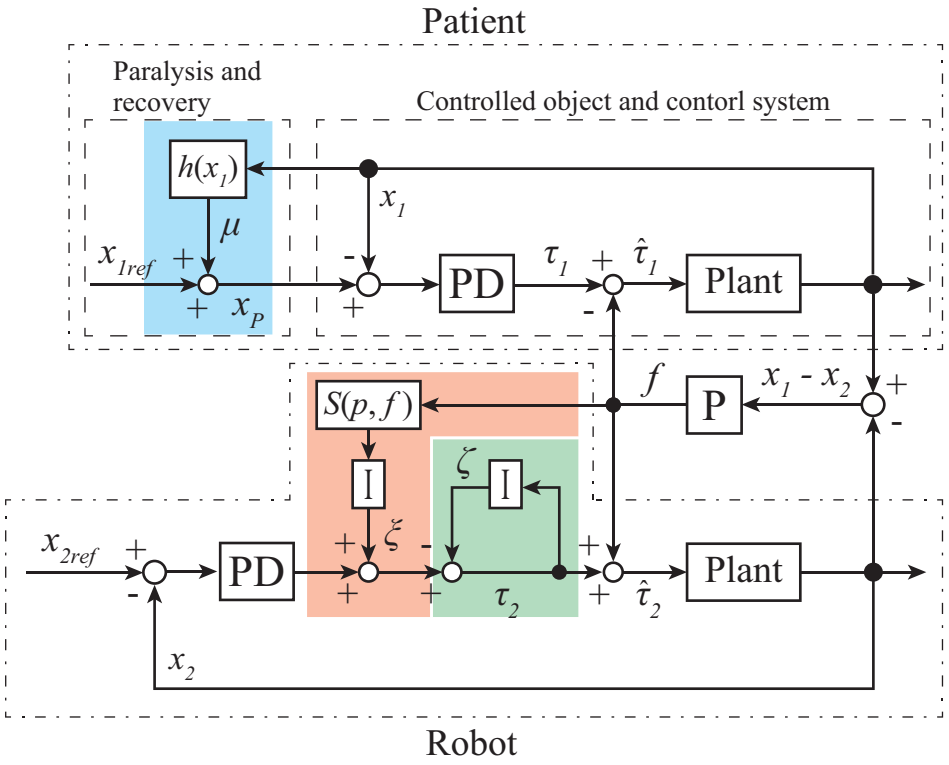

Fig. 5.2: Block diagram of whole system including the patient and robot (see Chapter 5.3 for details).

5.3 Robot controller realizing proposed robot rehabilitation strategy

5.3.1 Model of robot, patient, and relationship

To construct a theoretical basis of the robot rehabilitation, the discussion is started with a simplified model where the state of the patient and the robot with one DoF. The interaction between the robot and the patient is assumed as a position-dependent reaction force, so the patient-robot is described as a mass-spring model.

The motion equation is

$$\begin{cases} m_1\ddot{x}_1 = k(x_2 - x_1) + \tau_1 & (5.6) \\ m_2\ddot{x}_2 = k(x_1 - x_2) + \tau_2, & (5.7) \end{cases}$$

where m_1 and m_2 are the masses that the patient and the robot control, x_1 and x_2

represent the positions of the patient and the robot, and τ_1 and τ_2 are the driving forces of the patient and the robot, respectively. k is a spring coefficient between the robot and the patient. The models of the patient and the robot are simplified to make it easier to apply a proposed system to different rehabilitation robots and sensors. Its effectiveness is shown through experimental results of a walking experiment using a lower limb exoskeleton robot in Chapter 5.6.

5.3.2 Controller for realizing the proposed robot rehabilitation strategy

Figure 5.2 shows the whole system including the patient and the robot. The upper part of the block diagram represents the patient's plant and controller including the recovery function. The bottom part of the block diagram represents the robot's plant and controller designed with tacit learning.

The patient generates the driving force, τ_1, to converge the position to a reference position. Thus, the driving force, τ_1, is represented with the proportional–derivative (PD) controller as

$$\tau_1 = k_{p1}(x_P - x_1) - k_{d1}\dot{x}_1, \tag{5.8}$$

where k_{p1} is the proportional (P) gains of the PD controller, k_{d1} is the derivative (D) gains of the PD controller, and x_P is as same as Eq. (5.1).

The driving force of the robot, τ_2, is written as

$$\tau_2 = k_{p2}(x_{2ref} - x_2) - k_{d2}\dot{x}_2 - \zeta + \xi, \tag{5.9}$$

where k_{p2} is P gain, k_{d2} is D gain, and x_{2ref} is the reference position of the robot.

Value ζ consists of an accumulation of τ_2,

$$\zeta = k_{t1} \int \tau_2 dt, \tag{5.10}$$

where k_{t1} is a coefficient of an integrator that accumulates the driving force. This accumulation corresponds to tacit learning and adjusts the driving force of the robot through the robot-patient interaction. k_{t1} can change the adaptation level. This

accumulation controls the exoskeleton robot to reduce the burden on the user's muscles in the BioMot Project [84]. In this paper, the feedback control loop is called an adaptation loop and is shown in the green part of Fig. 5.2.

Value ξ consists of the integration of the interaction force,

$$\xi = k_{t2} \int S(p, f)dt, \tag{5.11}$$

$$S(p, f) = sign(f + p)|f|, \tag{5.12}$$

$$f = k(x_1 - x_2), \tag{5.13}$$

where f is the interaction force on the robot generated from the spring and p is a constant value determining the direction of the support force. This accumulation is an application of tacit learning and gradually changes the robot behavior based on the direction of the support force. In this paper, this feedback control loop is called a support loop and is shown in the pink part of Fig. 5.2.

The whole system can be expressed by combining Eqs. (5.1), (5.6), (5.7), (5.8), and (5.9) as

$$\begin{cases} m_1\ddot{x}_1 = k(x_2 - x_1) + k_{p1}(x_{1ref} + \mu - x_1) - k_{d1}\dot{x}_1 & (5.14) \\ m_2\ddot{x}_2 = k(x_1 - x_2) + k_{p2}(x_{2ref} - x_2) - k_{d2}\dot{x}_2 - \zeta + \xi. & (5.15) \end{cases}$$

Equations. (5.14) and (5.15) can be written as

$$\begin{cases} \boldsymbol{\tau} = \boldsymbol{A}(\boldsymbol{r} - \boldsymbol{x}) - \boldsymbol{B}\dot{\boldsymbol{x}} + \boldsymbol{\eta} & (5.16) \\ \boldsymbol{M}\ddot{\boldsymbol{x}} + \boldsymbol{K}\boldsymbol{x} = \boldsymbol{A}(\boldsymbol{r} - \boldsymbol{x}) - \boldsymbol{B}\dot{\boldsymbol{x}} + \boldsymbol{\eta}, & (5.17) \end{cases}$$

where

$$\boldsymbol{x} = \begin{bmatrix} x_1 & x_2 \end{bmatrix}^T, \quad \dot{\boldsymbol{x}} = \begin{bmatrix} \dot{x}_1 & \dot{x}_2 \end{bmatrix}^T, \tag{5.18}$$

$$\boldsymbol{A} = \begin{bmatrix} k_{p1} & 0 \\ 0 & k_{p2} \end{bmatrix}, \quad \boldsymbol{B} = \begin{bmatrix} k_{d1} & 0 \\ 0 & k_{d2} \end{bmatrix}, \tag{5.19}$$

$$\boldsymbol{M} = \begin{bmatrix} m_1 & 0 \\ 0 & m_2 \end{bmatrix}, \quad \boldsymbol{K} = \begin{bmatrix} k & -k \\ -k & k \end{bmatrix}, \tag{5.20}$$

$$\boldsymbol{r} = \begin{bmatrix} x_{1ref} + \mu & x_{2ref} - \frac{1}{k_{p2}}\zeta \end{bmatrix}^T, \boldsymbol{\eta} = \begin{bmatrix} 0 & \xi \end{bmatrix}^T. \tag{5.21}$$

5.3.3 Stability analysis of controller

Shimoda et al. [123] analyzed the stability of a control system using tacit learning by using the singular perturbation method. The singular perturbation separates the system into the FMS and the SMS, verifying the stability of each system. As it was written before, the part of the robot controller adapting the robot to the patient is the FMS, and the part of the controller changing the motion of the patient is the SMS.

(i) Analysis of FMS

First, the stability of the FMS is verified. The change caused by the SMS is much slower than that caused by the FMS, so the time differentiation of the support and the recovery are

$$\dot{\mu} \simeq 0, \ \dot{\boldsymbol{\eta}} \simeq 0. \tag{5.22}$$

From Eqs. (5.16) and (5.17), the whole system can be written as

$$\begin{cases} \boldsymbol{\tau} = \boldsymbol{A}(\boldsymbol{r} - \boldsymbol{x}) - \boldsymbol{B}\dot{\boldsymbol{x}} + \boldsymbol{\eta} \\ \boldsymbol{M}\ddot{\boldsymbol{x}} + \boldsymbol{K}\boldsymbol{x} = \boldsymbol{A}(\boldsymbol{r} - \boldsymbol{x}) - \boldsymbol{B}\dot{\boldsymbol{x}} + \boldsymbol{\eta} \end{cases} \tag{5.23}$$

$$\Leftrightarrow \begin{cases} \boldsymbol{\tau} = \boldsymbol{A}(\boldsymbol{r} + \boldsymbol{A}^{-1}\boldsymbol{\eta} - \boldsymbol{x}) - \boldsymbol{B}\dot{\boldsymbol{x}} \\ \boldsymbol{M}\ddot{\boldsymbol{x}} + \boldsymbol{K}\boldsymbol{x} = \boldsymbol{A}(\boldsymbol{r} + \boldsymbol{A}^{-1}\boldsymbol{\eta} - \boldsymbol{x}) - \boldsymbol{B}\dot{\boldsymbol{x}}. \end{cases} \tag{5.24}$$

A candidate for the Lyapunov function is defined as

$$V = \frac{1}{2}\dot{\boldsymbol{x}}^T\boldsymbol{M}\dot{\boldsymbol{x}} + \frac{1}{2}\boldsymbol{x}^T\boldsymbol{K}\boldsymbol{x} + \frac{1}{2}\{\boldsymbol{x} - (\boldsymbol{r} + \boldsymbol{A}^{-1}\boldsymbol{\eta})\}^T\boldsymbol{A}\{\boldsymbol{x} - (\boldsymbol{r} + \boldsymbol{A}^{-1}\boldsymbol{\eta})\}. \tag{5.25}$$

$\boldsymbol{M}$ and $\boldsymbol{A}$ are positive definite matrices. $\boldsymbol{K}$ is semi-positive definite matrix, but the second term on the right side of Eq. (5.25) is written as

$$\frac{1}{2}\boldsymbol{x}^T\boldsymbol{K}\boldsymbol{x} = \frac{1}{2}\begin{bmatrix} x_1 & x_2 \end{bmatrix}\begin{bmatrix} k & -k \\ -k & k \end{bmatrix}\begin{bmatrix} x_1 \\ x_2 \end{bmatrix} \tag{5.26}$$

$$= \frac{1}{2}\left(kx_1^2 - 2kx_1x_2 + kx_2^2\right) \tag{5.27}$$

$$= \frac{1}{2}k\left(x_1 - x_2\right)^2, \tag{5.28}$$

so Eq. (5.25) is positive for arbitrary values except for a condition: $\boldsymbol{x} = \boldsymbol{0}$, $\boldsymbol{x} = \boldsymbol{r} + \boldsymbol{A}^{-1}\boldsymbol{\eta}, \dot{\boldsymbol{x}} = \boldsymbol{0}$, and $x_1 = x_2$.

The time differentiation of Eq. (5.25) is

$$
\begin{aligned}
\dot{V} &= \dot{\boldsymbol{x}}^T\boldsymbol{M}\ddot{\boldsymbol{x}} + \dot{\boldsymbol{x}}^T\boldsymbol{K}\boldsymbol{x} + \{\dot{\boldsymbol{x}} - (\dot{\boldsymbol{r}} + \boldsymbol{A}^{-1}\dot{\boldsymbol{\eta}})\}^T\boldsymbol{A}\{\boldsymbol{x} - (\boldsymbol{r} + \boldsymbol{A}^{-1}\boldsymbol{\eta})\} \\
&= \dot{\boldsymbol{x}}^T\left[\boldsymbol{M}\ddot{\boldsymbol{x}} + \boldsymbol{K}\boldsymbol{x} + \boldsymbol{A}\{\boldsymbol{x} - (\boldsymbol{r} + \boldsymbol{A}^{-1}\boldsymbol{\eta})\}\right] - (\dot{\boldsymbol{r}} + \boldsymbol{A}^{-1}\dot{\boldsymbol{\eta}})^T\boldsymbol{A}\{\boldsymbol{x} - (\boldsymbol{r} + \boldsymbol{A}^{-1}\boldsymbol{\eta})\} \\
&= -\dot{\boldsymbol{x}}^T\boldsymbol{B}\dot{\boldsymbol{x}} - (\dot{\boldsymbol{r}} + \boldsymbol{A}^{-1}\dot{\boldsymbol{\eta}})^T\boldsymbol{A}\{\boldsymbol{x} - (\boldsymbol{r} + \boldsymbol{A}^{-1}\boldsymbol{\eta})\} \quad (\because Eq.\ (5.17)) \\
&= -\dot{\boldsymbol{x}}^T\boldsymbol{B}\dot{\boldsymbol{x}} + (\dot{\boldsymbol{r}} + \boldsymbol{A}^{-1}\dot{\boldsymbol{\eta}})^T(\boldsymbol{\tau} + \boldsymbol{B}\dot{\boldsymbol{x}}) \quad (\because Eq.\ (5.16)) \\
&= -\dot{\boldsymbol{x}}^T\boldsymbol{B}\dot{\boldsymbol{x}} + \dot{\boldsymbol{r}}^T(\boldsymbol{\tau} + \boldsymbol{B}\dot{\boldsymbol{x}}) \quad (\because \dot{\boldsymbol{\eta}} \simeq 0) \\
&= -\dot{\boldsymbol{x}}^T\boldsymbol{B}\dot{\boldsymbol{x}} + \begin{bmatrix} \dot{\mu} \\ -\frac{1}{k_{p2}}\dot{\zeta} \end{bmatrix}^T(\boldsymbol{\tau} + \boldsymbol{B}\dot{\boldsymbol{x}}) \quad (\because Eq.\ (5.21)) \\
&= -\dot{\boldsymbol{x}}^T\boldsymbol{B}\dot{\boldsymbol{x}} + \begin{bmatrix} 0 \\ -\frac{1}{k_{p2}}k_{t1}\tau_2 \end{bmatrix}^T(\boldsymbol{\tau} + \boldsymbol{B}\dot{\boldsymbol{x}}) \quad (\because \dot{\mu} \simeq 0, \dot{\zeta} = k_{t1}\tau_2) \\
&= -\dot{\boldsymbol{x}}^T\boldsymbol{B}\dot{\boldsymbol{x}} - \left(\begin{bmatrix} 0 & 0 \\ 0 & \frac{1}{k_{p2}}k_{t1} \end{bmatrix}\begin{bmatrix} \tau_1 \\ \tau_2 \end{bmatrix}\right)^T(\boldsymbol{\tau} + \boldsymbol{B}\dot{\boldsymbol{x}}) \\
&= -\dot{\boldsymbol{x}}^T\boldsymbol{B}\dot{\boldsymbol{x}} - (\boldsymbol{C}\boldsymbol{\tau})^T(\boldsymbol{\tau} + \boldsymbol{B}\dot{\boldsymbol{x}}) \\
&= -\dot{\boldsymbol{x}}^T\boldsymbol{B}\dot{\boldsymbol{x}} - \boldsymbol{\tau}^T\boldsymbol{C}^T\boldsymbol{\tau} + \boldsymbol{\tau}^T\boldsymbol{C}^T\boldsymbol{B}\dot{\boldsymbol{x}} \\
&= -\dot{\boldsymbol{x}}^T\boldsymbol{B}\dot{\boldsymbol{x}} - \left(\boldsymbol{\tau} + \frac{1}{2}\boldsymbol{B}\dot{\boldsymbol{x}}\right)^T\boldsymbol{C}^T\left(\boldsymbol{\tau} + \frac{1}{2}\boldsymbol{B}\dot{\boldsymbol{x}}\right) + \frac{1}{4}(\boldsymbol{B}\dot{\boldsymbol{x}})^T\boldsymbol{C}^T(\boldsymbol{B}\dot{\boldsymbol{x}}) \\
\therefore\ &= -\dot{\boldsymbol{x}}^T\left(\boldsymbol{B} - \frac{1}{4}\boldsymbol{B}^T\boldsymbol{C}^T\boldsymbol{B}\right)\dot{\boldsymbol{x}} - \left(\boldsymbol{\tau} + \frac{1}{2}\boldsymbol{B}\dot{\boldsymbol{x}}\right)^T\boldsymbol{C}^T\left(\boldsymbol{\tau} + \frac{1}{2}\boldsymbol{B}\dot{\boldsymbol{x}}\right). \qquad (5.29)
\end{aligned}
$$

When k_{t1} is a positive value, the matrix $\boldsymbol{C}^T$ is a positive semi-definite matrix, so the second term on the right side of Eq. (5.29) will be negative. The necessary and sufficient condition where Eq. (5.29) is definitely negative is that a matrix $\left(\boldsymbol{B} - \frac{1}{4}\boldsymbol{B}^T\boldsymbol{C}^T\boldsymbol{B}\right)$ is a positive definite matrix. Matrix $\boldsymbol{B}$ and matrix $\boldsymbol{C}$ are

$$
\boldsymbol{B} = \begin{bmatrix} k_{d1} & 0 \\ 0 & k_{d2} \end{bmatrix}, \boldsymbol{C} = \begin{bmatrix} 0 & 0 \\ 0 & \frac{1}{k_{p2}}k_{t1} \end{bmatrix}, \qquad (5.30)
$$

and

$$\begin{aligned}\boldsymbol{B}-\frac{1}{4}\boldsymbol{B}^T\boldsymbol{C}^T\boldsymbol{B} &= \begin{bmatrix} k_{d1} & 0 \\ 0 & k_{d2} \end{bmatrix} - \frac{1}{4}\begin{bmatrix} k_{d1} & 0 \\ 0 & k_{d2} \end{bmatrix}^T \begin{bmatrix} 0 & 0 \\ 0 & \frac{1}{k_{p2}}k_{t1} \end{bmatrix}^T \begin{bmatrix} k_{d1} & 0 \\ 0 & k_{d2} \end{bmatrix} \\ &= \begin{bmatrix} k_{d1} & 0 \\ 0 & k_{d2} \end{bmatrix} - \frac{1}{4}\begin{bmatrix} 0 & 0 \\ 0 & \frac{k_{d2}^2}{k_{p2}}k_{t1} \end{bmatrix} \\ &= \begin{bmatrix} k_{d1} & 0 \\ 0 & k_{d2}-\frac{1}{4}\frac{k_{d2}^2}{k_{p2}}k_{t1} \end{bmatrix}. \end{aligned} \tag{5.31}$$

A condition where the matrix $\left(\boldsymbol{B}-\frac{1}{4}\boldsymbol{B}^T\boldsymbol{C}^T\boldsymbol{B}\right)$ becomes the positive definite matrix is that all leading principal minors of that matrix are positives. That condition is

$$\begin{cases} k_{d1}>0 \\ k_{d2}-\frac{1}{4}\frac{k_{d2}^2}{k_{p2}}k_{t1}>0 \end{cases} \Leftrightarrow \begin{cases} k_{d1}>0 \\ k_{d2}>0 \\ k_{t1}<\frac{4k_{p2}}{k_{d2}}. \end{cases} \tag{5.32}$$

Consequently, when k_{t1} is small, the time differentiation of Eq. (5.25) becomes negative, so Eq. (5.25) is the Lyapunov function, and $\boldsymbol{x}=\boldsymbol{0}$, $\boldsymbol{x}=\boldsymbol{r}+\boldsymbol{A}^{-1}\boldsymbol{\eta}, \dot{\boldsymbol{x}}=\boldsymbol{0}$, and $x_1=x_2$ will be the asymptotically stable points. The results show that FMS is an asymptotically stable system.

(ii) Analysis of SMS

Next, the stability of the SMS is verified. The FMS is an asymptotically stable system. Convergence points for the FSM are described as $\overline{\bullet}$. $\ddot{\boldsymbol{x}}$, $\dot{\boldsymbol{x}}$, and $\dot{\zeta}$ converge to zero. At that time, the whole system can be written as

$$\begin{cases} k(\overline{x_1}-\overline{x_2})=\overline{\tau_1} & (5.33) \\ k(-\overline{x_1}+\overline{x_2})=\overline{\tau_2} & (5.34) \\ \overline{\tau_1}=k_{p1}\left(x_{1ref}+\overline{\mu}-\overline{x_1}\right) & (5.35) \\ \overline{\tau_2}=k_{p2}\left(x_{2ref}-\frac{1}{k_{p2}}\overline{\zeta}+\frac{1}{k_{p2}}\overline{\xi}-\overline{x_2}\right) & (5.36) \\ \dot{\overline{\xi}}=k_{t2}S(p,\overline{f}) & (5.37) \\ \dot{\overline{\zeta}}=k_{t1}\overline{\tau_2}=0. & (5.38) \end{cases}$$

From Eqs. (5.34) and (5.38), the interaction force on the robot becomes

$$k(\overline{x_1} - \overline{x_2}) = 0. \tag{5.39}$$

At that time, from Eqs. (5.12), (5.37), and (5.39),

$$\dot{\overline{\xi}} = 0. \tag{5.40}$$

From Eq. (5.36), the time differentiation of $\overline{x_2}$ will be

$$\begin{aligned} \overline{\tau_2} &= k_{p2}\left(x_{2ref} - \frac{1}{k_{p2}}\overline{\zeta} + \frac{1}{k_{p2}}\overline{\xi} - \overline{x_2}\right) \\ 0 &= -\frac{1}{k_{p2}}\dot{\overline{\zeta}} + \frac{1}{k_{p2}}\dot{\overline{\xi}} - \dot{\overline{x_2}} \\ \dot{\overline{x_2}} &= 0 \quad (\because \tau_2 = 0, Eqs.\ (5.38)\ and\ (5.40)). \end{aligned}$$

On the other hand, from Eqs. (5.33), (5.35), and (5.39),

$$k(\overline{x_1} - \overline{x_2}) = k_{p1}\left(x_{1ref} + \overline{\mu} - \overline{x_1}\right) \tag{5.41}$$

$$0 = k_{p1}\left(x_{1ref} + \overline{\mu} - \overline{x_1}\right) \tag{5.42}$$

$$\overline{x_1} = x_{1ref} + \overline{\mu}. \tag{5.43}$$

a candidate for the Lyapunov function is defined as

$$V = \frac{1}{2}\dot{\overline{x_1}}^2. \tag{5.44}$$

This function is positive for arbitrary values except for $\dot{\overline{x_1}} = 0$.

From Eq. (5.44), the time differentiation of the function is

$$\begin{aligned} \dot{V} &= \frac{\mathrm{d}}{\mathrm{d}t}\left(\frac{1}{2}\dot{\overline{x_1}}^2\right) \\ &= \frac{\mathrm{d}\dot{\overline{\mu}}}{\mathrm{d}t}\dot{\overline{\mu}} \quad (\because Eq.\ (5.43) \rightarrow \dot{\overline{x_1}} = \dot{\overline{\mu}}) \\ &= \frac{\mathrm{d}\overline{\mu}}{\mathrm{d}t}\frac{\mathrm{d}\overline{x_1}}{\mathrm{d}\overline{\mu}}\frac{\mathrm{d}\dot{\overline{\mu}}}{\mathrm{d}\overline{x_1}}\dot{\overline{\mu}} \\ &= \dot{\overline{\mu}}\frac{\mathrm{d}\overline{x_1}}{\mathrm{d}\overline{\mu}}\frac{\mathrm{d}\dot{\overline{\mu}}}{\mathrm{d}\overline{x_1}}\dot{\overline{\mu}} \\ &= \dot{\overline{\mu}}\frac{\mathrm{d}\dot{\overline{\mu}}}{\mathrm{d}\overline{x_1}}\dot{\overline{\mu}} \quad (\because Eq.\ (5.43) \rightarrow \frac{\mathrm{d}\overline{x_1}}{\mathrm{d}\overline{\mu}} = 1) \\ \therefore &= \frac{\mathrm{d}\dot{\overline{\mu}}}{\mathrm{d}\overline{x_1}}\dot{\overline{\mu}}^2. \end{aligned} \tag{5.45}$$

Thus, Eq. (5.45) becomes negative under the condition of Eq. (5.3). At that time, Eq. (5.44) is the Lyapunov function. Therefore, the SMS is an asymptotically stable system, and $\dot{\overline{x_1}} = 0$ is the asymptotically stable point. The final stable point is not specified in the controller but that is automatically decided depending on the features of the plant. This feature is discussed in our previous paper referred in [123]. As a result, it can show that SMS no longer changes after a sufficient time, and x_1 converges to a certain state. The convergence state of x_1 depends on the recovery function.

5.3.4 Recovery process in system having models of human and robot

In the recovery process, the patient gradually recovers from the paralysis with a long-time training.

Therefore, the system is analyzed as the singular perturbation system. In a fast motion subsystem(FMS), the change of the adaptation loop, ζ, is faster than the change of the recovery function, μ, and the support loop, ξ. FMS can be represented by using μ and ξ as

$$\begin{cases} \boldsymbol{M}\ddot{\boldsymbol{x}} + \boldsymbol{K}\boldsymbol{x} = \boldsymbol{A}(\boldsymbol{r} - \boldsymbol{x}) - \boldsymbol{B}\dot{\boldsymbol{x}} + \boldsymbol{\eta} & (5.46) \\ \dot{\mu} \simeq 0 & (5.47) \\ \dot{\xi} \simeq 0 & (5.48) \\ \dot{\zeta} = k_{t1}\tau_2. & (5.49) \end{cases}$$

This FMS can be proved to be an asymptotically stable system as proved in previous sub-chapter at the equilibrium state of FMS. At the equilibrium state, $\ddot{\boldsymbol{x}}$, $\dot{\boldsymbol{x}}$, and $\dot{\zeta}$ become zero, then Eq. (5.7) show

$$\begin{aligned} m_2\ddot{x}_2 &= k(x_1 - x_2) + \tau_2 \\ k(x_1 - x_2) &= 0 \\ x_1 &= x_2. \end{aligned} \quad (5.50)$$

It means that the robot can adapt to the motion of the patients.

A slow motion subsystem can be described as follow:

$$\begin{cases} \boldsymbol{K}\overline{\boldsymbol{x}} = \boldsymbol{A}(\boldsymbol{r} - \overline{\boldsymbol{x}}) + \overline{\boldsymbol{\eta}} & (5.51) \\ \dot{\overline{\mu}} = \dfrac{\mathrm{d}h(\overline{x_1})}{\mathrm{d}t} & (5.52) \\ \dot{\overline{\xi}} = k_{t2} S(p, \overline{f}) & (5.53) \\ \dot{\overline{\zeta}} = 0, & (5.54) \end{cases}$$

where $\overline{\bullet}$ means variables in the steady state. This SMS can be also proved to be an asymptotically stable system at previous sub-chapter, then $\overline{x_1}$ is converged to

$$\overline{x_1} = x_{1ref} + \overline{\mu}. \tag{5.55}$$

It means that the convergence state of x_1 depends on the recovery function. It is shown that x_1 is converged to the better state by the robot rehabilitation steps.

5.4 Point-to-point motion simulation with proposed controller and results

In this chapter, two simulations using the controller is described. Our system is applied to a reaching motion control of the patient and the robot. The patient moves his/her operating point from an initial position to his/her reference position. At that time, the robot gradually changes its operating point in order to support the patient during the motion according to the robot rehabilitation strategy.

The first simulation demonstrates that the controller can improve the patient's state stably. The second simulation demonstrates that the proposed robot rehabilitation strategy is realized even if the controller is used intermittently in each training session, similar to rehabilitation training.

The masses are $m_1 = 1.0, m_2 = 1.0$. The spring constant is $k = 50.0$. The gains are $k_{p1} = 1.0, k_{d1} = 3.0, k_{p2} = 1.0, k_{d2} = 3.0, k_{t1} = 2.5 \times 10^{-4}$, and $k_{t2} = 1.0 \times 10^{-5}$. The references are $x_{1ref} = 1.5$ and $x_{2ref} = 0.0$. The direction of the support force is defined as the direction in which the position of the patient changes. To apply positive

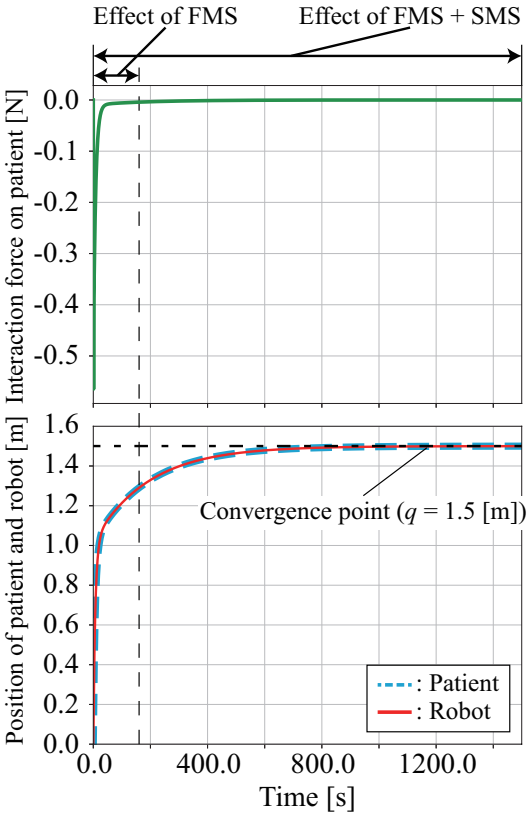

Fig. 5.3: Time series of the positions of the patient and robot using the controller in a continuous simulation (bottom), and a time series of the interaction force on the patient (top). In this simulation, recovery speed k_t is set to 5.0×10^{-6}, inhibition of the recovery C is set as 0.5 [m], and recovery potential q is set as 1.5 [m]. The interaction force on the patient quickly decreases to zero, and this is the effect of the FMS that adapts the robot to the patient. The patient and robot gradually converge to 1.5 $[m]$, and this is the combined effect of the FMS and SMS that improves the patient's state. These results show that our system is stable.

force of $0.1[N]$ on the patient to change their position, $p = 0.05$, and p is decided by trial and error.

The recovery function is designed as

$$\mu = h(x_1) = k_t \int (q - x_1)\, dt - C. \tag{5.56}$$

This function satisfies the condition of Eq. (5.3). k_t represents the speed of the recovery to q, that is, the recovery speed. q represents the patient recovery potential. C is a constant that represents the extent of the inhibition of the patient's movement.

In this chapter, enhancing the motion of human beings is focused on, especially

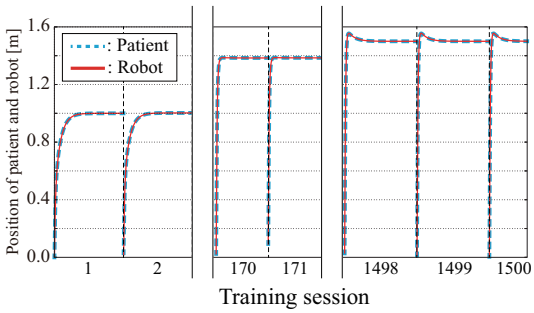

(a) Time series of the positions of the patient and robot with $k_t = 5.0 \times 10^{-4}$ and $q = 1.5$ in the recovery function

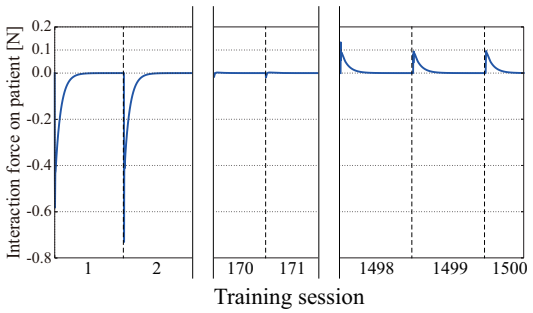

(b) Time series of the interaction force on the patient with $k_t = 5.0 \times 10^{-4}$ and $q = 1.5$ in the recovery function

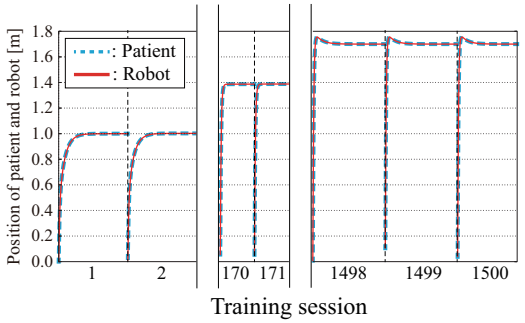

(c) Time series of the positions of the patient and robot with $k_t = 3.0 \times 10^{-4}$ and $q = 1.7$ in the recovery function

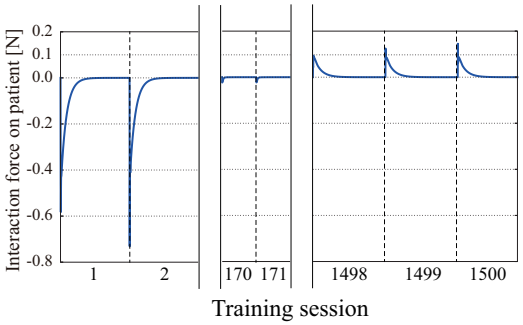

(d) Time series of the interaction force on the patient with $k_t = 3.0 \times 10^{-4}$ and $q = 1.7$ in the recovery function

Fig. 5.4: Effects of using the controller intermittently on motion and interaction force in each session: (a) Time series of the positions of the patient and robot with $k_t = 5.0 \times 10^{-4}$ and $q = 1.5$ in the recovery function. The robot moves to follow the motion of the patient based on adaptation loop ζ, gradually changing its behavior to support the motion of the patient. (b) Time series of the interaction force on the patient with $k_t = 5.0 \times 10^{-4}$ and $q = 1.5$ in the recovery function. The patient initially receives a negative force, but the robot gradually changes its behavior to apply a positive force to support the motion of the patient. (c) Time series of the positions of the patient and robot with $k_t = 3.0 \times 10^{-4}$ and $q = 1.7$ in the recovery function. (d) Time series of the interaction force on the patient with $k_t = 3.0 \times 10^{-4}$ and $q = 1.7$ in the recovery function. These figures show that even if the coefficients are different, the controller can cope with the difference.

post-stroke patients base on Neuro-synergy model. Since it is the simulation, the mean value of the time taken for one control cycle is calculated as the time required for automatic motion generation. A computer used in this study has 16.0 GB memory

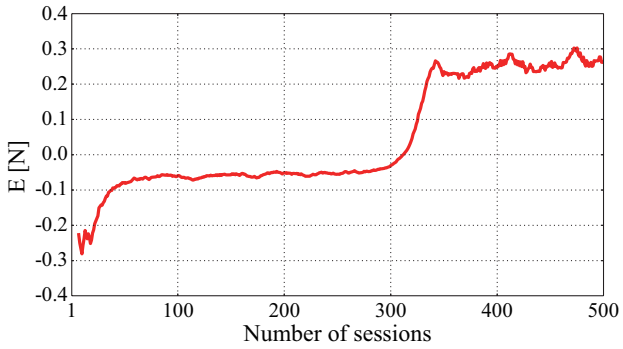

Fig. 5.5: Summation of $\tau_2 - \tau_1$ when τ_2 and τ_1 are both positive in each session when $k_{t1} = 2.5 \times 10^{-4}$ and $k_{t2} = 1.0 \times 10^{-5}$. Recovery speed k_t is set to 5.0×10^{-6}, inhibition of the recovery C is set as 0.5 [m], and recovery potential q is set as 1.5 [m]. The value of E is the negative value in the early stage of the session and gradually becomes the positive value as the session goes on, suggesting that the torque of the robot is not large enough to support the motion of the patient, but it gradually becomes larger than that of the patient and supports the motion of the patient. This shows the robot gradually changes its motion to support the patient when the patient attempts to move forward.

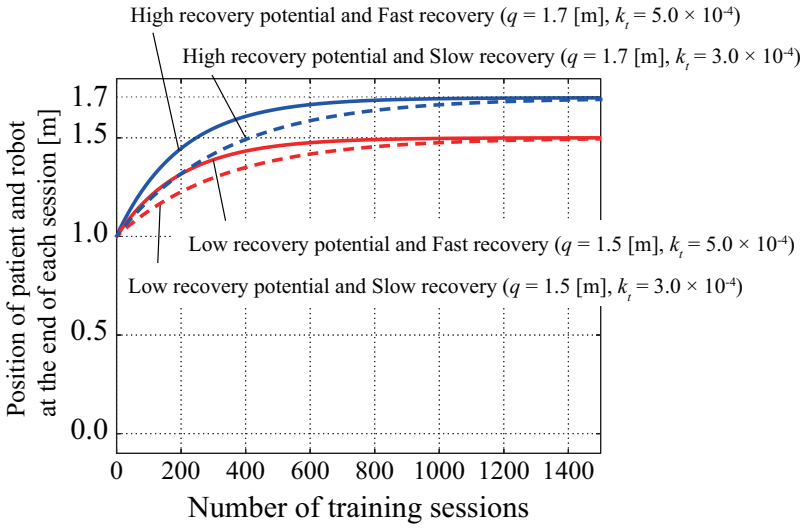

Fig. 5.6: Difference in changes of final position of the patient and the robot in each training session in intermittently using proposed controller. After starting the simulation, the robot quickly adapts to the patient, and then the robot gradually changes its behavior to support the patient at the end of each session. It shows that even if the potential of the patient recovery q and the extent of a recovery speed k_t are different from patient to patient, the proposed controller can deal with that difference.

and Intel® Core™ i7-8565U CPU @ 1.80 GHz 1.99 GHz, and python2.7 is installed. The mean value of the time required for automatic motion generation is 2.8×10^{-4} [s].

This result is faster than previous results. It is thought that the model is simple, and the performance of the computer is high.

5.4.1 Point-to-point motion simulation to show stability of whole system

k_t is set as 5.0×10^{-6}, q is set as 1.5, and C is set as 0.5. Figure 5.3 shows the time series of the position of the robot and the patient using the controller and the time series of the interaction force on the patient.

Initially, the interaction force on the patient quickly decreases to zero, owing to the effect of the FMS that adapts the robot to the patient. The patient and robot gradually converge to 1.5 through the combined effect of the FMS and SMS that improves the patient's state. These results show that the system is stable.

5.4.2 Point-to-point motion simulation in intermittently using proposed controller for training sessions

This simulation is conducted as follows.

1. The patient and the robot are placed in the same position.
2. The patient moves horizontally and the robot provides adaptation and support based on the controller.
3. The simulation is ended when $\dot{x}_1$ and $\dot{x}_2$ become smaller than 1.0×10^{-6}.
4. Values except for ξ and μ are set to the initial values, re-starting the simulation from (1).

One cycle from steps (1) to (4) is defined as one training session in the rehabilitation. The value of μ is updated at the completion of each cycle. $k_t = 5.0 \times 10^{-4}$ and $k_t = 3.0 \times 10^{-4}$ are used. It is bigger than previous simulation because the update of μ at the completion of each cycle.

Figure 5.4 shows that influence of using the controller intermittently on motion and interaction force in each session. Figure 5.4(a) is time series of position of the

patient and the robot with $k_t = 5.0 \times 10^{-4}$ and $q = 1.5[m]$ in recovery function. The patient moves his/her operating point from the initial position ($0.0[m]$) to the reference position that is $x_P = 1.0[m]$ in the early session, and the robot also converges to same position of the patient thanks to the adaptation loop ζ. Figure 5.4(b) is time series of interaction force on patient with $k_t = 5.0 \times 10^{-4}$ and $q = 1.5[m]$ in recovery function. The robot moves to follow the motion of the patient thanks to the adaptation loop ζ, gradually changing its behavior to support the motion of the patient thanks to the support loop ξ. The patient gets negative force at first, but the robot gradually changes its behavior to apply positive force on the patient to support the motion of the patient.

Figure 5.4(c) is time series of position of patient and robot with $k_t = 3.0 \times 10^{-4}$ and $q = 1.7[m]$ in recovery function. Figure 5.4(d) is time series of interaction force on patient with $k_t = 3.0 \times 10^{-4}$ and $q = 1.7[m]$ in recovery function. These figures show that even if the coefficients are different, the controller can cope with the difference.

Figure 5.5 is the summation E of the difference between the torque of the patient and the torque of the robot when these torques are both positive in each session. E is calculated from

$$E = \begin{cases} 0 & (sign(\tau_2) \neq sign(\tau_1)) \\ \int_{t_s}^{t_e} \tau_2 - \tau_1 dt & (\tau_1 > 0 \ and \ \tau_2 > 0) \end{cases}, \tag{5.57}$$

when t_s is the time of the start of the session, and t_e is the time of the end of the session. The value of E is zero at the start of each session. A red line in Fig. 5.5 means the average of E calculated when 14 sessions window is moved to the right one session by one session. In the early stage of the session, E is the negative value, suggesting that the torque of the robotτ_2 is not large enough to support the motion of the patient. However, E gradually become the positive value as the session goes on, suggesting that the torque of the robotτ_2 becomes larger than that of the patient. In order for the robot to support the patient, the torque of the robot should be larger than the torque of the patient at least when the patient attempts to move forward, in other ward, the torque of the patient is positive. This result shows the robot gradually changes its motion to support the patient when the patient attempts to move forward.

Figure 5.6 shows the difference in the changes in the final position of the patient and the robot in each training session when the controller is used intermittently for

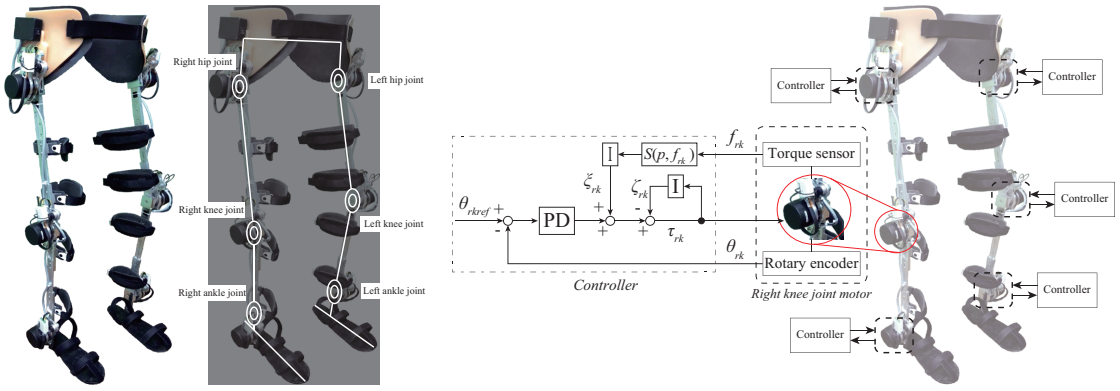

(a) Lower limb exoskeleton robot (b) Block diagram for exoskeleton robot

Fig. 5.7: (a) Lower limb exoskeleton robot. (b) Block diagram for exoskeleton robot(see Chapter 5.5 for details).

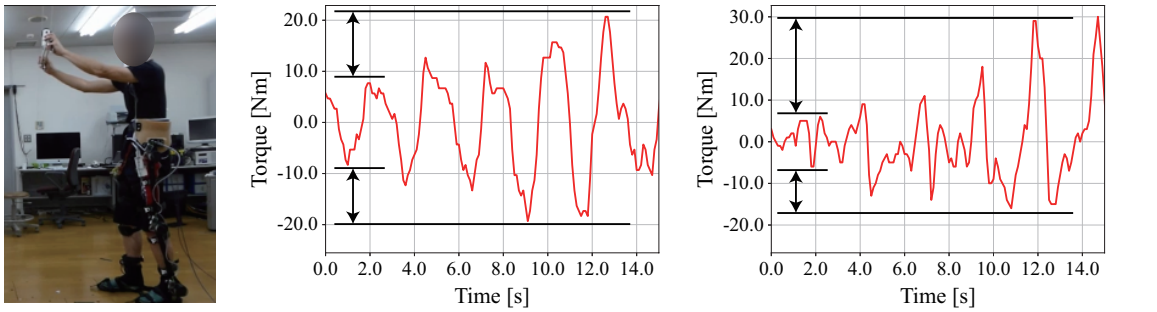

(a) Overview of walking experiment (b) Torque on left hip joint of lower limb exoskeleton robot (c) Torque on left knee joint of lower limb exoskeleton robot

Fig. 5.8: Overview and time series of torques in walking experiment. (a) Overview of walking experiment. (b) Torque on left hip joint of lower limb exoskeleton robot. (c) Torque on left knee joint of lower limb exoskeleton robot. It is shown that both torque can be increased during the action.

training sessions. Figure 5.6 indicates even if the patient recovery potential, q, and the recovery speed, k_t, are different from patient to patient, the controller can handle differences in q and k_t between patients.

5.5 Walking experiment with exoskeleton robot

In this chapter, it is shown how to use the proposed system to a lower limb exoskeleton robot. In addition to that, the validity of the model is indirectly shown by showing the effectiveness of the system in controlling the lower limb exoskeleton robot, which is designed using the model. Six DoF exoskeleton robot called H2 [149] is used

as shown in Fig. 5.7(a). Each joint of H2 has an actuator with a torque sensor and a rotary encoder. Five healthy males participate in the experiment, and subjects wear the exoskeleton robot and walk 5.0 [m] with the exoskeleton robot. The change of the torque of the robot is measured in actuators.

In this experiment, the mean value of the time required for automatic motion generation could not be calculated. After conducting the experiment, H2 was returned to the university in Spain. Therefore, the experiment could not be conducted again for calculating the mean value of the time.

5.5.1 Walking controller for exoskeleton robot to realize robot rehabilitation strategy

Figure 5.7 shows controllers for the exoskeleton robot. Term $\boldsymbol{\theta} \in \boldsymbol{R}^6$ is vectors of state variables of the exoskeleton robot. Term $\boldsymbol{\theta}_{ref} \in \boldsymbol{R}^6$ is a vector of angle references for the exoskeleton robot, and the same joint trajectories as trajectories in Fig. 1.4 is used for $\boldsymbol{\theta}_{ref}$. The torque vector $\hat{\boldsymbol{\tau}} \in \boldsymbol{R}^6$ for each joint is represented as

$$\boldsymbol{\tau} = \boldsymbol{A}(\boldsymbol{\theta}_{ref} - \boldsymbol{\theta}) - \boldsymbol{B}\dot{\boldsymbol{\theta}} + \boldsymbol{\xi} - \boldsymbol{\zeta}, \tag{5.58}$$

$$\dot{\boldsymbol{\zeta}} = \boldsymbol{C}\boldsymbol{\tau}, \tag{5.59}$$

$$\boldsymbol{\theta} = \begin{bmatrix} \theta_{lh} & \theta_{lk} & \theta_{la} & \theta_{rh} & \theta_{rk} & \theta_{ra} \end{bmatrix}^T, \boldsymbol{\theta}_{ref} = \begin{bmatrix} \theta_{lhref} & \cdots & \theta_{raref} \end{bmatrix}^T, \tag{5.60}$$

$$\boldsymbol{f} = \begin{bmatrix} f_{lh} & \cdots & f_{ra} \end{bmatrix}^T, \boldsymbol{\xi} = \begin{bmatrix} \xi_{lh} & \cdots & \xi_{ra} \end{bmatrix}^T, \boldsymbol{\zeta} = \begin{bmatrix} \zeta_{lh} & \cdots & \zeta_{ra} \end{bmatrix}^T, \tag{5.61}$$

where $\boldsymbol{f}$ is a vector consisting of torques created by the wearer, and it plays the role of the interaction force in Fig. 5.2. $\boldsymbol{\zeta}$ is a vector consisting of the integral values of tacit learning that is as same as the adapting loop used in the simulation. $\boldsymbol{\xi}$ is a vector consisting of torques and used as the role of the supporting loop in the simulation.

Term $\boldsymbol{A}$, $\boldsymbol{B}$, and $\boldsymbol{C}$ are diagonal matrices:

$$\boldsymbol{A} = diag(\begin{bmatrix} k_{p1} & \cdots & k_{p6} \end{bmatrix}), \tag{5.62}$$

$$\boldsymbol{B} = diag(\begin{bmatrix} k_{d1} & \cdots & k_{d6} \end{bmatrix}), \tag{5.63}$$

$$\boldsymbol{C} = diag(\begin{bmatrix} k_{i1} & \cdots & k_{i6} \end{bmatrix}), \tag{5.64}$$

where $k_{p1} \cdots k_{p6}$ are proportional (P) gains set as 10, and $k_{d1} \cdots k_{d6}$ are derivative (D) gains set as 0.1. $k_{i1} \cdots k_{i6}$ are coefficients of the adapting loop decided by the subject as a coefficient easy to walk. In the stability study, these coefficients should be smaller than a value calculated from the coefficients of the subjects in order for the system to be stable. In many cases, it is difficult to estimate biological coefficients, but at least, the system will be stable when the coefficients of the adapting loop are small. In this case, the coefficients of the adapting loop are set as 1.0×10^{-2}. The subject can stop the motion of the exoskeleton robot as soon as possible when the subject feels discomfort.

5.5.2 Walking results with healthy subjects

The subjects were asked to just walk with the exoskeleton robot. Figure 5.8(a) is an example of an overview in the experiment. All subjects did not lose balance at the beginning of walking like Fig. 1.4(b), suggesting there is small conflict between the robot motion and human motion intention. Subjects could walk with the exoskeleton robot properly.

Figure 5.8(b)(c) are time series of the torque of a left knee joint and the torque of a left hip joint of the exoskeleton robot when one subject walks, and each torque is set so that the average becomes zero. You can see that the torque of the left knee joint and the left hip joint of the exoskeleton robot is gradually increasing. After the experiment, the subjects said that they did not feel the disturbance from the robot in the early stage of the experiment and feel that the support force from the robot gradually increased. This result and subjects' opinions suggest that there is small conflict between the robot motion and human motion intention.

5.5.3 Discussion of Walking Experiment

In the experiment, by using the system, the exoskeleton robot could change its motion. The subject did not feel the disturbance from the robot in the early stage of the experiment and feel that the support force from the robot gradually increased.

As it is written before, the proposed model represents the recovery capability of human beings. In other words, it is considered to be the capability of changing subjects' motion, for instance, increasing the stride length in walking. Because the proposed model can represent that feature, the system designed based on the model can appropriately support the subject in response to the motion changing in the experiment, then the subject can conduct the rehabilitation training without feeling big conflict.

The extent of the recovery capability strongly depends on patients, but all patients may have small or big recovery capability. In that case, the patients will be able to recover from the motion paralysis by the rehabilitation training with supporting. In addition to that, by using our system, the patient will recover from the motion paralysis with not feeling the stress and feeling that he/she just conducts walking training.

5.6 Conclusion

In this chapter, the theoretical basis for robot rehabilitation was proposed. An important issue in robot rehabilitation was clarified based on a previous failure in our experiments and proposed a robot rehabilitation process.

A possible controller was discussed to complete the proposed rehabilitation steps based on two assumptions about paralysis and recovery. The theoretical analysis showed that the controller can adapt the robot motion to the patient motions in the first step of the rehabilitation, improve the state of the patient, and finally converge to the recovery state.

Two motion simulations were conducted using the controller to demonstrate that the controller stably improves the patient state and that the proposed rehabilitation steps were achieved with the controller, even if the controller was used intermittently for training sessions, similar to actual rehabilitation training. The simulations showed that the controller was stable when it was used both continuously and intermittently. In addition, the controller, which included an adaptation loop and support loop, provided the force support for the patient, which was not achieved with only an adaptation loop in the BioMot Project.

Chapter 6

Conclusion

6.1 Conclusion of doctoral dissertation

Our research motivation was to develop the robot could be the good partner for helping human beings. It was considered that in order for the robot to be the partner robot, it is not enough for the robot to generate its action from the symbolized action purpose such as “Walk”, “Go to station”, and “Cook”. In addition to that ability, it was considered that the robot needed to support the motion of human beings without disturbing the motion. Therefore, in this study, we aimed to establish technologies for the robot to automatically generate the detailed control signals from the symbolized action purposes and to promote human actions by the support, especially for the post-stroke patients.

Human beings have naturally achieved the motion generation and the motion support. Human activities are generated based on the biological information processing structure. Therefore we thought that it was better to develop methods realizing the motion generation and the motion support by imitating the biological information processing structure of human beings. That is, in order for the robot to generate the action from the symbolized action purpose like human beings, it is reasonable to develop the control method by imitating the biological information processing structure. In addition to that, it is necessary to to develop the support method to promote the human action based on understanding what kind of reaction human beings do based

on the biological information processing structure.

In this Ph.D. dissertation, the biological information processing structure was modeled as Neuro-synergy model. Neuro-synergy model was a model consisting of multi layers. The essence of Neuro-synergy model is that the action is generated from the combination of the top-down process and the bottom-up process. The top-down process is that the symbolized action purpose is gradually divided into detail control signals to the muscles. The bottom-up process is that the feedback control loops in each layer work to adjust the signals to adapt the body to the environment. The motion generation research and the motion support research were conducted based on the scheme of Neuro-synergy model from the aspects of the robot side and the human side.

6.1.1 Robot motion generation study based on Neuro-synergy model

In the robotics research, it was attempted to clarify the mechanisms of automatically generating motor commands from the symbolized action purpose, that is, the low-dimensional control signals. This problem was addressed by developing the artificial controller that embodied a mechanism generating motor commands from the low-dimensional control signals. From the view point of Neuro-synergy model, human beings make the action with two way, the first is to select the appropriate behavior that progresses in a top-down manner, and the second is to adjust the behavior according to the environment, which is a bottom-up process that progresses through body–environment interactions.

To clarify the effect of the bottom-up process on a robot motion control, the standing balance control of the two DoF inverted pendulum was studied. The control signals to each joint were transferred to another space computed using the mechanical resonance mode. Tacit learning was applied in MRM-space as the feedback control loops. The pendulum maintained standing against from small disturbance to big disturbance by using the controller designed using tacit learning and the mechanical resonance mode. The results of the simulation and experiment showed that the capability of

the standing balance was increased when the robot was controlled with MRM-space. It suggests that the simple adaptation mechanism working as the feedback control loops is enough to enhance the performance of standing balance when behavior control is conducted in a space where the direction of behavior can be set according to the disturbance. The similarities between the modes of the two DoF inverted pendulum and human's hip/ankle strategies also indicate the importance of dealing with various disturbances in the space in which physical features of the robot are well represented.

To clarify the effect of the top-down process and the bottom-up process on a robot motion control, the bipedal walking control of 27 DoF humanoid robot and NAO were studied. To represent the top-down process in which the action purpose was selected, the appropriate mechanical resonance mode for adjusting was chosen to achieve the desired motion. In walking simulations and experiments, the humanoid robot and NAO changed the walking motion to walk forward/backward and turn left/right while maintaining walking balance when the parameters of the first mode and the eighth mode were manually adjusted. From the view point of selecting the mode and changing the action, the signals added to the specified mode control can be considered as the top-down process. Walking balance was maintained by tacit learning which was applying in [81] to joint space in the same way as two DoF inverted pendulum control as a bottom-up process.

The purpose of this study was not to control robot walking but to generate the motion from adjusting the low-dimensional control signals. In the study of walking, the ZMP normative walking is the major method, and the smoothness and speed of walking is better than our method. However, walking using the mode and tacit learning has an advantage. It is that the motion of the whole body can be automatically generated by using the mode, unlike the ZMP normative walking which determines the position to put the foot from the center of gravity position. In other words, even when maintaining balance on a slope, the robot will be balanced in the whole body like a human being by using the mode. If the walking control using the modes is further studied, the walking motion that is potentially present in robot dynamics will be derived, which is different from ZMP approach.

These results suggest that transferring the signals to the appropriate control space

is the key process for reducing the complexity of the signals from the environment, and activating the feedback control loops in each space makes it possible to realize the symbolized action purpose. On the other hand, the application scope of this scheme, that is, the control using the mechanical resonance mode and tacit learning, must be discussed. In this study, this control method was applied from a robot with a small degree of freedom to a robot with a large degree of freedom(the two DoF inverted pendulum and the 27 DoF humanoid robot). From the viewpoint of a mechanism of the robot, the application scope will be a wide, but it is limited to cases where the target motion and mode are clearly known.

It is needed to decide a target motion in advance and to visually select the modes that seems to contribute to the target motion. From the result of simulations and experiments, by using the mode and tacit learning, the robot becomes robust against the disturbance and can change its motion with the adjustment of a few parameters. In order to apply this method to more wide variety robots and motions, a method is needed to be established, which is to automatically select and adjust the parameter of the modes to achieve the target motion by using such as reinforce learning or deep neural network. If such steps are to be more accumulated to form a larger network as Neuro-synergy model, various behaviors of the robot can be controlled from the more-symbolized action target such as “Go to the station.”

6.1.2 Human motion support study based on Neuro-synergy model

In the human side research, the support method was aimed to be proposed to enhance the motion of human beings, especially the post-stroke patients in this study. The robotic research showed that simultaneous activation of the symbolized action purpose and the feedback control loop in Neuro-synergy model was a key factor to generate the action. The motion support method for the post-stroke patient was developed based on this scheme.

The post-stroke patient has suffered from the motion paralysis because they got the damage in the part of a primary motor cortex. In many cases, they can make the

intention to move, but the action cannot be generated, suggesting that the top-down process in Neuro-synergy model of the patient does not works well to generate the detail control signals to the muscles. In general, the rehabilitation training, that is, the intervention of the therapists to the patients' motion is necessary for the patients to recover from the motion paralysis.

Simply speaking, the patient will be able to generate the voluntary action again when an appropriate neural network among the sensory area, the part of the brain playing the role of the intention, and the part surrounding the damaged motor area can be formed to bypass the damaged motor area. Almost rehabilitation training for the motion paralysis have been proposed to form the appropriate neural network since a long-long time ago.

Forming the appropriate neural network is, in some sense, the result of learning. The living things can acquire skilled actions after learning, and it is known that Hebb's rule underlies that process. Hebb's rule is a simple rule of learning in neuro-science, which is that the connectivity among the neurons becomes strong when the neurons fire simultaneously. Therefore, if the sensory area, the part playing the role of the intention, and the part surrounding the damaged motor area activate simultaneously, the connection among them becomes strong, then a network that is not affected by damage is formed. Such rehabilitation training intended to strengthen the connection between neurons is called as neuro-rehabilitation.

It is difficult to activate the sensory area from the muscle activities because the patient cannot generate the muscle activities with the intention. However, from the view point of Neuro-synergy model, even though the motor cortex gets the damage, the feedback control loops seem not to get the damage. Therefore, if the feedback control loops can be intervened by a physical support, the patient will generate a reactive motion, that is, the muscle activities. It can be thought that the un-functional neural network is not formed by using reactive motion to activate the sensory area because feedback control loops originally exist in the patients. From that point of view, the support method of neuro-rehabilitation was developed based on Neuro-synergy model to promote the motion of the post-stroke patient and to lead the recovery from the motion paralysis by intervening in the feedback control loops.

Two researches were conducted as follows. First, the grasping-training robot was developed, which could activate the grasping motion by intervening the simple feedback control loop. Second, the rehabilitation robot control method was theoretically developed by extending its scheme to more general action.

In the grasping-training robot study, in order to intervene the feedback control loops by the external physical support, the grasping reflex was used. In addition to that, the grasping-training robot was designed to support synergistic grasping that we normally conducted, which consisted of the finger flexion, the wrist extension, and the thumb opposition.

The proposed robot consisted of the four-finger glove with a curving mechanism, the bascule bridge mechanism, the thumb fixer, the shaft, and threads. The threads were connected to the curving mechanism of the glove and the edge of the bascule bridge mechanism. The glove could extend and bend, and the bascule bridge mechanism could down and up repeatedly by pulling the threads with the shaft. The thumb was opposed by the constraint with the thumb fixer as the wrist was extended.

The proposed robot had important features as below. When the robot motion support with intervening the feedback control loop was applied to the post-stroke patient, sEMG signals were detected from the paralyzed hand. These results indicated that appropriate motion support and the grasping of an elastic bar could induced the grasping reflex of the patients.

In the research of the theoretical approach, the scheme of intervening the feedback control loops of the post-stroke patients was expanded to more general action. The robot control system should be designed to support the patient even though patients' recovery potential and recovery speed are different in each patient. In particular, not knowing how much the patient recovers makes it difficult to design the rehabilitation robot controller. It was established that the robot rehabilitation strategy through clinical tests of walking with the exoskeleton robot, which is to gradually support the action while maintaining the activation of the feedback control loops.

For theoretical analysis, the robot controller was discussed to achieve the rehabilitation strategy based on two assumptions about paralysis and recovery and modeled the recovery of the patient. The theoretical analysis showed that the controller can

adapt the robot motion to the patient motions in the first step of the rehabilitation, improve the state of the patient, and finally converge to the recovery state.

The simulations showed that the controller was stable when it was used both continuously and intermittently. In addition to that, the controller could realize the robot rehabilitation strategy even if there are differences between patients. In addition to that, the experiment was conducted to verify the validity of the proposed controller by using the lower limb exoskeleton. From the stability study, it was showed that the robot would be stable when the coefficient of the adaptive loop was small. The coefficient of the adaptive loop of the exoskeleton robot was set based on that result. The robot could work maintaining the stable, and the subject said that they did not feel the disturbance from the robot in the early stage of the experiment and feel that the support force from the robot gradually increased.

6.1.3 Discussion of motion generation study and motion support study

(i) Looking at motion generation study from motion support study

The motion support study suggested that intervention to the feedback control loop by the physical support realized to promote the motion, and it is necessary to intervene to specific feedback control loops in order to promote specific motion. For instance, in case of the grasping rehabilitation, the grasping reflex was induced in order to promote grasping.

In case of the motion generation, it can be understood that interaction force between the robot and the environment plays the role of the intervention to the feedback control loops. The interaction force is changed by the change of the motion with adjusting the variables in the MRM space. Therefore, in order to promote specific motions of the robot, it is necessary to carefully adjust the variables in the MRM space to intervene to specific feedback control loops. For instance, the robot could walk forward/backward and turn left/right because appropriate variables in MRM space was adjusted.

In the motion support, because the grasping motion was the target, the feedback

control loop to intervene was identified. In case of the robot, however, even if the target motion is decided, it is difficult to decide the variables in MRM space to adjust from the target motion. Therefore, it is better to make a database of motions based on the fact that the motion is achieved by intervening the feedback control loops with adjusting some variables in MRM space. If it is possible, the robot will be able to perform wide variety actions like human beings.

(ii) Looking at motion support study from motion generation study

The motion generation study suggested that simultaneous activating the symbolized action purpose and the feedback control loops realized the motion generation. At that time, the joint motions could be generated from the adjustment of a few parameters by using the mechanical resonance mode calculated from the physical features of the robot.

In the motion support study, it can be understood that the physical support contributes to the activation of the feedback control loops, and the target motion of the rehabilitation plays the role of the symbolized action purpose. However, unlike the case of robots, it is difficult to promote complex motions such as turning, as long as the motion is promoted intervening to the feedback control loops by the physical support.

It is necessary to create new support method that can induce motion patterns based on the physical feature of the patient. From the robot study, one solution is to create the method based on the mechanical resonance mode estimated from the physical feature of the patient. If it is possible, the patient can conduct an effective rehabilitation training to restore the complex motion.

(iii) Common between motion generation study and motion support study

The above is the conclusions when looking at each study from each other's point of view. On the other hand, when looking at an essence common to each study, the essence underlying the motion generation and the motion support is to selectively intervene to the feedback control loops, although there is a difference between the intrinsic factor and the extrinsic factor. In case of the motion generation, the intrinsic factor such as the symbolized action purpose intervenes in the feedback control loops as the result

of the action output. In case of the motion support, the extrinsic factor such as the physical support intervenes in the feedback control loops directory. That is, simple functional action could be realized by utilizing and intervening the feedback control loops in both robots and post-stroke patients in this study.

It is expected that more complicated functional action can be realized by integrating multiple simple functional actions by combining with top-down processes. Of course, since the robot motion generated from the symbolized action purpose must be a motion that promotes the human motion, a task is remained which designs robot's feedback control loops to generate the motion promoting the human motion. However, the robot will be a better partner for human, if the human and the robot could share the same objective for a task completion, carry out a portion of that task and adjust their tasks based on the progress of their sub-task checked each other.

6.2 Future work

Future works for each study are enumerated before global future work. There are three future works.

First, it is about the generation of the robot action form the symbolized action purpose. It is reasoned that the extent to which a symbolized target that is represented by the lower-dimensional signals is used to create the robot behavior is the critical assessment for evaluating the extent to which the robot behavior is human-like. The results in this research are just one step up from pure motor-control signals, implying far from human-like behavior. Further discussion is required to elevate the proposed system to using more-symbolized action targets such as "Go to the station." A key problem is automatic creation of the mechanical resonance mode. Non-linear transfer for more complicated environment is another important problem. Even in the control of human behavior, the process of creating muscle synergy remains mysterious. We are now on the way to clarifying the process to a more hierarchical system in both physiological and artificial ways.

Second, it is about the grasping-training robot. As discussed in Chapter 4.1, inducing the grasping reflex is one factor constituting the grasp training. In addition, a

system is required to stimulate motion intention at the same time that the grasping reflex is stimulated. A virtual reality system is currently developed for stimulating motion intention. Further discussions are required from the perspective of clinical applications, such as how much time is acceptable clinically for setting up the robot. However, it is impossible to discuss such detailed clinical issues without a proposal for a complete system and associated in-depth training plans. Once the whole system has been developed, detailed discussions with clinicians should be conducted.

Third, it is about the theoretical approach of the rehabilitation robot control. There were fundamental assumptions in the patient model. For instance, there are many types of paralysis and recovery is not monotonic like the results in the simulations. Therefore, the controller is need to be fine-tuned to fit to each patient's condition, however the discussion in this research provides a starting point for robot rehabilitation because all states are modeled simply as an ideal state. The model should be tuned based on the patients and the rehabilitation targets to adapt the monotonic situation to the real target. For instance, the recovery function reflecting the real state should be used. A discussion is currently conducted to fit real situations.

As said in Chapter 1, it is considered that if the post-stroke patient and the robot can share the top-down signal and generate the action respond to not only the environment but also each action instead of generating each action from each top-down signal, the robot will be closer to the post-stroke patient. In this study, technologies were established for the robot to automatically generate the detailed control signals from the symbolized action purposes and to enhance human actions. There is no doubt that the above three future works are important for making the robot being the partner and should be solved. However, it will be discuss that not such detailed future works but more extensive future work here.

The definition of the partner in this study is a thing sharing same objective, cooperating with human beings to achieve the objective, and working for helping to enrich the human life. From the view point of the definition, the partner is not limited to the robot, but it can extend to the space around human beings, moreover to a social system. In other words, it is possible for a house, a town, a city, and a prefecture such kind of environment around human beings to be included in the category of the

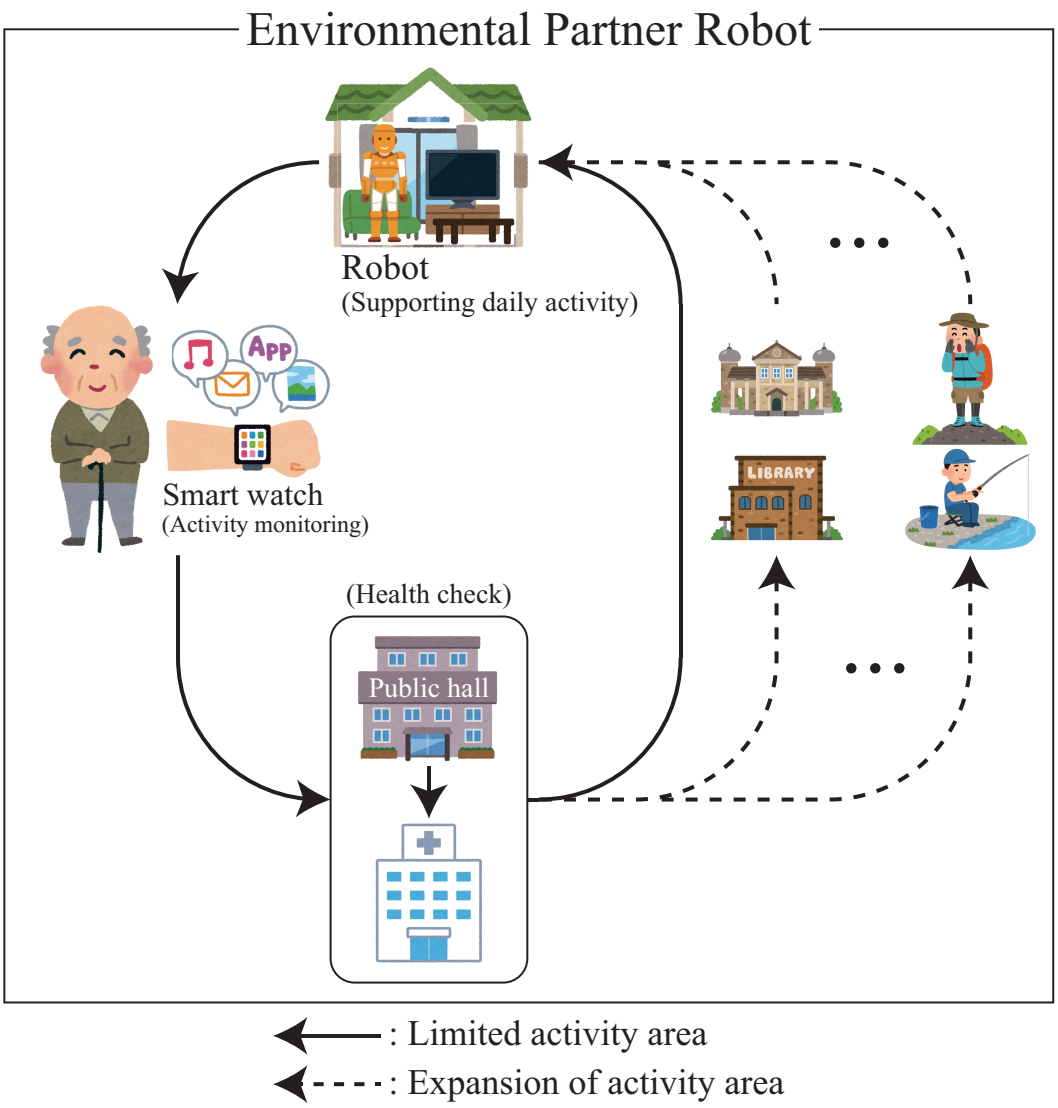

Fig. 6.1: Overview of environmental partner robot. In this case, the elderly people equip with a device such as a smart watch, assuming the smart watch to estimate the symbolized action purpose based on measured signals. In addition to that, the smart watch records elderly people's behavior and vital data, and the elderly people get health check and health advice in public halls and hospitals based on the daily health data. While repeating the round trip between the house and the public hall or the hospital, the environmental-partner robot estimates the preference of the elderly people from the daily activities and provides information in order to gradually expand the activity area

partner robot. In order for all human beings to benefit from the partner robot, we consider that it is necessary for the environment to perform as the partner robot.

What the environment becomes the partner does not mean that the environment

is embedded in Internet of Things(IoT), and people can easily access the environment. The environment actively effects on human being to maximize what human beings can do like the partner robot. We will call such kind of environment as environmental partner robot.

If it will be possible, the life will be unknowingly enriched just living in that environment. When we feel sleepy, it will recommend a cup of coffee, or when we feel cold, it will adjust the degree of an air conditioner, or when we get signs of illness, it will make a reservation for the hospital. It is like having an invisible partner robot nearby. Especially, elderly people will be able to benefit from it.

Figure 6.1 shows one example of the activity of elderly people in the environment supporting the elderly people. In this case, the elderly people equip with a device such as a smart watch, assuming the smart watch to estimate the symbolized action purpose based on measured signals. The smart watch records elderly people's behavior and vital data, and the elderly people get health check and health advice in public halls and hospitals based on the daily health data. While repeating the round trip between the house and the public hall or the hospital, the environmental partner robot estimates the preference of the elderly people from the daily activities and provides information in order to gradually expand the activity area(dots arrows in Fig. 6.1).

This is nothing less than enhancing human activity by the support, and it is an important role as the partner robot. In many cases, the elderly people live in constant area, and the decline of their body reduces what they can do. To increase the well-being of not only the elderly people but also people around the elderly people, not only the local viewpoint of the partner robot but also the introspective viewpoint of the environmental-partner robot will be necessary. We keep researching about the partner robot and aim for realizing the environmental partner robot.

Publication list

I. Journal paper

1. Shotaro Okajima, Maxime Tournier, Fady S. Alnajjar, Mitsuhiro Hayashibe, Yasuhisa Hasegawa, and Shingo Shimoda, "Generation of Human-Like Movement from Symbolized Information", Frontiers in Neurorobotics, Vol. 12, pp. 43-55, (2018).

2. Shotaro Okajima, Fady S. Alnajjar, Álvaro Costa-García, Guillermo Asin-Prieto, Jose L. Pons, Juan C. Moreno, Yasuhisa Hasegawa, and Shingo Shimoda, "Theoretical Approach for Designing the Rehabilitation Robot Controller", pp. 1-13, Advanced Robotics, Published online:
05 Jul 2019 doi.org/10.1080/01691864.2019.1633402.

II. International conference

1. Shotaro Okajima, Shingo Shimoda, and Yasuhisa Hasegawa, "Acquisition of Adaptive Behavior of Robot through Bow-tie structure", 2016 Joint IEEE International Conference on Development and Learning and Epigenetic Robotics (ICDL-EpiRob), September 19-22, p. 156-157 (2016).

2. Shotaro Okajima, Fady S. Alnajjar, Hiroshi Yamasaki, Matti Itkonen, Álvaro Costa-García, Yasuhisa Hasegawa, and Shingo Shimoda, "Grasp-training Robot to Activate Neural Control Loop for Reflex and Experimental Verification", 2018 IEEE International Conference on Robotics and Automation (ICRA), May 21-25, pp. 1849-1854 (2018).

3. Shotaro Okajima, Fady S. Alnajjar, Yasuhisa Hasegawa, and Shingo Shimoda, "Cooperative Movement in Grasping and Development of Grasping-training Robot", 2018 International Symposium on Micro-NanoMechatronics and Human Science(From Micro & Nano Scale Systems to Robotics & Mechatronics Systems) Symposium (MHS), Dec. 9-12, (2018).

III. Awards

1. MHS Best Paper Awards, 2018.

Reference

[1] Kawasaki Heavy Industries Ltd. `https://global.kawasaki.com/en/stories/articles/vol59/`.

[2] Marc H Raibert. Legged robots that balance. MIT press, 1986.

[3] Hooshang Hemami and B t Wyman. Modeling and control of constrained dynamic systems with application to biped locomotion in the frontal plane. IEEE Transactions on Automatic Control, 24(4):526–535, 1979.

[4] Suguru Arimoto and Fumio Miyazaki. A hierarchical control scheme for biped robots. Journal of the Robotics Society of Japan, 1(3):167–175, 1983.

[5] Atsuo Takanishi, Masami Ishida, Yoshiaki Yamazaki, and Ichiro Kato. The realization of dynamic walking by the biped walking robot wl-10 rd. Journal of the Robotics Society of Japan, 3(4):325–336, 1985.

[6] Tsutomu Mita, Toru Yamaguchi, Toshio Kashiwase, and Taro Kawase. Realization of a high speed biped using modern control theory. International Journal of Control, 40(1):107–119, 1984.

[7] Syuji KAJITA and Akira KOBAYASHI. Dynamic walk control of a biped robot with potential energy conserving orbit. Transactions of the Society of Instrument and Control Engineers, 23(3):281–287, 1987.

[8] Fumio Miyazaki and Suguru Arimoto. A control theoretic study on dynamical biped locomotion. Journal of Dynamic Systems, Measurement, and Control, 102(4):233–239, 1980.

[9] J Furusho and M Masubuchi. Control of a dynamical biped locomotion system for steady walking. Journal of Dynamic Systems, Measurement, and Control, 108(2):111–118, 1986.

[10] J Furusho and M Masubuchi. A theoretically motivated reduced order model for the control of dynamic biped locomotion. Journal of Dynamic Systems, Measurement, and Control, 109(2):155–163, 1987.

[11] Akihito Sano and Junji Furusho. 3d dynamic walking of biped robot by controlling the angular momentum. Transactions of the Society of Instrument and Control Engineers, 26(4):459–466, 1990.

[12] Ltd. Honda Motor Co. Robot development history. `https://global.honda/innovation/robotics/robot-development-history.html`.

[13] Kazuhito Yokoi, Fumio Kanehiro, Kenji Kaneko, Kiyoshi Fujiwara, Shuji Kajita, and Hirohisa Hirukawa. A honda humanoid robot controlled by aist software. In Proc. of the IEEE-RAS International Conference on Humanoid Robots, pages 259–264, 2001.

[14] Hitoshi Hasunuma, Masami Kobayashi, Hisashi Moriyama, Toshiyuki Itoko, Yoshitaka Yanagihara, Takao Ueno, Kazuhisa Ohya, and Kazuhito Yokoil. A tele-operated humanoid robot drives a lift truck. In Proceedings 2002 IEEE International Conference on Robotics and Automation (Cat. No. 02CH37292), volume 3, pages 2246–2252. IEEE, 2002.

[15] Kenji Kaneko, Fumio Kanehiro, Shuuji Kajita, Kazuhiko Yokoyama, Kazuhiko Akachi, Toshikazu Kawasaki, Shigehiko Ota, and Takakatsu Isozumi. Design of prototype humanoid robotics platform for hrp. In IEEE/RSJ International Conference on Intelligent Robots and Systems, volume 3, pages 2431–2436. IEEE, 2002.

[16] K. Kaneko, F. Kanehiro, S. Kajita, H. Hirukawa, T. Kawasaki, M. Hirata, K. Akachi, and T. Isozumi. Humanoid robot hrp-2. In IEEE International Conference on Robotics and Automation, 2004. Proceedings. ICRA '04. 2004, volume 2, pages 1083–1090. IEEE, 2004.

[17] Kenji Kaneko, Kensuke Harada, Fumio Kanehiro, Go Miyamori, and Kazuhiko Akachi. Humanoid robot hrp-3. In 2008 IEEE/RSJ International Conference on Intelligent Robots and Systems, pages 2471–2478. IEEE, 2008.

[18] Kenji Kaneko, Fumio Kanehiro, Mitsuharu Morisawa, Kazuhiko Akachi, Go Miyamori, Atsushi Hayashi, and Noriyuki Kanehira. Humanoid robot hrp-4-

humanoid robotics platform with lightweight and slim body. In 2011 IEEE/RSJ International Conference on Intelligent Robots and Systems, pages 4400–4407. IEEE, 2011.

[19] Iori Kumagai, Mitsuharu Morisawa, Shin'ichiro Nakaoka, Takeshi Sakaguchi, Hiroshi Kaminaga, Kenji Kaneko, and Fumio Kanehiro. Perception based locomotion system for a humanoid robot with adaptive footstep compensation under task constraints. In 2018 IEEE/RSJ International Conference on Intelligent Robots and Systems (IROS), pages 713–719. IEEE, 2018.

[20] R. Cisneros, M. Benallegue, A. Benallegue, M. Morisawa, H. Audren, P. Gergondet, A. Escande, A. Kheddar, and F. Kanehiro. Robust humanoid control using a qp solver with integral gains. In 2018 IEEE/RSJ International Conference on Intelligent Robots and Systems (IROS), pages 7472–7479, 2018.

[21] K. Kaneko, H. Kaminaga, T. Sakaguchi, S. Kajita, M. Morisawa, I. Kumagai, and F. Kanehiro. Humanoid robot hrp-5p: An electrically actuated humanoid robot with high-power and wide-range joints. IEEE Robotics and Automation Letters, 4(2):1431–1438, 2019.

[22] Masato Hirose and Kenichi Ogawa. Honda humanoid robots development. Philosophical Transactions of the Royal Society A: Mathematical, Physical and Engineering Sciences, 365(1850):11–19, 2006.

[23] Soya Takagi. Toyota partner robots. Journal of the Robotics Society of Japan, 24(2):208–210, 2006.

[24] T-HR3. Toyota motor corporation. `https://global.toyota/en/detail/19666346`.

[25] HSR. Toyota motor corporation. `https://global.toyota/en/detail/8709541/`.

[26] DARPA Robotics Challenge 2015 Program Day01. `https://www.youtube.com/watch?v=QauIL-TKvYU`.

[27] A Compilation of Robots Falling Down at the DARPA Robotics Challenge. https://www.youtube.com/watch?v=g0TaYhjpOfo.

[28] Atlas. Boston dynamics. https://www.bostondynamics.com/atlas.

[29] Handle. Boston dynamics. https://www.bostondynamics.com/handle.

[30] SpotMini. Boston dynamics. https://www.bostondynamics.com/spot-mini.

[31] M. Kanazawa, S. Nozawa, Y. Kakiuchi, Y. Kanemoto, M. Kuroda, K. Okada, M. Inaba, and T. Yoshiike. Robust vertical ladder climbing and transitioning between ladder and catwalk for humanoid robots. In 2015 IEEE/RSJ International Conference on Intelligent Robots and Systems (IROS), pages 2202–2209, 2015.

[32] Takahide Yoshiike, Mitsuhide Kuroda, Ryuma Ujino, Hiroyuki Kaneko, Hirofumi Higuchi, Shingo Iwasaki, Yoshiki Kanemoto, Minami Asatani, and Takeshi Koshiishi. Development of experimental legged robot for inspection and disaster response in plants. In 2017 IEEE/RSJ International Conference on Intelligent Robots and Systems (IROS), pages 4869–4876. IEEE, 2017.

[33] Takumi Kamioka, Hiroyuki Kaneko, Toru Takenaka, and Takahide Yoshiike. Simultaneous optimization of zmp and footsteps based on the analytical solution of divergent component of motion. In 2018 IEEE International Conference on Robotics and Automation (ICRA), pages 1763–1770. IEEE, 2018.

[34] Yoshiki Kanemoto, Takahide Yoshiike, Masaaki Muromachi, and Masahiko Osada. Compact and high performance torque-controlled actuators and its implementation to disaster response robot. In 2018 IEEE International Conference on Robotics and Automation (ICRA), pages 1–7. IEEE, 2018.

[35] Takumi Kamioka, Hiroyuki Kaneko, Mitsunide Kuroda, Chiaki Tanaka, Shinya Shirokura, Masanori Takeda, and Takahide Yoshiike. Dynamic gait transition between walking, running and hopping for push recovery. In 2017 IEEE-RAS 17th International Conference on Humanoid Robotics (Humanoids), pages 1–8. IEEE, 2017.

[36] Kaname Narukawa, Takahide Yoshiike, Kenta Tanaka, and Mitsuhide Kuroda. Real-time collision detection based on one class svm for safe movement of humanoid robot. In 2017 IEEE-RAS 17th International Conference on Humanoid Robotics (Humanoids), pages 791–796. IEEE, 2017.

[37] LBR iiwa. Kuka. `https://www.kuka.com/en-us/products/robotics-systems/industrial-robots/lbr-iiwa`.

[38] Panda. Franka emika. `https://www.franka.de/technology`.

[39] Ming Ding, Ryojun Ikeura, Toshiharu Mukai, Hiromichi Nagashima, Shinya Hirano, Kazuya Matsuo, Minghui Sun, Chang'an Jiang, and Shigeyuki Hosoe. Comfort estimation during lift-up using nursing-care robot riba. In Innovative Engineering Systems (ICIES), 2012 First International Conference on, pages 225–230, 2012.

[40] Kazuyoshi Wada, Takanori Shibata, Tomoko Saito, and Kazuo Tanie. Analysis of factors that bring mental effects to elderly people in robot assisted activity. In IEEE/RSJ International Conference on Intelligent Robots and Systems, volume 2, pages 1152–1157. Ieee, 2002.

[41] Kazuyoshi Wada, Takanori Shibata, Tomoko Saito, and Kazuo Tanie. Effects of robot-assisted activity for elderly people and nurses at a day service center. Proceedings of the IEEE, 92(11):1780–1788, 2004.

[42] Kazue Takayanagi, Takahiro Kirita, and Takanori Shibata. Comparison of verbal and emotional responses of elderly people with mild/moderate dementia and those with severe dementia in responses to seal robot, paro. Frontiers in Aging Neuroscience, 6:257, 2014.

[43] Takanori Shibata. Therapeutic seal robot as biofeedback medical device: Qualitative and quantitative evaluations of robot therapy in dementia care. Proceedings of the IEEE, 100(8):2527–2538, 2012.

[44] Pocobee. Toyota motor corporation. `https://www.toyota-global.com/innovation/partner_robot/robot/`.

[45] Pepper. Softbank group corp. `https://www.softbank.jp/en/robot/`.

[46] Fumihide Tanaka, Kyosuke Isshiki, Fumiki Takahashi, Manabu Uekusa, Rumiko Sei, and Kaname Hayashi. Pepper learns together with children: Development of an educational application. In 2015 IEEE-RAS 15th International Conference on Humanoid Robots (Humanoids), pages 270–275. IEEE, 2015.

[47] Ahmed Hussain Qureshi, Yutaka Nakamura, Yuichiro Yoshikawa, and Hiroshi Ishiguro. Robot gains social intelligence through multimodal deep reinforcement learning. In 2016 IEEE-RAS 16th International Conference on Humanoid Robots (Humanoids), pages 745–751. IEEE, 2016.

[48] Google Home. Google llc. `https://store.google.com/product/google_home`.

[49] Amazon Echo. Amazon.com, inc. `https://www.amazon.com/dp/B00X4WHP5E/`.

[50] Portal. Facebook, inc. `https://portal.facebook.com/`.

[51] Homepad. Apple inc. `https://www.apple.com/homepod/`.

[52] Roomba. irobot corporation. `https://www.irobot.com/`.

[53] George Konidaris. Constructing abstraction hierarchies using a skill-symbol loop. In IJCAI: proceedings of the conference, volume 2016, page 1648. NIH Public Access, 2016.

[54] George Konidaris, Leslie Pack Kaelbling, and Tomas Lozano-Perez. From skills to symbols: Learning symbolic representations for abstract high-level planning. Journal of Artificial Intelligence Research, 61:215–289, 2018.

[55] Tomohiko Takei, Joachim Confais, Saeka Tomatsu, Tomomichi Oya, and Kazuhiko Seki. Neural basis for hand muscle synergies in the primate spinal cord. Proceedings of the National Academy of Sciences, 114(32):8643–8648, 2017.

[56] N. A. Bernshtein. The co-ordination and regulation of movements. Oxford, New York, Pergamon Press, 1967.

[57] Andrea d'Avella, Philippe Saltiel, and Emilio Bizzi. Combinations of muscle synergies in the construction of a natural motor behavior. Nature Neuroscience, 6:300–308, 2003.

[58] Jose Gonzalez-Vargas, Massimo Sartori, Strahinja Dosen, Diego Torricelli, Jose Pons, and Dario Farina. A predictive model of muscle excitations based on muscle modularity for a large repertoire of human locomotion conditions. Frontiers in Computational Neuroscience, 9:114, 2015.

[59] Filipe O. Barroso, Diego Torricelli, Juan C. Moreno, Julian Taylor, Julio Gomez-Soriano, Elisabeth Bravo-Esteban, Stefano Piazza, Cristina Santos, and Jose L. Pons. Shared muscle synergies in human walking and cycling. Journal of Neurophysiology, 112:1984–1998, 2014.

[60] Matthew C. Tresch, Philippe Saltiel, and Emilio Bizzi. The construction of movement by the spinal cord. Nature Neuroscience, 2:162–167, 1999.

[61] Stacie A. Chvatal, Gelsy Torres-Oviedo, Seyed A. Safavynia, and Lena H. Ting. Common muscle synergies for control of center of mass and force in nonstepping and stepping postural behaviors. Journal of Neurophysiology, 106:999–1015, 2011.

[62] Fady Shibata Alnajjar, Tytus Wojtara, hidenori kimura, and Shingo Shimoda. Muscle synergy space: learning model to create an optimal muscle synergy. Frontiers in Computational Neuroscience, 7:136, 2013.

[63] Alvaro Costa-Garcia, Matti Itkonen, Hiroshi Yamasaki, Fady Shibata-Alnajjar, and Shingo Shimoda. A novel approach to the segmentation of semg data based on the activation and deactivation of muscle synergies during movement. IEEE Robotics and Automation Letters, 3:1972–1977, 2018.

[64] Hiroki Kogami, Qi An, Ningjia Yang, Hiroshi Yamakawa, Yusuke Tamura, Atsushi Yamashita, Hajime Asama, Shingo Shimoda, Hiroshi Yamasaki, Matti Itkonen, Fady Shibata-Alnajjar, Noriaki Hattori, Makoto Kinomoto, Kouji Takahashi, Takanori Fujii, Hironori Otomune, and Ichiro Miyai. Effect of physical

therapy on muscle synergy structure during standing-up motion of hemiplegic patients. IEEE Robotics and Automation Letters, 3:2229–2236, 2018.

[65] Mark L. Latash. The organization of quick corrections within a two-joint synergy in conditions of unexpected blocking and release of a fast movement. Clinical Neurophysiology, 111:975–987, 2000.

[66] Margaret Schenkman, Richard A Berger, Patrick O Riley, Robert W Mann, and W Andrew Hodge. Whole-body movements during rising to standing from sitting. Physical Therapy, 70:638–648, 1990.

[67] Hiroshi R. Yamasaki and Shingo Shimoda. Spatiotemporal modular organization of muscle torques for sit-to-stand movements. Journal of Biomechanics, 49:3268–3274, 2016.

[68] Mark L. Latash. Synergy. Oxford university press, 2008.

[69] Fady Shibata-Alnajjar, Matti Itkonen, Vincent Berenz, Maxime Tournier, Chikara Nagai, and Shingo Shimoda. Sensory synergy as environmental input integration. Frontiers in Neuroscience, 8:436, 2015.

[70] Lena H. Ting. Dimensional reduction in sensorimotor systems: a framework for understanding muscle coordination of posture. In Computational Neuroscience: Theoretical Insights into Brain Function, volume 165, pages 299–321. Elsevier, 2007.

[71] G. E. Hinton and R. R. Salakhutdinov. Reducing the dimensionality of data with neural networks. Science, 313:504–507, 2006.

[72] E. Hosseini-Asl, J. M. Zurada, and O. Nasraoui. Deep learning of part-based representation of data using sparse autoencoders with nonnegativity constraints. IEEE Transactions on Neural Networks and Learning Systems, 27:2486–2498, 2016.

[73] Chelsea Finn, Xin Yu Tan, Yan Duan, Trevor Darrell, Sergey Levine, and Pieter Abbeel. Deep spatial autoencoders for visuomotor learning. In 2016 IEEE International Conference on Robotics and Automation (ICRA), pages 512–519, 2016.

[74] H. van Hoof, N. Chen, M. Karl, P. van der Smagt, and J. Peters. Stable reinforcement learning with autoencoders for tactile and visual data. In 2016 IEEE/RSJ International Conference on Intelligent Robots and Systems (IROS), pages 3928–3934, 2016.

[75] Y. Kondo and Y. Takahashi. Real-time whole body imitation by humanoic robot based on particle filter and dimension reduction by autoencoder. In 2017 Joint 17th World Congress of International Fuzzy Systems Association and 9th International Conference on Soft Computing and Intelligent Systems (IFSA-SCIS), pages 1–6, 2017.

[76] Kuniaki Noda, Hiroaki Arie, Yuki Suga, and Tetsuya Ogata. Multimodal integration learning of robot behavior using deep neural networks. Robotics and Autonomous Systems, 62:721–736, 2014.

[77] Emanuel Todorov. Compositionality of optimal control laws. In Advances in Neural Information Processing Systems 22, pages 1856–1864. Curran Associates, Inc, 2009.

[78] Takamitsu Matsubara, Takaya Asakura, and Kenji Sugimoto. Dynamic linear bellman combination of optimal policies for solving new tasks. IEICE Transactions on Fundamentals of Electronics, Communications and Computer Sciences, E98.A:2187–2190, 2015.

[79] E. Uchibe and K. Doya. Combining learned controllers to achieve new goals based on linearly solvable mdps. In 2014 IEEE International Conference on Robotics and Automation (ICRA), pages 5252–5259, 2014.

[80] Shingo Shimoda and Hidenori Kimura. Biomimetic approach to tacit learning based on compound control. IEEE Transactions on Systems, Man, and Cybernetics, Part B (Cybernetics), 40:77–90, 2010.

[81] Shingo Shimoda, Yuki Yoshihara, and Hidenori Kimura. Adaptability of tacit learning in bipedal locomotion. IEEE Transactions on Autonomous Mental Development, 5:152–161, 2013.

[82] Mitsuhiro Hayashibe and Shingo Shimoda. Synergetic motor control paradigm for optimizing energy efficiency of multijoint reaching via tacit learning. Frontiers in Computational Neuroscience, 8:21, 2014.

[83] Shintaro Oyama, Shingo Shimoda, Fady S. K. Alnajjar, Katsuyuki Iwatsuki, Minoru Hoshiyama, Hirotaka Tanaka, and Hitoshi Hirata. Biomechanical reconstruction using the tacit learning system: Intuitive control of prosthetic hand rotation. Frontiers in Neurorobotics, 10:19, 2016.

[84] Shingo Shimoda, Álvaro Costa, Guillermo Asin-Prieto, Shotaro Okajima, Eduardo Ináez, Yasuhisa Hasegawa, Jose M Azorín, Jose L. Pons, and Juan C. Moreno. Joint stiffness tuning of exoskeleton robot h2 by tacit learning. In Symbiotic Interaction, pages 138–144, 2015.

[85] Paul D. MacLean. The Triune Brain in Evolution: Role in Paleocerebral Functions. Springer US, 1990.

[86] Chris Eliasmith, Terrence C Stewart, Xuan Choo, Trevor Bekolay, Travis DeWolf, Yichuan Tang, and Daniel Rasmussen. A large-scale model of the functioning brain. science, 338(6111):1202–1205, 2012.

[87] Karl Friston. Hierarchical models in the brain. PLoS computational biology, 4(11):e1000211, 2008.

[88] Uri Hasson, Janice Chen, and Christopher J Honey. Hierarchical process memory: memory as an integral component of information processing. Trends in cognitive sciences, 19(6):304–313, 2015.

[89] Thomas Parr and Karl J Friston. The anatomy of inference: Generative models and brain structure. Frontiers in computational neuroscience, 12, 2018.

[90] Kunihiko Fukushima and Sei Miyake. Neocognitron: A self-organizing neural network model for a mechanism of visual pattern recognition. In Competition and cooperation in neural nets, pages 267–285. Springer, 1982.

[91] Steve Lawrence, C Lee Giles, Ah Chung Tsoi, and Andrew D Back. Face recognition: A convolutional neural-network approach. IEEE transactions on neural networks, 8(1):98–113, 1997.

[92] Yann LeCun, Yoshua Bengio, et al. Convolutional networks for images, speech, and time series. The handbook of brain theory and neural networks, 3361(10):1995, 1995.

[93] Masakazu Matsugu, Katsuhiko Mori, Yusuke Mitari, and Yuji Kaneda. Subject independent facial expression recognition with robust face detection using a convolutional neural network. Neural Networks, 16(5-6):555–559, 2003.

[94] Christopher D Malon and Eric Cosatto. Classification of mitotic figures with convolutional neural networks and seeded blob features. Journal of pathology informatics, 4, 2013.

[95] Mike Schuster and Kuldip K Paliwal. Bidirectional recurrent neural networks. IEEE Transactions on Signal Processing, 45(11):2673–2681, 1997.

[96] Tomáš Mikolov, Martin Karafiát, Lukáš Burget, Jan Černockỳ, and Sanjeev Khudanpur. Recurrent neural network based language model. In Eleventh annual conference of the international speech communication association, 2010.

[97] Yunong Zhang and Shuzhi Sam Ge. Design and analysis of a general recurrent neural network model for time-varying matrix inversion. IEEE Transactions on Neural Networks, 16(6):1477–1490, 2005.

[98] Hermann Mayer, Faustino Gomez, Daan Wierstra, Istvan Nagy, Alois Knoll, and Jürgen Schmidhuber. A system for robotic heart surgery that learns to tie knots using recurrent neural networks. Advanced Robotics, 22(13-14):1521–1537, 2008.

[99] Zhan Li, Mitsuhiro Hayashibe, Charles Fattal, and David Guiraud. Muscle fatigue tracking with evoked emg via recurrent neural network: toward personalized neuroprosthetics. IEEE Computational Intelligence Magazine, 9(2):38–46, 2014.

[100] Volodymyr Mnih, Koray Kavukcuoglu, David Silver, Andrei A Rusu, Joel Veness, Marc G Bellemare, Alex Graves, Martin Riedmiller, Andreas K Fidjeland, Georg Ostrovski, et al. Human-level control through deep reinforcement learning. Nature, 518(7540):529, 2015.

[101] Timothy P Lillicrap, Jonathan J Hunt, Alexander Pritzel, Nicolas Heess, Tom Erez, Yuval Tassa, David Silver, and Daan Wierstra. Continuous control with deep reinforcement learning. arXiv preprint arXiv:1509.02971, 2015.

[102] Hado Van Hasselt, Arthur Guez, and David Silver. Deep reinforcement learning with double q-learning. In Thirtieth AAAI Conference on Artificial Intelligence, 2016.

[103] Dalin Zhang, Lina Yao, Sen Wang, Kaixuan Chen, Zheng Yang, and Boualem Benatallah. Fuzzy integral optimization with deep q-network for eeg-based intention recognition. In Pacific-Asia Conference on Knowledge Discovery and Data Mining, pages 156–168. Springer, 2018.

[104] Nicolas Heess, Srinivasan Sriram, Jay Lemmon, Josh Merel, Greg Wayne, Yuval Tassa, Tom Erez, Ziyu Wang, SM Eslami, Martin Riedmiller, et al. Emergence of locomotion behaviours in rich environments. arXiv preprint arXiv:1707.02286, 2017.

[105] Yoshihisa Tsurumine, Yunduan Cui, Eiji Uchibe, and Takamitsu Matsubara. Deep reinforcement learning with smooth policy update: Application to robotic cloth manipulation. Robotics and Autonomous Systems, 112:72–83, 2019.

[106] Alec Radford, Luke Metz, and Soumith Chintala. Unsupervised representation learning with deep convolutional generative adversarial networks. arXiv preprint arXiv:1511.06434, 2015.

[107] Christian Ledig, Lucas Theis, Ferenc Huszár, Jose Caballero, Andrew Cunningham, Alejandro Acosta, Andrew Aitken, Alykhan Tejani, Johannes Totz, Zehan Wang, et al. Photo-realistic single image super-resolution using a generative adversarial network. In Proceedings of the IEEE conference on computer vision and pattern recognition, pages 4681–4690, 2017.

[108] Emily L Denton, Soumith Chintala, Rob Fergus, et al. Deep generative image models using a laplacian pyramid of adversarial networks. In Advances in neural information processing systems, pages 1486–1494, 2015.

[109] Xi Chen, Yan Duan, Rein Houthooft, John Schulman, Ilya Sutskever, and Pieter Abbeel. Infogan: Interpretable representation learning by information maximizing generative adversarial nets. In Advances in neural information processing systems, pages 2172–2180, 2016.

[110] Ngoc-Dung T Tieu, Huy H Nguyen, Hoang-Quoc Nguyen-Son, Junichi Yamagishi, and Isao Echizen. Spatio-temporal generative adversarial network for gait anonymization. Journal of Information Security and Applications, 46:307–319, 2019.

[111] Sepp Hochreiter and Jürgen Schmidhuber. Long short-term memory. Neural computation, 9(8):1735–1780, 1997.

[112] Alex Graves and Jürgen Schmidhuber. Framewise phoneme classification with bidirectional lstm and other neural network architectures. Neural Networks, 18(5-6):602–610, 2005.

[113] Haşim Sak, Andrew Senior, and Françoise Beaufays. Long short-term memory recurrent neural network architectures for large scale acoustic modeling. In Fifteenth annual conference of the international speech communication association, 2014.

[114] Haşim Sak, Andrew Senior, and Françoise Beaufays. Long short-term memory based recurrent neural network architectures for large vocabulary speech recognition. arXiv preprint arXiv:1402.1128, 2014.

[115] Jiachen Zhao, Fang Deng, Yeyun Cai, and Jie Chen. Long short-term memory-fully connected (lstm-fc) neural network for pm2. 5 concentration prediction. Chemosphere, 220:486–492, 2019.

[116] Volodymyr Mnih, Adria Puigdomenech Badia, Mehdi Mirza, Alex Graves, Timothy Lillicrap, Tim Harley, David Silver, and Koray Kavukcuoglu. Asynchronous methods for deep reinforcement learning. In International conference on machine learning, pages 1928–1937, 2016.

[117] Marie Csete and John Doyle. Bow ties, metabolism and disease. Trends in Biotechnology, 22(9):446–450, 2004.

[118] Jing Zhao, Hong Yu, Jian-Hua Luo, Zhi-Wei Cao, and Yi-Xue Li. Hierarchical modularity of nested bow-ties in metabolic networks. BMC Bioinformatics, 7(1):386, Aug 2006.

[119] Rodney Brooks. A robust layered control system for a mobile robot. IEEE journal on robotics and automation, 2(1):14–23, 1986.

[120] Rodney A Brooks and Jonathan H Connell. Asynchronous distributed control system for a mobile robot. In Mobile Robots I, volume 727, pages 77–85. International Society for Optics and Photonics, 1987.

[121] NAO. softbank robotics. `https://www.ald.softbankrobotics.com/en/robots/nao`.

[122] P.G. Kry, L. Reveret, F. Faure, and M.-P Cani. Modal locomotion: Animating virtual characters with natural vibrations. Computer Graphics Forum, 28:289–298, 2009.

[123] Shingo Shimoda, Yuki Yoshihara, Kenji Fujimoto, Takashi Yamamoto, Iwao Maeda, and Hidenori Kimura. Stability analysis of tacit learning based on environmental signal accumulation. In 2012 IEEE/RSJ International Conference on Intelligent Robots and Systems, pages 2613–2620, 2012.

[124] F. B. Horak and L. M. Nashner. Central programming of postural movements: adaptation to altered support-surface configurations. Journal of Neurophysiology, 55:1369–1381, 1986.

[125] C. F Runge, C. L Shupert, F. B Horak, and F. E Zajac. Ankle and hip postural strategies defined by joint torques. Gait & Posture, 10:161–170, 1999.

[126] Stephen N. Robinovitch, Britta Heller, Andrew Lui, and Jeffrey Cortez. Effect of strength and speed of torque development on balance recovery with the ankle strategy. Journal of Neurophysiology, 88:613–620, 2002.

[127] NASA. Man-system integration standards. 1, `http://msis.jsc.nasa.gov/sections/section03.htm`.

[128] Kazumi Kawahira, Megumi Shimodozono, Seiji Etoh, Katsuya Kamada, Tomokazu Noma, and Nobuyuki Tanaka. Effects of intensive repetition of a new facilitation technique on motor functional recovery of the hemiplegic upper limb and hand. Brain Injury, 24(10):1202–1213, 2010.

[129] HI Krebs, BT Volpe, ML Aisen, and N Hogan. Increasing productivity and quality of care: Robot-aided neuro-rehabilitation. Journal of rehabilitation research and development, 37(6):639–652, 2000.

[130] Angelo Basteris, Sharon M Nijenhuis, Arno HA Stienen, Jaap H Buurke, Gerdienke B Prange, and Farshid Amirabdollahian. Training modalities in robot-mediated upper limb rehabilitation in stroke: a framework for classification based on a systematic review. Journal of neuroengineering and rehabilitation, 11(1):111, 2014.

[131] ReoGo. Motorika. `http://motorika.com/product-1/`.

[132] Lori Sledziewski, Roseann C Schaaf, and Julie Mount. Use of robotics in spinal cord injury: A case report. American Journal of Occupational Therapy, 66(1):51–58, 2012.

[133] Shigeki Kubota, Yoshio Nakata, Kiyoshi Eguchi, Hiroaki Kawamoto, Kiyotaka Kamibayashi, Masataka Sakane, Yoshiyuki Sankai, and Naoyuki Ochiai. Feasibility of rehabilitation training with a newly developed wearable robot for patients with limited mobility. Archives of physical medicine and rehabilitation, 94(6):1080–1087, 2013.

[134] Atsushi Tsukahara, Ryota Kawanishi, Yasuhisa Hasegawa, and Yoshiyuki Sankai. Sit-to-stand and stand-to-sit transfer support for complete paraplegic patients with robot suit hal. Advanced robotics, 24(11):1615–1638, 2010.

[135] Power assist hand. Lap co., ltd. `http://www.t-atom.com/`.

[136] Hand of Hope. Rehab-robotics. `http://rehab-robotics.com/index.html`.

[137] Christopher N Schabowsky, Sasha B Godfrey, Rahsaan J Holley, and Peter S Lum. Development and pilot testing of hexorr: hand exoskeleton rehabilitation robot. Journal of neuroengineering and rehabilitation, 7(1):36, 2010.

[138] Sung-Sik Yun, Brian Byunghyun Kang, and Kyu-Jin Cho. Exo-glove pm: an easily customizable modularized pneumatic assistive glove. IEEE Robotics and Automation Letters, 2(3):1725–1732, 2017.

[139] Hossein Taheri, Justin B Rowe, David Gardner, Vicki Chan, Kyle Gray, Curtis Bower, David J Reinkensmeyer, and Eric T Wolbrecht. Design and preliminary evaluation of the finger rehabilitation robot: controlling challenge and quantifying finger individuation during musical computer game play. Journal of neuroengineering and rehabilitation, 11(1):10, 2014.

[140] AMADEO. Tyromotion. `https://tyromotion.com/en/produkte/amadeo/`.

[141] Pinhas Ben-Tzvi, Jerome Danoff, and Zhou Ma. The design evolution of a sensing and force-feedback exoskeleton robotic glove for hand rehabilitation application. Journal of Mechanisms and Robotics, 8(5):051019, 2016.

[142] Kaci E Madden and Ashish D Deshpande. On integration of additive manufacturing during the design and development of a rehabilitation robot: A case study. Journal of Mechanical Design, 137(11):111417, 2015.

[143] Pyung Hun Chang, Seung-Hee Lee, Kwang-Min Koo, Seung-Hyun Lee, Sang-Hyun Jin, Sang Seok Yeo, Jeong Pyo Seo, and Sung Ho Jang. The cortical activation pattern by a rehabilitation robotic hand: a functional nirs study. Frontiers in human neuroscience, 8:49, 2014.

[144] RjG Lee and WG Tatton. Motor responses to sudden limb displacements in primates with specific cns lesions and in human patients with motor system disorders. Canadian Journal of Neurological Sciences, 2(3):285–293, 1975.

[145] C Ghez and Y Shinoda. Spinal mechanisms of the functional stretch reflex. Experimental Brain Research, 32(1):55–68, 1978.

[146] K Darton, OC Lippold, M Shahani, and U Shahani. Long-latency spinal reflexes in humans. Journal of Neurophysiology, 53(6):1604–1618, 1985.

[147] BioMot Project. `http://www.biomotproject.eu/`.

[148] Shotaro Okajima, Maxime Tournier, Fady S Alnajjar, Mitsuhiro Hayashibe, Yasuhisa Hasegawa, and Shingo Shimoda. Generation of human-like movement from symbolized information. Frontiers in neurorobotics, 12, 2018.

[149] H2. Technaid s.l. `https://www.technaid.com/products/robotic-exoskeleton-exo-exoesqueleto/`.